

603.246

155 p \$5.00hc

\$1.00mf

(UNCLASSIFIED)

MIT Fluid Dynamics Research
Laboratory Report No. 64-2

UNSTEADY LOADS ON HYDROFOILS INCLUDING
FREE SURFACE EFFECTS AND CAVITATION

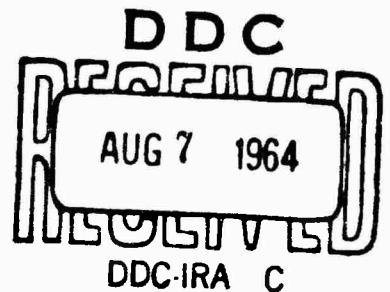
by

Sheila Evans Widnall

MASSACHUSETTS INSTITUTE OF TECHNOLOGY

June 1964

Contract No. Nonr 1841(81)



This research was carried out under the Bureau of Ships
Fundamental Hydromechanics Research Program, S-R009 01 01,
Administered by the David Taylor Model Basin.

Reproduction in whole or in part is permitted for any purpose
of the United States Government.

(UNCLASSIFIED)

UNSTEADY LOADS ON HYDROFOILS
INCLUDING FREE SURFACE EFFECTS AND CAVITATION

by

Sheila Evans Widnall

ABSTRACT

Linearized three-dimensional lifting surface theory is applied to a variety of problems of interest in hydrofoil application. The resulting integral equations are solved by numerical techniques on a high-speed digital computer to predict steady and oscillatory loads.

The following cases are discussed: thin non-planar hydrofoils at infinite Froude number, the effect of gravity waves on the forces on an oscillating hydrofoil near the free surface, supercavitating hydrofoils of finite span in steady and oscillatory motion. Numerical results for lift and moment are presented and comparison with experiment is made whenever possible.

Results of these calculations indicate that this numerical solution is a very practical and efficient way to obtain accurate prediction of unsteady loads for flutter calculations.

ACKNOWLEDGEMENTS

The author wishes to acknowledge the time and enthusiasm given by her thesis committee consisting of Professors Marter Landahl, Holt Ashley and John Dugundji. Appreciation is also due to Dick Kaplan for comradeship and competition during the graduate years, to husband Bill and infant son Bill for unbelievable cooperation, and to Linda Hodgens, who typed the manuscript.

This research was performed under Contract Nonr 1841(81) administered by the David Taylor Model Basin. Common interests and discussions shared with members of the Model Basin staff were gratefully appreciated.

In addition, the M.I.T. Computation Center provided a most efficient staff and computer time of the IBM 7094 under problem M2429.

TABLE OF CONTENTS

| <u>Chapter No.</u> | | <u>Page No.</u> |
|--------------------|---|-----------------|
| <u>I</u> | <u>Lifting Surface Theory for Nonplanar Surfaces</u> | |
| | 1.1 Introduction | 1 |
| | 1.2 The Integral Equation for a Nonplanar Lifting Surface | 4 |
| | 1.3 The Kernel Function For a Nonplanar Hydrofoil at Infinite Froude Number | 13 |
| | 1.4 The Singularity in the Kernel Function | 16 |
| | 1.5 Numerical Method for a Nonplanar Fully Wetted Lifting Surface | 21 |
| <u>II</u> | <u>The Effect of Gravity Waves on the Lift and Moment On an Oscillating Hydrofoil</u> | |
| | 2.1 Introduction | 30 |
| | 2.2 The Kernel Function for Two-Dimensional Foils at Arbitrary Froude Number | 32 |
| | 2.3 Numerical Solution and Results for Arbitrary Froude Number | 43 |
| | 2.4 The Kernel Function in Three Dimensions | 47 |
| <u>III</u> | <u>Unsteady Loads on Supercavitating Hydrofoils</u> | |
| | 3.1 Introduction | 63 |
| | 3.2 Linearized Theory For Three-Dimensional Supercavitating Hydrofoils | 64 |
| | 3.3 Numerical Method For Three-Dimensional Supercavitating Hydrofoils | 75 |
| | 3.3a Numerical Calculations for a Steady Symmetric Wedge | 80 |
| | 3.3b Numerical Results for a Symmetric Wedge | 86 |
| | 3.3c Numerical Method for a Supercavitating Flat Plate | 88 |
| | 3.3d Comparison With Steady Two-dimensional Linearized Theory | 98 |

| | | |
|-----------|---|------|
| 3.3e | Comparison With Other Three-Dimensional Theories and Experiment | 105 |
| 3.3f | Lift and Moment on an Oscillating Supercavitating Hydrofoil of Finite Span | 111 |
| <u>IV</u> | <u>Conclusion and Recommendations</u> | 120a |
| <u>V</u> | <u>References</u> | 121 |
| <u>VI</u> | <u>Appendix</u> | |
| 1 | Evaluation of Kernel Functions for Steady and Unsteady Three-Dimensional Flow | 125 |
| 11 | The Kernel Function for Nonplanar Surfaces | 135 |
| 111 | Transformation of the Fourier Inversion Integral | 139 |

List of Figures

| | | |
|-----|--|----|
| 1.1 | Configuration of a Nonplanar Surface | 8 |
| 1.2 | The Neighborhood of the Singular Point | 18 |
| 1.3 | Comparison with Experiment--Spanwise Distribution of Lift Due to Bending ($k = .6$) | 26 |
| 1.4 | Comparison with Experiment--Spanwise Distribution of Lift Due to Bending ($k = .8$) | 27 |
| 1.5 | Comparison with Experiment--Spanwise Distribution of Lift Due to Bending ($k = 1.2$) | 28 |
| 1.6 | Comparison with Experiment--Spanwise Distribution of Lift Due to Bending ($k = 2.0$) | 29 |
| 2.1 | Location of the Poles of Equation (2.44) for Constant \mathcal{F} , Increasing K . ($f = k\mathcal{F}^2$) | 39 |
| 2.2 | Lift Coefficient Due to Heave vs. k for a Two-dimensional Hydrofoil | 59 |
| 2.3 | Lift Coefficient Due to Pitch vs. k for a Two-dimensional Hydrofoil | 60 |
| 2.4 | Moment Coefficient Due to Heave vs. k for a Two-dimensional Hydrofoil | 61 |
| 2.5 | Moment Coefficient Due to Pitch vs. k for a Two-dimensional Hydrofoil | 62 |

Figures (con't)

| | | |
|------|---|----|
| 3.1 | Closed Surface of Cavity and Foil | 66 |
| 3.2 | The Projection of S on to the x y plane | 68 |
| 3.3 | Model for a Supercavitating Wedge | 81 |
| 3.4 | The Function $h(\eta, \eta_1, \eta_2)$ vs η | 82 |
| 3.5 | The set of Functions $f_c(\xi)$ | 83 |
| 3.6 | Typical $f(\xi)$ | 84 |
| 3.7 | Control Point Locations on S_c for a Symmetric Wedge Solution | 85 |
| 3.8 | Comparison of Chordwise Pressure Distributions on a Symmetric Wedge by Two-Dimensional Theory and Three-Dimensional Numerical Results on the Center Section of an Aspect Ratio 6 Wedge $\sigma = 0$ $\alpha = .1$ | 87 |
| 3.9 | Comparison of Pressure Source Distribution in the Cavity Behind a Symmetric Wedge by Two-Dimensional Theory and Three-Dimensional Numerical Results at the Center Section of An Aspect Ratio 6 Wedge $\sigma = 0$ $\alpha = .1$ | 87 |
| 3.10 | Typical $f(\xi)$ for a Supercavitating Flat Plate | 91 |
| 3.11 | Modes of $f(\xi)$ | 92 |
| 3.12 | Configuration for Numerical Solution for a Supercavitating Flat Plate Showing Control Point Location x_k, y_k . | 93 |

Figures (con't)

- 3.13 Numerical Results for the Pressure Source Distribution on the Center Section of an Aspect Ratio 6 Supercavitating Flat Plate, Comparison with Two-Dimensional Linear Theory
 $\alpha = .1, \beta = 0, X_E = 5$ 100
- 3.14 Numerical Results for the Lift Distribution on the Center Section of an Aspect Ratio 6 Flat Plate, Comparison with Two-Dimensional Theory
 $\alpha = .1, \beta = 0, X_E = 5$ 101
- 3.15 Lift and Moment Coefficients vs. σ ($\alpha = .1$) Numerical Results for the Center Section of an Aspect Ratio 6 Flat Plate Foil; Two-Dimensional Theory 104
- 3.16 Experimental Results for Cavity Length vs. σ/α 109
- 3.17 Comparison Between Numerical Results and Experiment for an Aspect Ratio 6 Foil Lift Coefficient vs. Cavitation Number. 110
- 3.18 Lift Coefficient vs. Cavitation Number for an Aspect Ratio 4 Foil ($\alpha = 10^\circ$); Comparison with Experiment and Other Theories 110
- 3.19-3.22 Unsteady Aerodynamic Coefficients for an Aspect Ratio 6 Supercavitating Foil, Comparison with Two-Dimensional Theory 113
- 3.23-2.26 Unsteady Aerodynamic Coefficients for an Aspect Ratio one Supercavitating Foil 117

SYMBOLS

- Q_n - coefficient of the nth assumed pressure source mode
 R - aspect ratio
 b_n - coefficient of the nth assumed pressure doublet mode
 b_0 - root semichord
 C_L - lift coefficient
 C_M - moment coefficient
 DDW - matrix of upwash at x, y, z due to $\langle \frac{\partial P}{\partial \varphi} \rangle_n$
 DW - matrix of upwash at x_k, y_k, z_k due to ΔP_n
 DPM - matrix of pressure doublet strength at x_k, y_k, z_k due to ΔP_n
 E_i - complex exponential integral
 f - reduced frequency • (Froude Number)²
 $f_n(\eta)$ - assumed η function for $\Delta P^{(3, \eta)}$
 F - Froude number
 $f^{(3)}$ - assumed Ξ functions for $\langle \frac{\partial P}{\partial \varphi} \rangle^{(3, \eta)}$
 g - acceleration of gravity
 $h(\eta, \eta_1, \eta_2)$ - assumed spanwise functions for $\langle \frac{\partial P}{\partial \varphi} \rangle$, defined by equation (3.38)
 $H(x)$ - heavyside function
 I - number of streamwise rectangles on foil--cavity surface
 J - number of spanwise rectangles on foil--cavity surface
 k - reduced frequency
 χ - kernel function
 $\bar{\chi}$ - limiting form of kernel function
 h_n - chordwise assumed Ξ functions for $\Delta P^{(3, \eta)}$
 n - normal coordinate

- \mathcal{P} - fourier transform of P
 P - matrix of pressure at x_k, y_k due to $\langle \frac{\partial P}{\partial y} \rangle$
 \hat{P} - perturbation pressure
 P - nondimensional complex amplitude of pressure perturbation
 ΔP - pressure jump across the foil surface
 $\langle \frac{\partial P}{\partial n} \rangle$ - jump in normal derivative of pressure across the foil-cavity surface S .
 R - radius vector
 s - semispan/semichord
 S - surface of integration
 S_c - cavity surface (projection of)
 S_w - wetted surface (projection of)
 ds - element of area on surface S
 t - time
 U - free stream velocity
 $v(x, y)$ - upwash on wetted surface of foil
 x, y, z - nondimensional coordinates
 X_E - coordinate of trailing edge of cavity
 α - angle of attack
 $\delta(x)$ - delta function
 ϵ - small parameter defining width of region near singular point
 ξ, η, ζ - nondimensional coordinates
 $v(x, y, t)$ - shape of free surface
 ρ - free stream density

- σ - cavitation number
- τ - tangential coordinate
- ϕ - perturbation velocity potential
- φ - nondimensional complex amplitude of perturbation
velocity potential
- Φ - Fourier transform of φ
- ψ - slope angle of nonplanar surface

CHAPTER I
LIFTING SURFACE THEORY FOR
NONPLANAR SURFACES

1.1 Introduction

Before the availability of high speed digital computers, methods based on linearized theory for calculating loads on three dimensional lifting surfaces in incompressible fluids were restricted to special plan form shapes which could be handled analytically or to approximate methods suitable for hand calculation.

In steady flow, a lifting surface is represented by a vortex sheet, or by the horseshoe vortices which make up the vortex sheet. The boundary value problem is formulated using the velocity potential. By the principle of superposition, the upwash velocity on the wing is written as an integral of the upwash velocities from each element of the vortex sheet. This boundary value problem, together with auxiliary conditions such as the Kutta condition, is solved for the distribution of vortex strength and thus the distribution of lift on the surface.

Unfortunately this integral equation cannot be solved analytically for wings of arbitrary planform. For two limiting cases, wings of large aspect ratio and wings of small aspect ratio, analytical results have been obtained. For wings of arbitrary planform, approximate techniques have been used. For example, the wing is represented by a finite number of horseshoe vortices located on the surface

of the wing; their strength is determined by satisfying the known upwash condition at control points on the wing. A discussion of some of these techniques, as well as numerical and experimental results, is given by Thwaites, Ref. (1).

For planar lifting surfaces in oscillatory motion in an infinite incompressible fluid, analytical solutions have been given for wings of infinite aspect ratio (Ref. (2)), and for wings of circular planform, (Ref. (3), (4)). Some of the approximate techniques for finite wings described in Ref. (1), such as those of Falkner and Multhopp, have been modified for oscillating wings. A discussion of the numerical techniques for oscillating finite wings developed before the age of high speed computing machines is given in Ref. (7). These methods were always a compromise between "accuracy of results and computing labor required". (Ref. (7))

Taking advantage of high-speed stored program computing equipment, Watkins and his associates (Ref. (6), (7)) have developed a most satisfactory numerical method for calculation of the lift distribution on a finite planar wing in steady or oscillatory motion in an infinite subsonic flow. This method makes a direct attack on the integral equation relating upwash to lift distribution on the wing by assuming a set of modes for the lift distribution

with unknown coefficients. The coefficients of these lift modes are found by satisfying the boundary condition of a known upwash at suitably selected control points on the surface. The integrations required for this method would be completely impractical to do analytically but are quite straightforward numerically.

Much of the present work is an extension of these ideas to problems of interest in hydrofoil applications. Governing integral equations are derived for the following cases: in Chapter 1, three-dimensional nonplanar oscillating lifting surfaces in an infinite fluid or beneath a free surface at infinite Froude number; in Chapter 2, two- and three-dimensional oscillating foils beneath a free surface including the effects of gravity waves generated by the motion, (finite Froude number); in Chapter 3, three-dimensional steady and oscillating supercavitating hydrofoils in an infinite fluid. Numerical results are presented for most of these cases and comparisons are made with experiments where possible.

These integral equations are derived by taking advantage of the fact that in linearized theory for an incompressible fluid, the perturbation pressure satisfies Laplace's equation. As an introduction to these techniques we

shall discuss the integral equation for a nonplanar lifting surface in an infinite fluid.

1.2 The Integral Equation for a Nonplanar Lifting Surface

In the linearized theory for the flow of an incompressible fluid with free stream velocity U in the positive x direction about a thin lifting surface in steady or unsteady motion, the perturbation pressure is given by a linear operation on the perturbation velocity potential, namely by

$$-\frac{\hat{p}}{\rho} = \frac{\partial \phi}{\partial t} + U \frac{\partial \phi}{\partial x} \quad (1.1)$$

We consider simple harmonic motion with frequency ω

$$\hat{p} = p e^{i\omega t} \quad (1.2)$$

$$\phi = \varphi e^{i\omega t} \quad (1.3)$$

If we nondimensionalize all physical quantities with respect to free stream velocity U , density ρ , and root semichord b_0 , the complex amplitudes of \hat{p} and ϕ are related by equation (1.4)

$$-p = ik\varphi + \frac{\partial \varphi}{\partial x} \quad (1.4)$$

where p , φ , $\frac{\partial \varphi}{\partial x}$ are now dimensionless variables, k is the reduced frequency.

Equation (1.3) is solved for φ as a function of p with the boundary condition $\varphi(-\infty) = 0$.

$$\phi(x) = \int_{-\infty}^x P(\lambda) e^{ik(\lambda-x)} d\lambda \quad (1.5)$$

In the literature it is common to define an acceleration potential ψ .

$$\psi = ik\phi + \frac{\partial p}{\partial x} \quad (1.6)$$

$$\psi = -p \quad (1.7)$$

For convenience, however, we will work with pressure directly.

In the linearized theory for an incompressible irrotational flow, both p and ϕ are potential functions satisfying Laplace's equation,

$$\nabla^2 p = 0 \quad (1.8)$$

$$\nabla^2 \phi = 0 \quad (1.9)$$

Green's theorem (for a potential function) is written for a closed surface surrounding the fluid, in this case, a closed inner boundary plus the surface at infinity which does not contribute to the integrals (See reference (5) for a discussion of Green's Theorem). In standard notation

the normal vector would point out of the fluid; in aeronautical applications it is often written with the normal pointing into the fluid.

$$P(x, y, z) = \frac{1}{4\pi} \iint_S P(\xi, \eta, \zeta) \nabla \left(\frac{1}{R} \right) \cdot \vec{n} \, dS \quad (1.10)$$

$$- \frac{1}{4\pi} \iint_S \frac{\nabla P(\xi, \eta, \zeta) \cdot \vec{n}}{R} \, dS'$$

where \vec{n} is the outward normal to S into the fluid at the point ξ, η, ζ .

x, y, z are coordinates of a point in the fluid. ξ, η, ζ are coordinates of a point on the closed surface S .

The surface S is taken to be the "upper" and "lower" surfaces of a zero thickness wing, given by some function

$\zeta = \zeta(\eta, \xi)$. In linearized theory for thin wing-like configurations, (i.e. for $\frac{\partial \zeta}{\partial \xi} \ll 1$) we satisfy the upwash boundary condition on the mean position of the nonplanar surface, $\zeta = \zeta(\eta, 0) = \zeta(\eta)$.

We rewrite equation (1.10) as an integral of the jump in p and $\frac{\partial p}{\partial n}$ across an open surface $\zeta = \zeta(\eta)$.

$$P(x, y, z) = \frac{1}{4\pi} \iint_S \Delta p(\xi, \eta, \zeta(\eta)) \frac{\partial}{\partial n} \left(\frac{1}{R} \right) dS - \frac{1}{4\pi} \iint_S \left\langle \frac{\partial p}{\partial n} \right\rangle \frac{dS}{R} \quad (1.11)$$

$$\Delta p = p^- - p^+$$

$$\left\langle \frac{\partial p}{\partial n} \right\rangle = \frac{\partial p^-}{\partial n} - \frac{\partial p^+}{\partial n}$$

S^+ is the "top" of the surface

S^- is the "bottom" of the surface

n is the normal to the surface $f = f(\eta)$ positive "upward".

With an extremely nonplanar surface it is often quite arbitrary which is the top surface and which is the bottom surface; for planar wings the top and bottom are more easily defined.

Fig. (1.1) shows a typical nonplanar lifting surface configuration.

The nondimensional linearized momentum equation for the direction normal to S is

for S^+

$$-\frac{\partial p^+}{\partial n} = \frac{\partial v_n^+}{\partial x} + \frac{\partial v_n^+}{\partial t}$$

(1.12)

for S^-

$$-\frac{\partial p^-}{\partial n} = \frac{\partial v_n^-}{\partial x} + \frac{\partial v_n^-}{\partial t}$$

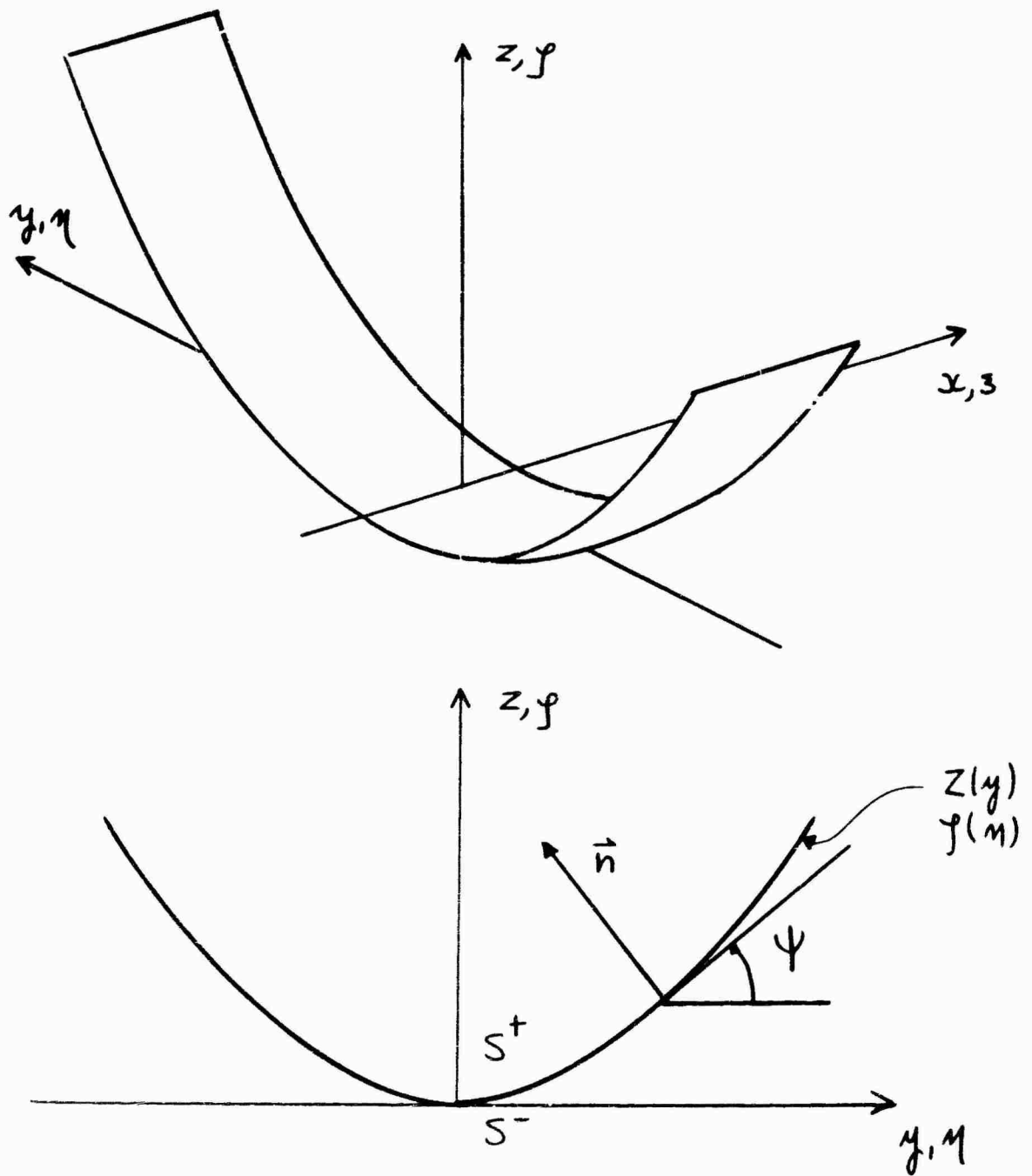


Figure 1.1 Configuration of a Nonplanar Surface

If we consider a zero-thickness surface in fully wetted flow the normal velocity V_n is continuous across the surface.

Therefore, for fully wetted flow the function $\left\langle \frac{\partial P}{\partial n}(\xi, \eta, f(\eta)) \right\rangle$ is zero on the surface.

Equation (1.8) then becomes

$$P(x, y, z) = -\frac{1}{4\pi} \iint_S \Delta P(\xi, \eta, f(\eta)) \frac{\partial}{\partial n} \left(\frac{1}{R} \right) dS \quad (1.13)$$

The singularity $-\frac{1}{4\pi} \frac{\partial}{\partial n} \left(\frac{1}{R} \right)$ is called a pressure doublet. This singularity causes a unit pressure jump across the surface at the point $x = \xi$, $y = \eta$,

$z(\eta) = f(\eta)$; n is the normal at that point.

The position of a nonplanar surface performing unsteady motions is given by some function of ξ, η, f and t .

$$f(\xi, \eta, f, t) = 0 \quad (1.14)$$

For small perturbations, the upwash velocity, normal to the mean position of the surface is formed from

$$V_n(x, y, z(\eta)) = \frac{Df}{Dt} = \frac{\partial f}{\partial t} + \frac{\partial f}{\partial x} \quad (1.15)$$

The velocity at a point x, y, z in the direction $n(y, z(y))$ is given by

$$v_n(x, y, z) = \frac{\partial}{\partial n} \phi(x, y, z) \quad (1.16)$$

The velocity potential $\phi(x, y, z)$ may be found by the operation indicated in equation (1.5)

$$\phi(x, y, z) = \iint_S \Delta p(s, \eta, \rho(\eta)) \left(\frac{1}{4\pi} \int_{-\infty}^{x-s} \frac{\partial}{\partial n(\eta, \rho)} \left(\frac{1}{R(\lambda)} \right) e^{ik(\lambda - (x-s))} d\lambda \right) dS \quad (1.17)$$

$$v_n(x, y, z) = \iint_S \Delta p(s, \eta, \rho(\eta)) \left(\frac{1}{4\pi} \frac{\partial}{\partial n(y, z)} \int_{-\infty}^{x-s} \frac{\partial}{\partial n(\eta, \rho)} \left(\frac{1}{R(\lambda)} \right) e^{ik(\lambda - (x-s))} d\lambda \right) dS \quad (1.18)$$

where

$$R(\lambda) = \sqrt{\lambda^2 + (y - \eta)^2 + (z - \rho)^2}$$

The velocity boundary condition (1.15) is satisfied in the limit as the point x, y, z approaches the surface

$x, y, z(y)$.

The kernel function for this problem is

$$\begin{aligned} K(x-\xi, y-\eta, z-f) &= \lim_{z \rightarrow z(y)} \\ &\left(\frac{1}{4\pi} \frac{\partial}{\partial n(y, z)} \int_{-\infty}^{x-\xi} \frac{\partial}{\partial n(\eta, f)} \left(\frac{1}{R(\lambda)} \right) e^{ik(\lambda - (x-\xi))} d\lambda \right) \end{aligned} \quad (1.19)$$

Referring to Fig. 1.1, we write the following expressions

for $\frac{\partial}{\partial n(y, z)}$ and $\frac{\partial}{\partial n(\eta, f)}$.

$$\frac{\partial}{\partial n(y, z)} = \cos \psi(y) \frac{\partial}{\partial z} - \sin \psi(y) \frac{\partial}{\partial y} \quad (1.20)$$

$$\frac{\partial}{\partial n(\eta, f)} = \cos \psi(\eta) \frac{\partial}{\partial f} - \sin \psi(\eta) \frac{\partial}{\partial \eta} \quad (1.21)$$

Since

$$\frac{\partial}{\partial \rho} \left(\frac{1}{R} \right) = - \frac{\partial}{\partial z} \left(\frac{1}{R} \right) \quad (1.22)$$

and

$$\frac{\partial}{\partial \eta} \left(\frac{1}{R} \right) = - \frac{\partial}{\partial y} \left(\frac{1}{R} \right) \quad (1.23)$$

then

$$\begin{aligned} \frac{\partial}{\partial n(y,z)} \frac{\partial}{\partial n(\eta,\rho)} = & - \left\{ \cos \psi(y) \cos \psi(\eta) \frac{\partial^2}{\partial z^2} + \sin \psi(y) \sin \psi(\eta) \frac{\partial^2}{\partial y^2} \right. \\ & \left. - (\sin \psi(y) \cos \psi(\eta) + \sin \psi(\eta) \cos \psi(y)) \frac{\partial^2}{\partial y \partial z} \right\} \end{aligned} \quad (1.24)$$

The complete form for this kernel function is given in Ref. (8). It is reproduced in Appendix 11. For a planar lifting surface, the kernel function becomes

$$\mathcal{K}(x-3, y-\eta, 0) = - \frac{\partial^2}{\partial z^2} \int_{-\infty}^{x-3} \frac{1}{R(\lambda)} e^{ik(\lambda-(x-3))} d\lambda \quad (1.25)$$

which agrees with references (6) and (7). With the kernel function defined by equation (1.19), the upwash velocity normal to the mean position of the nonplanar surface becomes

$$V_n(x, y, z(y)) = \iint_{S'} \Delta p(\xi, \eta, f(\eta)) K(x-\xi, y-\eta, z(y)-f(\eta)) dS' \quad (1.26)$$

This integral equation, relating the complex amplitude of the unsteady load on the surface to the complex amplitude of the upwash velocity normal to the mean surface, is solved numerically by a technique of assumed $\Delta p(\xi, \eta, f(\eta))$ modes. This method is discussed in section (1.4), and a few numerical results are given.

1.3 The Kernel Function for a Nonplanar Hydrofoil at Infinite Froude Number

For a hydrofoil traveling beneath a free surface at high velocities such that the Froude number $F = U/\sqrt{g b_0}$ can be taken equal to infinity, the free surface becomes a surface of zero perturbation pressure. The infinite Froude number approximation neglects the effects of gravity waves induced by the motion of the foil. In Chapter 2, these

effects are included and numerical results show that, at least for foils of infinite aspect ratio, a Froude number of 10 is essentially equivalent to infinity for the prediction of loads due to unsteady motion.

The singularity which causes a unit lift at the point x, η, ρ in the $\vec{n}(\eta, \rho(\eta))$ direction as well as causing no perturbation pressure on the free surface, located at $z = 0$, has the following form:

$$f(x-\xi, y-\eta, z-\rho) = -\frac{1}{4\pi} \frac{\partial}{\partial n(\eta, \rho)} \left(\frac{1}{\sqrt{(x-\xi)^2 + (y-\eta)^2 + (z-\rho)^2}} \right) \quad (1.27)$$

$$-\frac{1}{4\pi} \frac{\partial}{\partial n'(\eta, \rho)} \left(\frac{1}{\sqrt{(x-\xi)^2 + (y-\eta)^2 + (z-\rho)^2}} \right)$$

where

$$\frac{\partial}{\partial n(\eta, \rho)} = \cos \psi(\eta) \frac{\partial}{\partial \rho} - \sin \psi(\eta) \frac{\partial}{\partial \eta} \quad (1.28)$$

$$\frac{\partial}{\partial n'(\eta, \rho)} = \cos \psi(\eta) \frac{\partial}{\partial \rho} + \sin \psi(\eta) \frac{\partial}{\partial \eta} \quad (1.29)$$

It is convenient to think of this singularity as a pressure doublet with axis in the normal direction on the foil itself and a pressure doublet, of the same strength located at the image point with axis in the image normal direction. Thus a foil traveling beneath a free surface at infinite Froude number is represented by a foil and its image, equally loaded.

The kernel function for this problem representing the upwash normal to the foil at the point x, y, z , due to this doublet pair, is given by

$$K(x-z, y-\eta, z-f) = \lim_{z \rightarrow z(\eta)} \left\{ \frac{1}{4\pi} \frac{z}{\partial n(\eta, z)} \left[\frac{z}{\partial n(\eta, f)} \int_{-\infty}^{x-z} \frac{e^{ik(\lambda-(x-z))}}{R(\lambda, z-f)} d\lambda \right. \right. \\ \left. \left. + \frac{z}{\partial n'(\eta, f)} \int_{-\infty}^{x-z} \frac{e^{ik(\lambda-(x-z))}}{R(\lambda, z+f)} d\lambda \right] \right\} \quad (1.30)$$

For completeness, the final expression for this kernel function is given in Appendix 11. The expression for the kernel function is singular only at the line $y = \eta, z = f$ on the foil; the singular behavior of this kernel function is the same as that of the kernel function for a

nonplanar surface in an infinite fluid. The numerical integration can be handled by the same technique as those developed by Watkins (Ref. (7)) for the planar wing in an infinite fluid.

1.4 The Singularity in the Kernel Function

The kernel functions in equations (1.19), (1.25) and (1.30) become singular on the line $y = \eta$ $z(y) = \int (\eta)$ on the surface S. This is, of course, a familiar situation and the solution to the apparent problem is to find the proper definition of the improper integral. A full treatment of improper integrals which appear in two-dimensional theory was given by Mangler, Ref. (11). Mangler gives definitions for improper integrals which arise when the limit of a potential function is taken. For example, the Cauchy principal value integral is the limit of the following potential function.

$$\begin{aligned}
 g(t) &= \lim_{n \rightarrow 0} \int_a^b \frac{f(\tau)(t-\tau) d\tau}{(t-\tau)^2 + n^2} = \int_a^b \frac{f(\tau) d\tau}{(t-\tau)} \\
 &= \lim_{\epsilon \rightarrow 0} \left\{ \int_a^{t-\epsilon} \frac{f(\tau) d\tau}{(t-\tau)} + \int_{t+\epsilon}^b \frac{f(\tau) d\tau}{(t-\tau)} \right\} \quad (1.31)
 \end{aligned}$$

The function $\frac{t-\tau}{(t-\tau)^2+n^2}$ is a solution of Laplace's equation. Taking the t derivative of (1.31) defines the improper integral

$$g'(t) = \lim_{n \rightarrow 0} \left\{ \int_a^b \frac{f(\tau) d\tau}{(t-\tau)^2+n^2} \left(1 - \frac{2(t-\tau)^2}{(t-\tau)^2+n^2} \right) \right\} \quad (1.32)$$

Mangler shows that the proper definition of this integral is

$$g'(t) = \int_a^b \frac{f(\tau) d\tau}{(t-\tau)^2} = \lim_{\epsilon \rightarrow 0} \left\{ \int_a^{t-\epsilon} \frac{f(\tau) d\tau}{(t-\tau)^2} + \int_{t+\epsilon}^b \frac{f(\tau) d\tau}{(t-\tau)^2} - \frac{2f(t)}{\epsilon} \right\} \quad (1.33)$$

In order to apply Mangler's results which are valid for functions which satisfy the two-dimensional Laplace's equation, we must show that as we approach the singularity, the flow becomes a locally two-dimensional potential flow in the cross flow plane.

We isolate the region near the line $y = \eta$, $z = \zeta$

by a strip σ of width 2ϵ , along the chord. In this region we express the kernel function in coordinates normal and tangential to the surface at that point.

(See fig. 1.2)

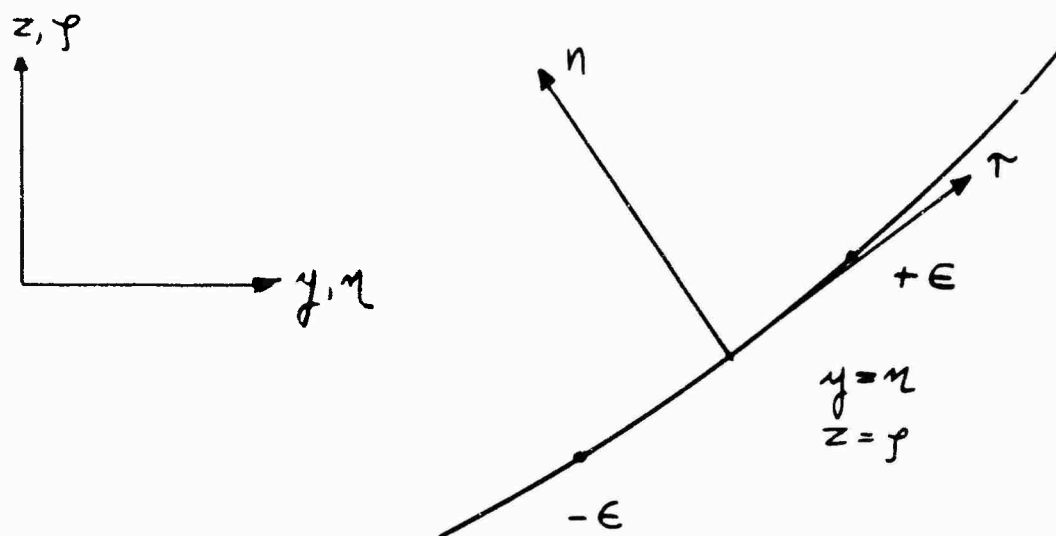


Figure 1.2 The Neighborhood of the Singular Point.

For ϵ small compared to the radius of curvature of the surface the kernel function is approximately

$$\mathcal{K} = -\frac{1}{4\pi} \frac{\partial^2}{\partial n^2} \int_{-\infty}^{\infty} \frac{e^{i k A - (x-3)\lambda}}{\sqrt{\lambda^2 + n^2 + \epsilon^2}} d\lambda \quad (1.34)$$

For small n and ϵ , equation (1.34) can be written

$$\begin{aligned}
 \chi(x-z, \eta, \epsilon) &= -\frac{e^{-ik(x-z)}}{4\pi} \left(1 + \frac{(x-z)}{|x-z|}\right) \left(\frac{1}{\eta^2 + \epsilon^2} - \frac{2\eta z}{(\eta^2 + \epsilon^2)^2}\right) \\
 &= \bar{K}(x-z) \left(\frac{1}{\eta^2 + \tau^2} - \frac{2\eta z}{(\eta^2 + \tau^2)^2}\right) \quad (1.35)
 \end{aligned}$$

(See Appendix 11).

Other singularities are present but are of lower order.

The upwash boundary condition is expressed as the limit of the normal velocity as the control point approaches the surface.

$$V_n(x, y, z(y)) = \lim_{\epsilon \rightarrow 0} \left[\iint_{S-\sigma} \Delta p(\xi, \eta, \rho(\eta)) \chi(x-z, y-\eta, z(y)-\rho(\eta)) dS' \right] \quad (1.36)$$

$$+ \lim_{\eta \rightarrow 0} \int_{-\epsilon}^{\epsilon} \left(\frac{1}{\eta^2 + \tau^2} - \frac{2\eta z}{(\eta^2 + \tau^2)^2}\right) d\tau \int \Delta p(\xi, \eta) \bar{K}(x-z) d\xi$$

In the narrow region σ , the pressure jump $\Delta p(\xi, \eta, \rho(\eta))$ can be expressed by the first term in the Taylor series.

$$\Delta p(\xi, \eta) = \Delta p(\xi, y) + O(\epsilon) \quad (1.37)$$

The form of equation (1.36) shows that as we approach the line $y = \eta$, $z = f$, the kernel function becomes a two-dimensional potential function in the cross flow direction.

The integral of this function over \mathcal{T} and the limit as $n \rightarrow 0$ has been shown by Mangler to be properly defined by equation (1.33). Thus in three-dimensional potential flow, the singularity of the kernel function for the upwash due to a pressure doublet is properly handled as a Mangler integral. The standard notation for this integral is

$$\begin{aligned}
 V_n(x, y, z(y)) &= \iint_{\mathcal{S}} K(x-z, y-\eta, z(y)-f(\eta)) \Delta p \, d\mathcal{S}' \\
 &= \lim_{\epsilon \rightarrow 0} \left\{ \iint_{\mathcal{S}-\sigma} K(x-z, y-\eta, z(y)-f(\eta)) \Delta p \, d\mathcal{S}' \right. \\
 &\quad \left. - \frac{2}{\epsilon} \int \Delta p(z, y) \bar{K}(x-z) \, dz \right\} \quad (1.38)
 \end{aligned}$$

1.5 Numerical Method for a Nonplanar Fully Wetted Lifting Surface.

The integral equation for a nonplanar lifting surface (1.38) is solved by essentially the method developed by Watkins et al. Ref. (7), for the planar wing. The unknown load distribution $\Delta p(z, \eta, f(\eta))$ on the surface is represented by a series of assumed modes with unknown coefficients. These coefficients are determined by satisfying the upwash velocity, equation (1.38), at control points on the surface.

$$V_n(x_k, y_k, z_k) = \sum b_i \int \Delta p_i \mathcal{K}(x_k - z, y_k - \eta, z_k - f(\eta)) dS \quad (1.39)$$

where x_k, y_k, z_k are coordinates of the kth point and

$\Delta p_i(z, \eta, f(\eta))$ is the ith assumed mode.

The integrals in equation (1.39) are evaluated numerically by Gaussian quadrature except for a thin strip of width 2ϵ about the line $y = \eta, z = f$ on the surface. If the width 2ϵ is small compared to the radius of curvature of the surface at this point, the method developed by Watkins to account for the singularity can be applied directly. The neighborhood of the point $y = \eta, z = f$ is shown in figure 1.2. We define a coordinate τ to be arc length measure from $y = \eta, z = f$. The result of the integrations in this strip which are done by Gaussian quadrature

is expanded in powers of S .

(1.40)

$$\text{then } \int_{LE}^{\tau_c} \Delta p_i \tau^2 K(x-z, \tau) d\zeta = \sum_{m=0}^M C_{i,m} \tau^m$$

$$v_{ki} = \iint_{S=0} \Delta p_i K dS + \int_{-e}^e \sum_{m=0}^M \frac{C_{i,m}}{\tau^2} \tau^m d\zeta \quad (1.41)$$

If the surface is symmetric in y and if the upwash velocity is purely symmetric or purely antisymmetric in y , the function $\Delta p(\zeta, \eta, f(\eta))$ will be symmetric or antisymmetric in η . The boundary condition in this case need be satisfied at control points on only half of the surface.

The assumed load series used by Watkins for a plane wing is

$$\Delta p(\zeta, \eta) = \sum_0^M \sum_0^N b_{n+(m-1)N} f_m(\eta) l_n(\zeta) \quad (1.42)$$

The surface is located such that the root semichord is between $\zeta = -1$, the leading edge, and $\zeta = +1$, the trailing edge.

The ξ functions are chosen in the following way.

Let

$$\xi = -b(\eta) \cos \theta + \xi_{LE}(\eta) \quad (1.43)$$

where $b(\eta)$ is the semichord at span η and $\xi_{LE}(\eta)$ is the leading edge coordinate at span η .

$$\rho_c(\xi) = \cot(\theta(\xi)/2) \quad (1.44)$$

$$\rho_n(\xi) = \frac{4}{2^{2n}} \sin(n\theta(\xi))$$

The $\rho_n(\xi)$ functions satisfy the Kutta condition at the trailing edge and the $\rho_0(\xi)$ function has a square root singularity at the leading edge. Analytical results for a flat plate in two-dimensional flow, and for a wing of circular plan form in three dimensions, show a square root singularity at the leading edge.

The $f_n(\eta)$ functions for symmetric upwash are

$$f_n(\eta) = (\eta/s)^{2n} \sqrt{1 - (\eta/s)^2} \quad (1.45)$$

The $f_n(\eta)$ functions for antisymmetric upwash are

$$f_n(\eta) = (\eta/s)^{2n+1} \sqrt{1 - (\eta/s)^2} \quad (1.46)$$

where s is the semispan. The $f_n(\eta)$ functions satisfy

the condition that the lift drops to zero at the wing tips. They also are the functions used in lifting line theory. In general, one should pick a set of functions to have properties as close as possible to the actual lift distribution. In this case, control point location is less critical and convergence is possible with fewer modes.

For a nonplanar surface, we could use this set of functions or replace the spanwise functions with a set more appropriate to a particular configuration. For surface piercing foils, it is not likely that the lift drops to zero at the water surface with infinite slope. For intersecting surfaces the load does not drop to zero at the corner and there is the additional constraint that the sum of the pressure jumps at the intersection is zero.

The result of these techniques give a set of complex linear algebraic equations for the unknown coefficients of the Δp modes.

$$\begin{aligned} \{v_k\} &= \left[v_{ki} \right] \{b_i\} \\ \{b_i\} &= \left[v_{ki} \right]^{-1} \{v_k\} \end{aligned} \quad (1.47)$$

Once the b_i 's have been found, the pressure jump distribution on the surface is known. From this, force and moment coefficients for the configuration may be calculated.

The numerical technique has been programmed for the IBM 7090. In practice, for simple configurations, calculations with 9, 16, and 25 control points have given good results. Time required for a calculation is under five minutes.

As an example of the method, calculations were done to compare with the experiments of Abramson and Ransleben, Ref. (12). For these, the unsteady lift and moment coefficients at several chordwise sections on the span of an aspect ratio 5 foil in bending and torsion oscillations were measured. Fig. 1.3 to 1.7 show numerical results for unsteady lift coefficient, magnitude and phase, along the span due to bending at reduced frequencies $K = .6, .8, 1.2, 2.0$. These calculations were carried out with 9, 16 and 25 control points. Results are in fair agreement at low reduced frequency; agreement is poor at higher reduced frequency.

This is perhaps due to a failure of the Kutta condition at high reduced frequencies. This is discussed by Ashley, Widnall and Landahl in Ref. (9) and some empirical modifications to the numerical method are suggested. Calculations were also performed for a planar wing below the free surface. These results were presented in Ref. (8).

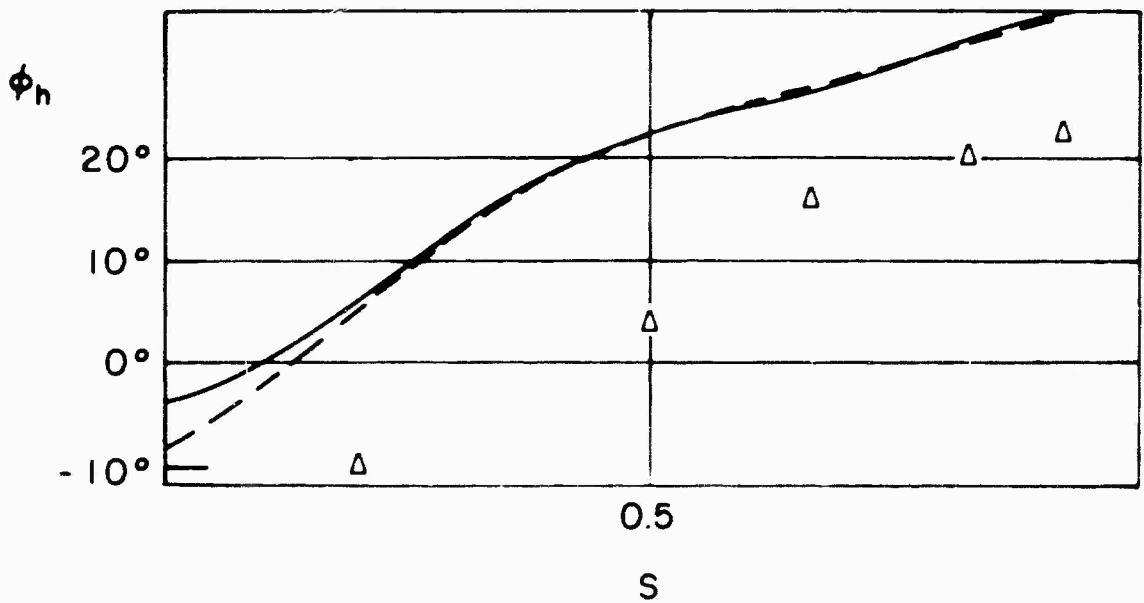
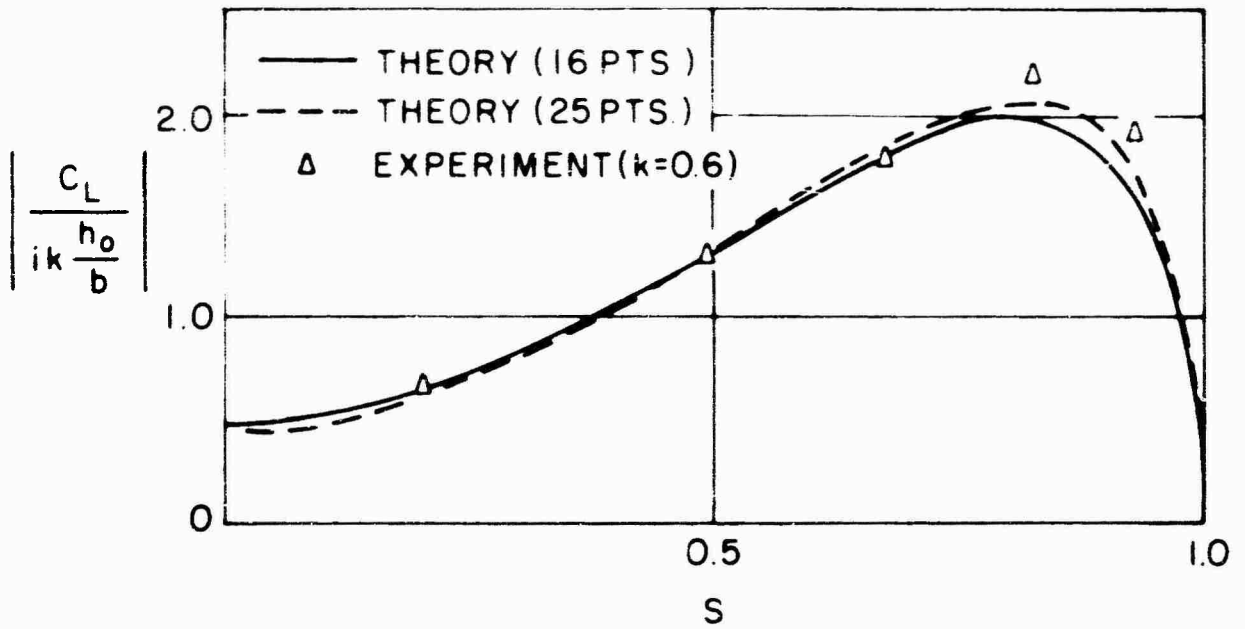


FIG. 13 COMPARISON WITH EXPERIMENT - SPANWISE DISTRIBUTION OF LIFT DUE TO BENDING (k=0.6)

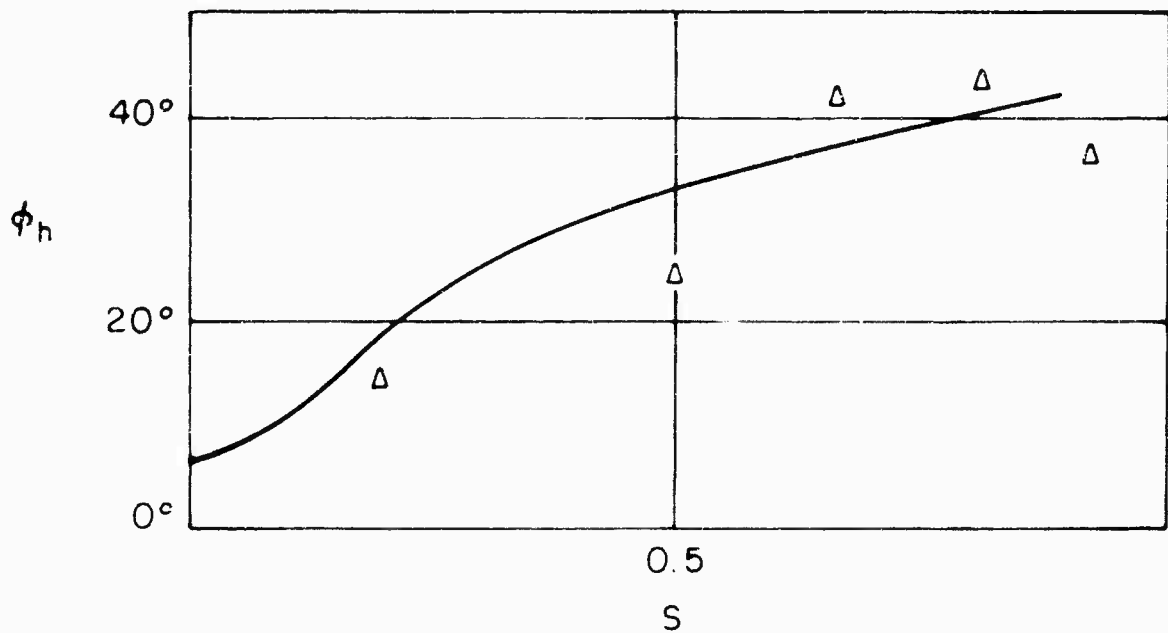
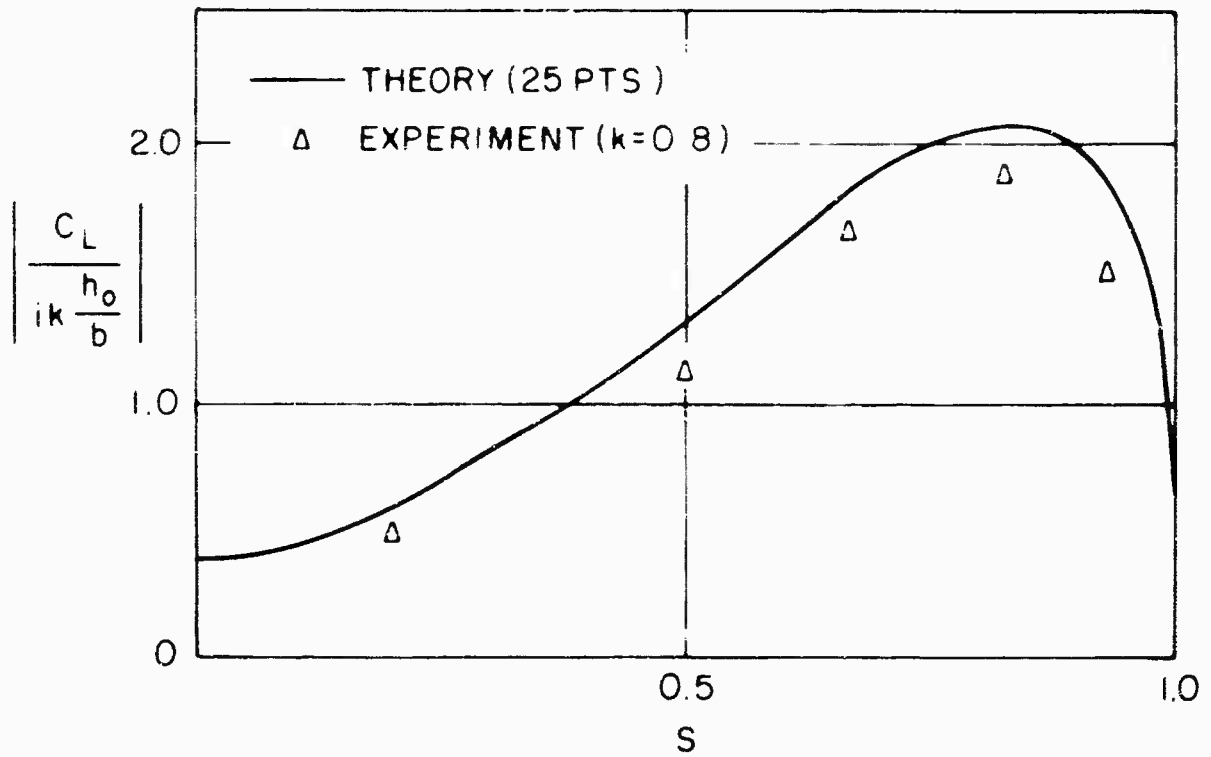


FIG 1.4 COMPARISON WITH EXPERIMENT - SPANWISE DISTRIBUTION OF LIFT DUE TO BENDING (k=0.8)

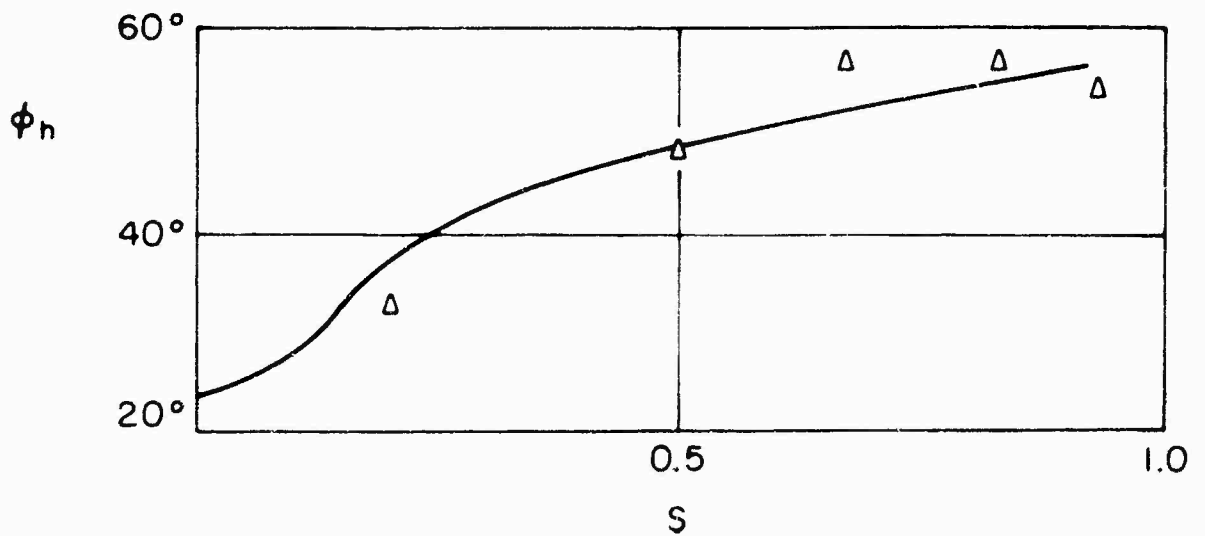
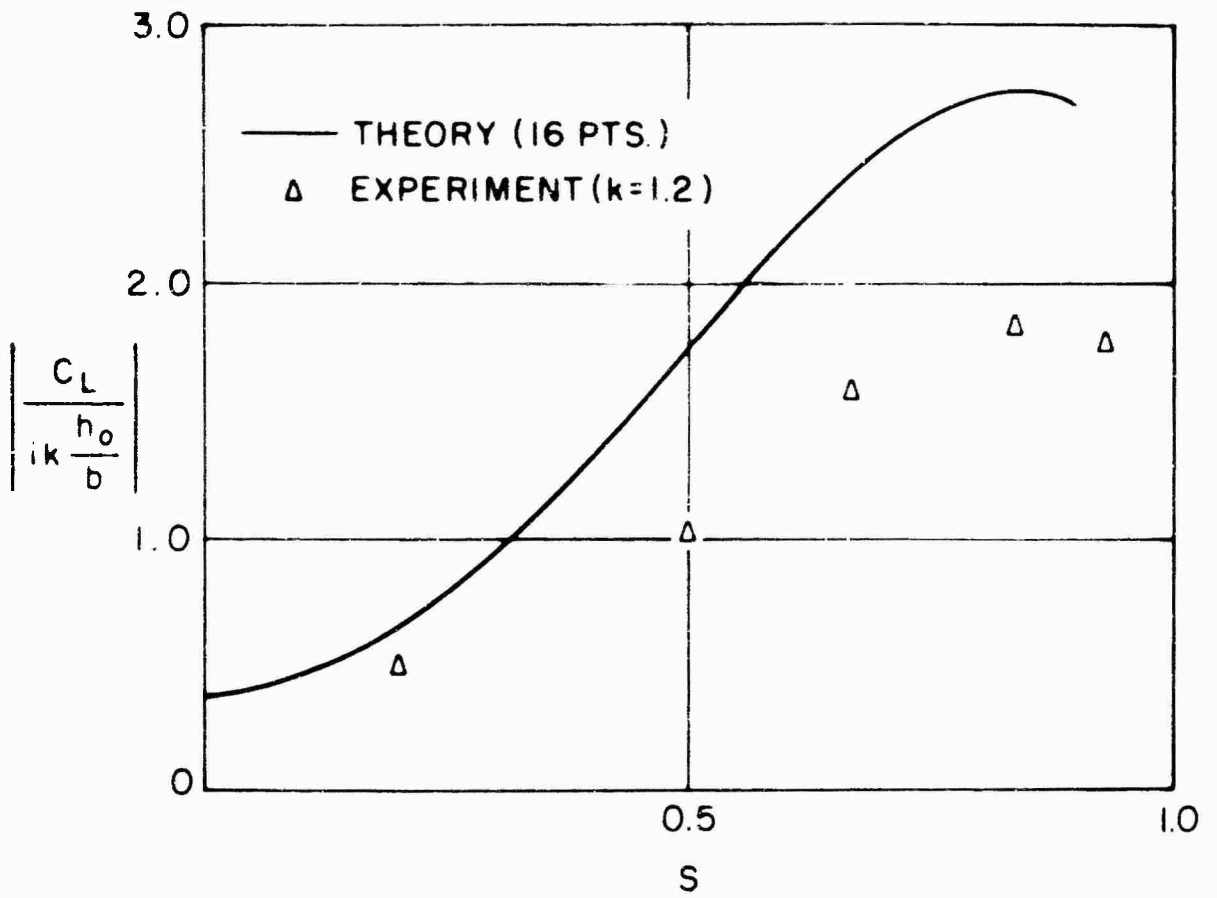


FIG 15 COMPARISON WITH EXPERIMENT - SPANWISE DISTRIBUTION OF LIFT DUE TO BENDING (k=1.2)

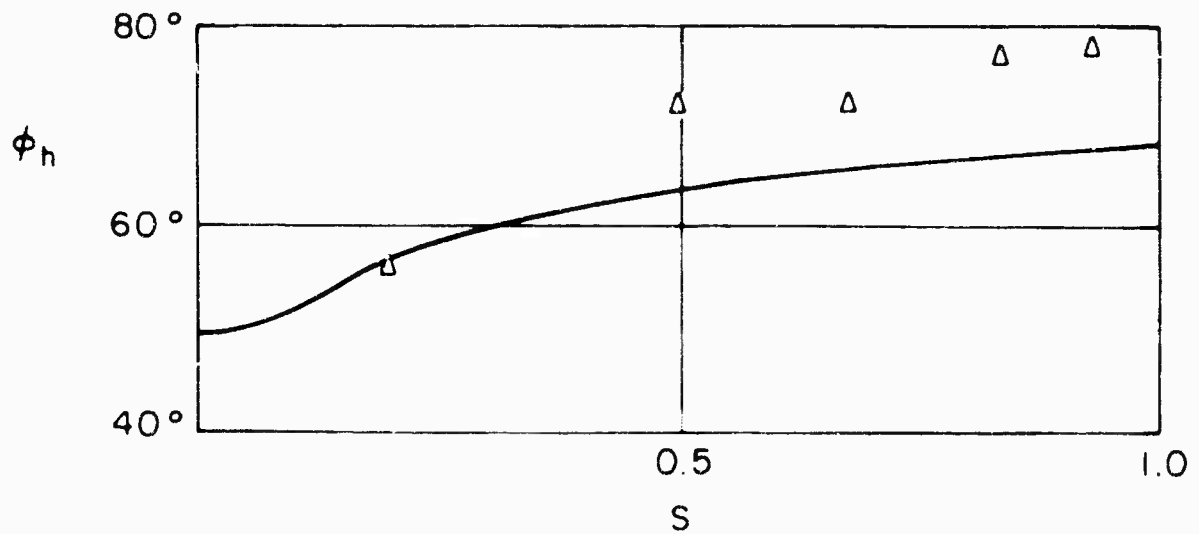
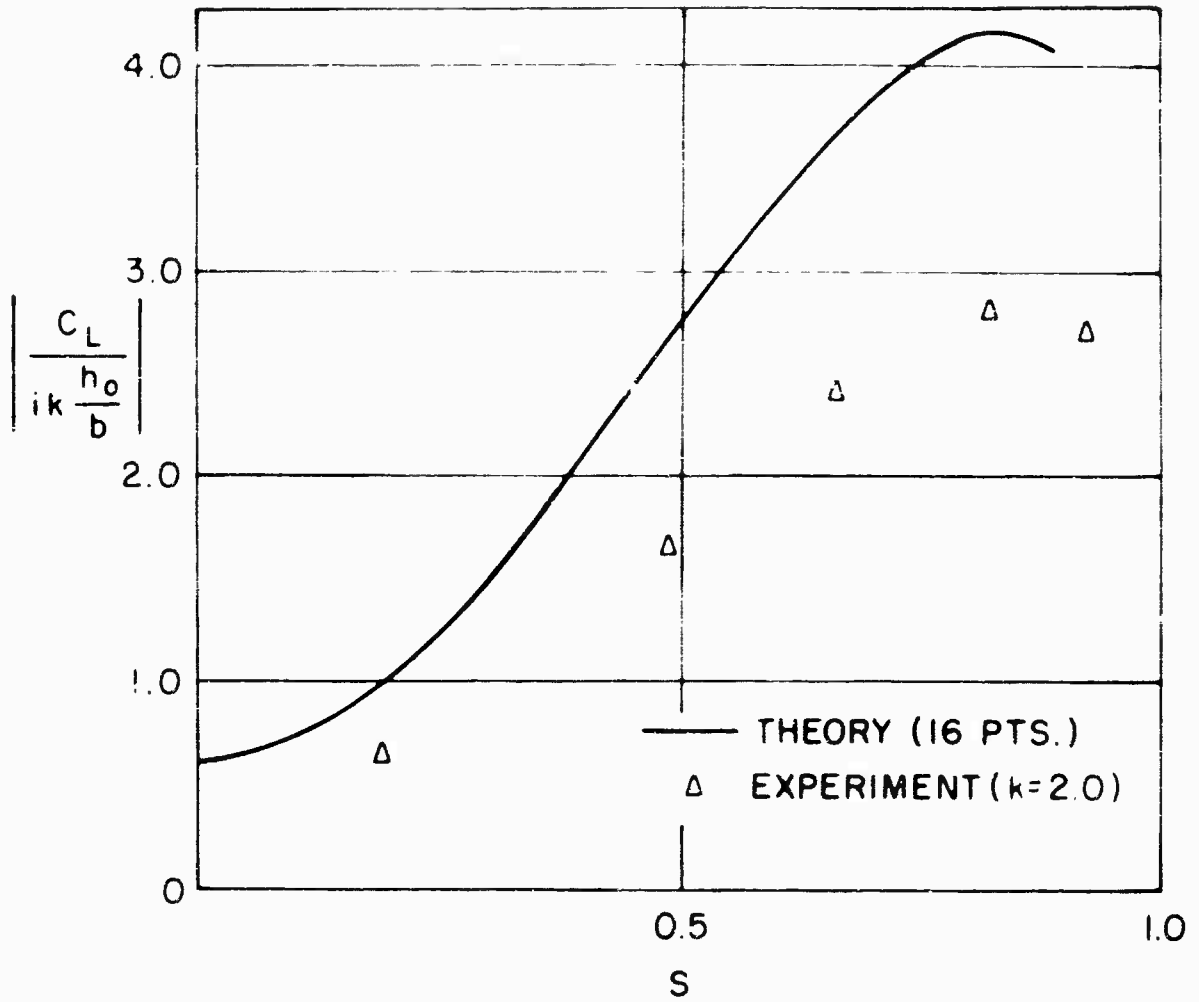


FIG. 1.6 COMPARISON WITH EXPERIMENT - SPANWISE DISTRIBUTION OF LIFT DUE TO BENDING ($k = 2.0$)

CHAPTER II

THE EFFECT OF GRAVITY WAVES ON THE UNSTEADY LIFT AND
MOMENT ON AN OSCILLATING HYDROFOIL2.1 Introduction

An intriguing question in the study of unsteady hydrofoil motions is whether the gravity waves induced by the motion influence the loading to any great extent. To answer this question we formulate the "exact linearized" integral equation relating the loading on an oscillating foil near the free surface to the upwash on the foil. In this problem, we represent the loading by a distribution of singularities on the foil surface which, in addition to producing a unit lift at a point, have a perturbation pressure field which satisfies the free surface boundary condition. The integral equation will then be solved by a method of assumed modes similar to that described in Chapter I.

We locate our coordinate system so that the mean position of the free surface is the x,y plane at $z = 0$. The free stream velocity is in the positive x direction. As seen in this coordinate system, the free surface will take some shape $\psi = \psi(x,y,t)$. The boundary condition on the free surface is that the perturbation pressure is equal to zero. (See ref. (14)).

The linearized Bernoulli equation for an incompressible irrotational flow in a gravity field is

$$\frac{\partial \phi}{\partial t} + \frac{\partial \phi}{\partial x} + \hat{p} + \frac{z}{F^2} = 0 \quad (2.1)$$

where the variables have been nondimensionalized with respect to free stream velocity U , density ρ , and root semichord b_0 .

F is the Froude number ($F = U/\sqrt{g b_0}$)

ϕ is the perturbation velocity potential

\hat{p} is the perturbation pressure

Applied at the free surface $\checkmark (x, y, t)$ this equation becomes

$$\frac{\partial \phi}{\partial t} + \frac{\partial \phi}{\partial x} + \frac{v(x, y, t)}{F^2} = 0 \quad (2.2)$$

The vertical velocity of a fluid particle on the free surface is related to the velocity potential by

$$\frac{\partial v}{\partial t} + \frac{\partial v}{\partial x} = \frac{\partial \phi}{\partial z} \quad (2.3)$$

A combination of equation (2.2) and (2.3) gives the free-surface boundary condition

$$\left(\frac{\partial}{\partial t} + \frac{\partial}{\partial x} \right)^2 \phi + \frac{1}{F^2} \frac{\partial \phi}{\partial z} = 0 \quad (2.4)$$

In the linearized problem, this boundary condition is applied on the mean position of the free surface, $z = 0$.

The same boundary condition must also be satisfied by the perturbation pressure.

$$\left(\frac{\partial}{\partial t} + \frac{\partial}{\partial x} \right) \hat{p} + \frac{1}{F^2} \frac{\partial \hat{p}}{\partial z} = 0 \quad @ z=0 \quad (2.5)$$

For simple harmonic motion with reduced frequency k

$$\hat{p} = p e^{ikt} \quad (2.6)$$

The complex amplitude of \hat{F} satisfies

$$\left(ik + \frac{\partial}{\partial x}\right)^2 P + \frac{\partial P}{\partial z} \frac{1}{F^2} z = 0 \quad \text{at } z = 0 \quad (2.7)$$

If the Froude number is infinite, this boundary condition reduces to zero pressure perturbation on the free surface. As was discussed in Chapter I, the singularity which causes a unit lift at a point and causes no perturbation pressure at $z = 0$, is a pressure doublet plus its image.

To find the singularity which causes a unit lift at a point on the foil and in addition produces a pressure field which satisfies the full free surface boundary condition is more complicated. For two-dimensional flow, analytical expressions for the kernel function can be found using Fourier transform techniques. The problem in three dimensions can be reduced to a single integral which could be done numerically.

When the upwash on the foil due to these singularities has been found, the problem may be expressed as

$$V(x, y) = \iint_{\Sigma} \Delta p(z, \eta) K(x-z, y-\eta) dz d\eta \quad (2.8)$$

where the integration is over the surface of the foil. All effects due to the free surface are contained in the kernel function.

2.2 The Kernel Function for Two Dimensional Flow at Arbitrary Froude Number

The complex amplitude of the perturbation pressure fields for a lifting element at $z = -d$ satisfies Laplaces

equation (2.9) with boundary conditions (2.10) - (2.13)

$$\nabla^2 p = 0 \quad (2.9)$$

$$(ik + \frac{\partial}{\partial x})^2 p + \frac{1}{F^2} \frac{\partial p}{\partial z} = 0 \quad @ z=0 \quad (2.10)$$

$$p(x; d^-) - p(x, -d^+) = \delta(x-s) \quad (2.11)$$

$$\frac{\partial p}{\partial x}(x, -d^-) - \frac{\partial p}{\partial x}(x, -d^+) = 0 \quad (2.12)$$

$$p(x, -\infty) = 0 \quad (2.13)$$

The complex amplitude of the upwash velocity due to this pressure field is given by

$$\chi(x-s, -d) = \frac{\partial \phi}{\partial z}(x-s; d) = \lim_{z \rightarrow -d} \left\{ -\frac{\partial}{\partial z} \int_{-\infty}^{x-s} p(\lambda) e^{i\kappa(\lambda - (x-s))} d\lambda \right\} \quad (2.14)$$

In addition to these conditions, we must impose a radiation condition requiring that all waves we consider have been generated by the motion of the foil. This may be done by letting the reduced frequency k have an infinitesimal negative imaginary part so that at time $t = -\infty$, there was no motion.

The derivation of the kernel function is similar to that of ref. (8). We apply Fourier transforms in x according to the definitions

$$p(x, z) = \frac{1}{\sqrt{2\pi}} \int_{-\infty}^{\infty} \mathcal{P}(s, z) e^{isx} ds \quad (2.15)$$

$$\mathcal{P}(s, z) = \frac{1}{\sqrt{2\pi}} \int_{-\infty}^{\infty} p(x, z) e^{-isx} dx \quad (2.16)$$

$$f(x, z) = \frac{1}{\sqrt{2\pi}} \int_{-\infty}^{\infty} \Phi(s, z) e^{isx} ds \quad (2.17)$$

$$\Phi(s, z) = \frac{1}{\sqrt{2\pi}} \int_{-\infty}^{\infty} \varphi(x, z) e^{-isx} dx \quad (2.18)$$

Equations (2.8) to (2.13), in the transform variables and become

$$\frac{d^2 \mathcal{P}}{dz^2} - s^2 \mathcal{P} = 0 \quad (2.19)$$

$$-(k+s)^2 \mathcal{P} + \frac{1}{F^2} \frac{d\mathcal{P}}{dz} = 0 \quad \text{at } z=0 \quad (2.20)$$

$$\mathcal{P}^-(s, -d) - \mathcal{P}^+(s, -d) = \frac{e^{-isd}}{\sqrt{2\pi}} \quad (2.21)$$

$$\frac{d\mathcal{P}^-}{dz}(s, -d) - \frac{d\mathcal{P}^+}{dz}(s, -d) = 0 \quad (2.22)$$

$$\mathcal{P}^-(s, -\infty) = 0 \quad (2.23)$$

$$\frac{d\Phi}{dz} = \frac{i}{(k+s)} \frac{d\mathcal{P}}{dz} \quad (2.24)$$

where \mathcal{P}^- is the solution for $z < -d$ and \mathcal{P}^+ is the solution for $z > -d$.

The solutions to equation (2.12) are

$$\mathcal{P}^+ = A^+ e^{1s|z} + B^+ e^{-1s|z} \quad (2.25)$$

$$\mathcal{P}^- = A^- e^{1s|z} + B^- e^{-1s|z} \quad (2.26)$$

Condition (2.23) requires $B^- = 0$. The functions $A^+ B^+ A^-$ are found from equation (2.20 - 2.22). The resulting expressions for \mathcal{L}^+ and \mathcal{L}^- are

$$\mathcal{L}^+ = -\frac{1}{2\sqrt{2\pi}} e^{-(z+d)|s|} e^{-is\beta} + \frac{1}{2\sqrt{2\pi}} e^{(z-d)|s|} e^{-is\beta} \left(\frac{F^2(s+k)^2 + |s|}{F^2(s+k)^2 - |s|} \right) \quad (2.27)$$

$$\mathcal{L}^- = \frac{1}{2\sqrt{2\pi}} e^{(z+d)|s|} e^{-is\beta} + \frac{1}{2\sqrt{2\pi}} e^{(z-d)|s|} e^{-is\beta} \left(\frac{F^2(s+k)^2 + |s|}{F^2(s+k)^2 - |s|} \right) \quad (2.28)$$

The kernel function can be found from either (2.27) or (2.28) by using equation (2.24) and (2.1')

$$K(x-\beta, -d) = \lim_{z \rightarrow -d^+} \left\{ \frac{1}{\sqrt{2\pi}} \int_{-\infty}^{\infty} \frac{1}{k+s} \left(\frac{dP^+}{dz} \right) e^{isx} ds \right\} \quad (2.29)$$

or

$$K(x-\beta, -d) = \lim_{z \rightarrow -d^-} \left\{ \frac{1}{\sqrt{2\pi}} \int_{-\infty}^{\infty} \frac{i}{k+s} \left(\frac{dP^-}{dz} \right) e^{isx} ds \right\} \quad (2.30)$$

The first term in equations (2.27) and (2.28) gives the kernel function for a pressure doublet in an infinite fluid. Thus

$$\mathcal{K}(x-\beta, -d) = \frac{1}{4\pi} \lim_{\epsilon \rightarrow 0} \left\{ \int_{-\infty}^{\infty} \frac{i|s|}{s+k} e^{-\epsilon|s| + is(x-\beta)} ds \right\} \quad (2.31)$$

We use the fact that k has a small negative imaginary part to move the pole off the axis of integration. Hence there results

$$\mathcal{K}^{\infty}(x-\beta, -d) = \lim_{\epsilon \rightarrow 0} \left\{ -\frac{1}{2\pi} \frac{x-\beta}{(x-\beta)^2 + \epsilon^2} + \frac{ik}{2\pi} e^{-ik(x-\beta)} \left[Ei(ik(x-\beta)) + \frac{\pi i}{2} \left(1 + \frac{x-\beta}{|x-\beta|} \right) \right] \right\} \quad (2.32)$$

where

$$E_i(w) = \int_{-\infty}^w \frac{e^{-t}}{t} dt \quad (2.33)$$

is the complex exponential integral with branch line along the positive real axis.

The proper definition of an integral over the generalized function $\lim_{\epsilon \rightarrow 0} \left\{ \frac{x-3}{(x-3)^2 + \epsilon^2} \right\}$ is the Cauchy principal value.

$$\lim_{\epsilon \rightarrow 0} \left\{ \int_a^b \frac{(x-3) f(z) dz}{(x-3)^2 + \epsilon^2} \right\} = \int_a^b \frac{f(z)}{(x-3)} dz \quad (2.34)$$

The first term in equation (2.32) contains the strongest singularity in the kernel function. The second term has only a logarithmic singularity and the additional terms due to free surface effects are not singular.

For infinite Froude number, the kernel function is just

$$K_{F=\infty} = \frac{1}{4\pi} \left(\lim_{\epsilon \rightarrow 0} \left\{ \int_{-\infty}^{\infty} \frac{i|s|}{s+k} e^{-\epsilon|s| + i s(x-3)} ds \right\} + \int_{-\infty}^{\infty} \frac{i|s|}{s+k} e^{-2d|s| + i s(x-3)} ds \right) \quad (2.35)$$

which gives

$$K_{F=\infty} = -\frac{1}{2\pi} \lim_{\epsilon \rightarrow 0} \left\{ \frac{x-3}{(x-3)^2 + \epsilon^2} \right\} - \frac{1}{2\pi} \left(\frac{x-3}{(x-3)^2 + (2d)^2} \right) + \frac{ik}{4\pi} e^{\delta_0^*} E_i(\delta_0^*) \\ + \frac{ik}{2\pi} e^{-ik(x-3)} \left[E_i(ik(x-3)) + \frac{\pi i}{2} \left(1 + \frac{(x-3)}{ix-3d} \right) \right] + \frac{ik}{4\pi} e^{-\delta_0} \left[E_i(\delta_0) + \pi i \left(1 + \frac{(x-3)}{(x-3)} \right) \right] \quad (2.36)$$

where

$$\bar{f}_0 = k(2d + i(x-3)) \quad (2.37)$$

$$\bar{f}_0^* = k(2d - i(x-3)) \quad (2.38)$$

It is interesting to note the asymptotic form of the kernel function for large values of $x - 3$. The asymptotic representation of the complex exponential integral is

$$E_i(w) \sim \frac{e^{-w}}{w} \quad (2.39)$$

The lowest order terms in equation (2.34) are thus

$$K \sim \frac{ik}{2\pi} \left[i\frac{\pi}{2} \left(1 + \frac{|x-3|}{(x-3)} \right) \right] e^{-iK(x-3)} \quad (2.40)$$

$$+ \frac{ik}{2\pi} \left[i\frac{\pi}{2} \left(1 + \frac{|x-3|}{(x-3)} \right) \right] e^{-2kd - iK(x-3)}$$

The behavior far downstream from the disturbance is that of a wave moving in the positive x direction with unit velocity.

$$K \propto \left(1 + \frac{(x-3)}{|x-3|} \right) e^{-ik(x-t)} \quad (2.41)$$

No wave exists upstream. This represents, of course, the shed wake vorticity, which is carried downstream by the free stream. Later on, we shall use these same ideas to find the gravity waves produced by the motion. At this point, we will note that the poles infinitesimally close to the axis of integration in eq. (2.33) give rise to waves which travel upstream or downstream. If the poles had been located at a finite distance μ from the real axis, the waves would be damped.

$$K \propto \left(1 + \frac{(x-3)}{|x-3|} \right) e^{-\mu(x-3)} = K(x-\epsilon) \quad (2.42)$$

The complete expression for the kernel for finite Froude number is

$$K(x-3, f) = K^\infty + K^F = \lim_{\epsilon \rightarrow 0} \left\{ \frac{1}{4\pi} \int_{-\infty}^{\infty} \frac{e^{i s(x-3) - \epsilon |s|}}{(s+k)} \right. \\ \left. + \frac{i}{4\pi} \int_{-\infty}^{\infty} e^{\frac{i s(x-3) - 2d|s|}{|s|}} \left(\frac{F^2(s+k)^2 + |s|}{F^2(s+k)^2 - |s|} \right) ds \right\} \quad (2.43)$$

where K^∞ is the kernel function for a pressure doublet in an infinite fluid and K^F is the correction term due to free surface effects. This correction term may be expressed as

$$K^F = \frac{i}{4\pi} \left\{ - \int_{-\infty}^0 \frac{s ds}{(s+k)} \left(\frac{F^2(s+k)^2 - s}{F^2(s+k)^2 + s} \right) e^{2sd + i s(x-3)} \right. \\ \left. + \int_{-\infty}^0 \frac{s ds}{(s-k)} \left(\frac{F^2(s+k)^2 + s}{F^2(s-k)^2 + s} \right) e^{2sd - i s(x-3)} \right\} \quad (2.44)$$

The first integral has poles at

$$s_0 = -k \quad (2.45)$$

$$s_1 = -k \left(1 + \frac{1}{2f} + \frac{1}{2f} \sqrt{4f+1} \right) \quad (2.46)$$

$$s_2 = -k \left(1 + \frac{1}{2f} - \frac{1}{2f} \sqrt{4f+1} \right) \quad (2.47)$$

where $f = kF^2$. These are all located infinitesimally close to the real axis along the path of integration.

The second integral has poles at

$$\bar{s}_0 = k \quad (2.48)$$

$$s_3 = k \left(1 - \frac{1}{2f} + \frac{1}{2f} \sqrt{1-4f} \right) \quad (2.49)$$

$$s_4 = k \left(1 - \frac{1}{2f} - \frac{1}{2f} \sqrt{1 - 4f} \right) \quad (2.50)$$

The location of these poles depends on the value of f . Thus, for $f < \frac{1}{4}$, they are located infinitesimally close to the real positive axis. For $\frac{1}{4} < f < \frac{1}{2}$, they are complex conjugates in the second and third quadrants. In the case of $\frac{1}{2} < f$, they are complex conjugates in the first and fourth quadrants. These poles, and their significance for the gravity waves generated by the motion, have been discussed by Tan, Ref. (12), and Kaplan, Ref. (13) and (14).

A root locus diagram is shown in fig. 2.1 for constant F , and increasing k .

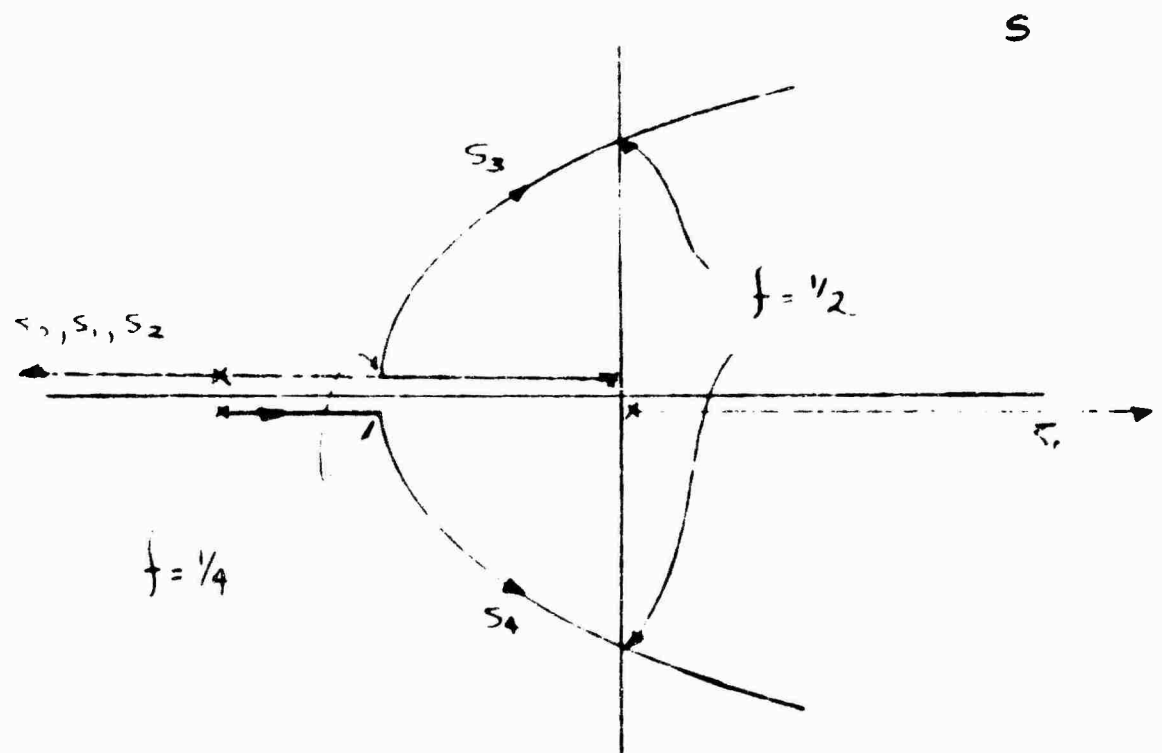


Fig. 2.1 Location of the poles of equation (2.44) for constant F , increasing k . ($f = kF^2$)

The integrands in equation (2.44) may be separated into partial fractions

$$\begin{aligned}
 K^F &= \frac{L}{4\pi} \int_{-\infty}^{\infty} \frac{|s|}{s} e^{-2|s|d + i s(x-3)} ds \\
 &+ \frac{L}{4\pi} \left\{ \int_{-\infty}^0 \left(\frac{-k}{(s+k)} + \frac{a_1}{s-s_1} + \frac{a_2}{s-s_2} \right) e^{2sd + i s(x-3)} ds \right. \\
 &\left. + \int_{-\infty}^0 \left(\frac{-k}{(s-k)} + \frac{a_3}{s-s_3} + \frac{a_4}{s-s_4} \right) e^{2sd - i s(x-3)} ds \right\}
 \end{aligned} \tag{2.51}$$

where

$$a_1 = k(1+f^{-1} + (3+f^{-1}))(4f+1)^{-1/2} \tag{2.52}$$

$$a_2 = k(1+f^{-1} - (3+f^{-1}))(4f+1)^{-1/2} \tag{2.53}$$

$$a_3 = k(1-f^{-1} - (3-f^{-1}))(1-4f)^{-1/2} \tag{2.54}$$

$$a_4 = k(1-f^{-1} - (3-f^{-1}))(1-4f)^{-1/2} \tag{2.55}$$

The first integral in equation (2.51) is the kernel function for a simple steady pressure doublet at the image point. The remaining integrals can be expressed as complex exponential integrals with or without a correction term depending on whether the path of integration of equation (2.51), after transformation into the exponential integral form, equation (2.33), crosses the branch line of this function.

This depends on the position of the poles in the complex plane which is a function of f . ($f = kF^2$)

For $f < 1/4$, the kernel function is

$$\begin{aligned}
 K^F = & \frac{1}{2\pi} \frac{(x-3)}{(x-3)^2 + 4d^2} - \frac{ik}{4\pi} e^{-\xi_0} \left[Ei(\xi_0) + \pi i \left(1 + \frac{(x-3)}{|x-3|} \right) \right] \\
 & + \frac{ia_1}{4\pi} e^{-\xi_1} \left[Ei(\xi_1) + \pi i \left(1 + \frac{x-3}{|x-3|} \right) \right] + \frac{ia_2}{4\pi} e^{-\xi_2} \left[Ei(\xi_2) + \pi i \left(1 + \frac{(x-3)}{|x-3|} \right) \right] \\
 & + \frac{ia_3}{4\pi} e^{-\xi_3} \left[Ei(\xi_3) + \pi i \left(1 - \frac{(x-3)}{|x-3|} \right) \right] + \frac{ia_4}{4\pi} e^{-\xi_4} \left[Ei(\xi_4) - \pi i \left(1 + \frac{(x-3)}{|x-3|} \right) \right] \\
 & - \frac{ik}{4\pi} e^{\xi_0^*} Ei(-\xi_0^*)
 \end{aligned} \tag{2.56}$$

where

$$\xi_0 = k(2d + i(x-3)) \tag{2.57}$$

$$\xi_1 = -s_1(2d + i(x-3)) \tag{2.58}$$

$$\xi_2 = -s_2(2d + i(x-3)) \tag{2.59}$$

$$\xi_3 = -s_3(2d - i(x-3)) \tag{2.60}$$

$$\xi_4 = -s_4(2d - i(x-3)) \tag{2.61}$$

For large values of $(x-3)$, the asymptotic form of the kernel for $f < 1/4$ is

$$\begin{aligned}
 K = & \frac{k}{4} e^{-2kd} \left[1 + \frac{(x-3)}{|x-3|} \right] e^{-ik(x-t)} - \frac{a_1}{4} e^{s_1 2d} \left[1 + \frac{(x-3)}{|x-3|} \right] e^{is_1(x + \frac{k}{s_1} t)} \\
 & - \frac{a_2}{4} e^{s_2 2d} \left[1 + \frac{(x-3)}{|x-3|} \right] e^{is_2(x + \frac{k}{s_2} t)} \\
 & - \frac{a_3}{4} e^{s_3 2d} \left[1 - \frac{(x-3)}{|x-3|} \right] e^{-is_3(x - \frac{k}{s_3} t)} \\
 & - \frac{a_4}{4} e^{s_4 2d} \left[1 + \frac{(x-3)}{|x-3|} \right] e^{-is_4(x - \frac{k}{s_4} t)}
 \end{aligned} \tag{2.62}$$

Since for $f < \frac{1}{4}$, s_1 to s_4 are real and negative, we can draw the conclusion that the disturbance produces four gravity waves, in addition to the wake. The s_1 and s_2 waves travel downstream behind the disturbance, the s_3 wave travels upstream ahead of the disturbance, and the s_4 wave travels upstream behind the disturbance.

In the limit as $f \rightarrow \frac{1}{4}$, the s_3 and s_4 waves have a group velocity which is equal to the velocity of the foil relative to the stationary fluid. (see Ref. 14) This is a singular point for the linearized problem, in some ways analogous to the Mach number unity problem for linearized compressible flow.

For $f > \frac{1}{4}$, the kernel function differs only in the contribution from the poles. Thus for $\frac{1}{4} < f < \frac{1}{2}$,

$$\begin{aligned}
 K^F = & \frac{(x-3)}{2\pi((x-3)^2 + 10^2)} - \frac{ik}{4\pi} e^{-\beta_0} \left[Ei(\beta_0) + \pi i \left(1 + \frac{(x-3)}{1x-3} \right) \right] \\
 & + \frac{ia_1}{4\pi} e^{-\beta_1} \left[Ei(\beta_1) + \pi i \left(1 + \frac{(x-3)}{1x-3} \right) \right] + \frac{ia_2}{4\pi} e^{-\beta_2} \left[Ei(\beta_2) + \pi i \left(1 + \frac{1x-3}{x-3} \right) \right] \\
 & + \frac{ia_3}{4\pi} e^{-\beta_3} \left[Ei(\beta_3) + \pi i \left(1 + \frac{I.P.(\beta_3)}{I.P.(\beta_3)} \right) \right] - \frac{ik}{4\pi} e^{\beta_0} Ei(\beta_0) \\
 & + \frac{ia_4}{4\pi} e^{-\beta_4} \left[Ei(\beta_4) - \pi i \left(1 - \frac{I.P.(\beta_4)}{I.P.(\beta_4)} \right) \right]
 \end{aligned}$$

(2.63)

whereas for $f > \frac{1}{2}$ the kernel function is

$$\begin{aligned}
 \chi^F = & -\frac{(x-z)}{2\pi((x-z)^2 + 4d^2)} - \frac{ik}{4\pi} e^{-\beta_0} \left[Ei(\beta_0) + \pi i \left(1 + \frac{|x-z|}{(x-z)} \right) \right] \\
 & + \frac{ia_1}{4\pi} e^{-\beta_1} \left[Ei(\beta_1) + \pi i \left(1 + \frac{(x-z)}{|x-z|} \right) \right] \\
 & + \frac{ia_2}{4\pi} e^{-\beta_2} \left[Ei(\beta_2) + \pi i \left(1 + \frac{(x-z)}{|x-z|} \right) \right] \\
 & + \frac{ia_3}{4\pi} e^{-\beta_3} Ei(\beta_3) + \frac{ia_4}{4\pi} e^{-\beta_4} Ei(\beta_4) \\
 & + \frac{ik}{4\pi} e^{\beta_0^*} Ei(\beta_0^*)
 \end{aligned}
 \tag{2.64}$$

The asymptotic form of the kernel function for $\frac{1}{4} < f$ shows that the gravity waves from the s_3 and s_4 poles are damped far from the origin. Only the gravity waves due to the s_1 and s_2 poles, plus the unsteady wake, extend downstream from the disturbance.

2.3 Numerical Solution and Results for Arbitrary Froude Number

The integral equation relating the complex amplitude of the upwash and the load distribution on a two-dimensional oscillating hydrofoil, traveling beneath a free surface is

$$v(x) = \int_{-1}^{+1} K(x-z) \Delta\rho(z) dz
 \tag{2.65}$$

where $K(x-z) = K^\infty + K^F$ as derived in section 2.2. As in the

three-dimensional case, the kernel function is the upwash at a point x due to an oscillating pressure doublet at a point ξ . This function contains the effects of the unsteady wake, the surface waves generated by the motion, and the depth of the foil below the free surface.

A numerical solution of this equation has been programmed for the IBM 7090. The method which was used involves a series of assumed modes, in a manner similar to that described in Chapter I. One assumes a series of pressure modes, each of which satisfies the Kutta condition, and solves for the coefficients of these modes from the known upwash distribution. Once the coefficients of the pressure modes are known, the unsteady lift and moment can easily be calculated.

The foil is located on the ξ axis from $\xi = +1$ to $\xi = -1$, the semichord thus being adopted as a reference length. The assumed lift functions are chosen as follows:

$$\Delta p(\xi) = b_0 \cot \theta/2 + \sum_{n=1}^N b_n \sin n\theta \quad (2.66)$$

$$\Delta f(\xi) = \sum_{n=0}^N b_n \ln(\theta(\xi)) \quad (2.67)$$

where

$$\xi = -\cos \theta \quad (2.68)$$

The b_n 's are the unknown complex coefficients. With this assumption for the lift distribution, equation (1.1) becomes

$$v(x) = \int_0^\pi \left(\sum_{n=0}^N b_n \ln(\theta) \right) K(x-\xi(\theta)) \sin \theta \, d\theta \quad (2.69)$$

Define a function

$$C_{in} = \int_0^\pi b_n \ln(\theta) K(x_i - \xi(\theta)) \sin \theta \, d\theta \quad (2.70)$$

In terms of the $C_{in}'s$, the integral equation becomes a complex matrix equation

$$\{v_i\} = [C_{in}] \{b_n\} \quad (2.71)$$

where v_1 is the known complex upwash evaluated at a preassigned set of control points x_1 . It would be possible to solve for N b_n 's by fitting the upwash at N points. Then $[C]$ would be a square matrix. Instead, the upwash is "fit" by a minimum mean-square error criterion at more points than the number of assumed modes. This device makes control-point location less critical.

Results of an analysis to choose the complex coefficients for a "best" fit have led to the following procedure: One writes a linear set of equations

$$\begin{matrix} 1 \times N \\ \{v_i\} \\ 1 \times M \end{matrix} = \begin{matrix} \\ [C_{in}] \\ M \times N \end{matrix} \begin{matrix} \\ \{b_n\} \\ \end{matrix} \quad (2.72)$$

where $M < N$.

Then premultiply both sides by the complex-conjugate transpose of $[C_{in}]$.

$$\begin{bmatrix} \overline{C_{in}} \end{bmatrix}^T \{v_i\} = \begin{bmatrix} \overline{C_{in}} \end{bmatrix}^T \begin{bmatrix} C_{in} \end{bmatrix} \{b_n\} \quad (2.73)$$

The result is an M th order set of linear equations for the M unknown complex coefficients. This procedure minimizes the dot product of the error and the conjugate of the error. This method is used in the program to fit the complex upwash $v(x)$ by

the sum of complex upwashes $C_{n(x)}$ due to the assumed lift modes.

In the present program, nineteen downwash points are chosen and a "best fit" is made with four or five pressure modes. When the complex coefficients have been found, unsteady lift and moment coefficients are computed by the familiar formulas

$$C_L = 2\pi (b_0 + b_1/2) \quad (2.74)$$

$$C_{M_{1/4}} = \pi/4 (b_2 - b_1) \quad (2.75)$$

The program for infinite depth reproduced the Theodorsen results, Ref. (1), to four significant figures.

Results for C_L and C_M for a two-dimensional hydrofoil oscillating in heave and pitch beneath a free surface are shown in Fig. 2.2. to 2.5.

Definitions of lift and moment coefficients are

$$C_{L_{hr}} + i C_{L_{hi}} = \frac{\text{Lift due to heave}}{\frac{\rho U^2}{2} i k h_0 c} \quad (2.76)$$

$$C_{M_{hr}} + i C_{M_{hi}} = \frac{\text{Moment due to heave}}{\frac{\rho U^2}{2} i k h_0 c^2} \quad (2.77)$$

where the nondimensional motion of the foil is

$$h(x,t) = h_0 e^{i k t} \quad (2.78)$$

and

$$C_{L_{pr}} + i C_{L_{pi}} = \frac{\text{Lift due to pitch}}{\frac{\rho U^2}{2} \alpha_0 c} \quad (2.79)$$

$$C_{M\alpha r} + i C_{M\alpha i} = \frac{\text{Moment due to pitch}}{\frac{\rho U^2}{2} \alpha \cdot c^2} \quad (2.80)$$

where the nondimensional motion of the foil is

$$h(x, t) = -\alpha_c \left(x + \frac{1}{2}\right) e^{ikt} \quad (2.81)$$

($x = \frac{1}{2}$ is the quarter chord.)

By these definitions, C_L has a quasi-steady value of 2π at infinite depth.

Results are shown for lift and moment coefficients vs. reduced frequency for various Froude numbers and depth below the free surface.

These results indicate that the coefficients predicted for Froude numbers of about 10 are equivalent to those predicted for infinite Froude numbers. Thus for hydrofoil operation in typical ranges of F , the effects of free surface waves are not significant.

The behavior of these coefficients near the singular point $kF^2 = 1/4$ is interesting from a mathematical point of view but seems to be of limited practical importance in problems of hydrofoil flutter.

2.4 The Kernel Function in Three Dimensions

To determine the form of the kernel function, we make use of Fourier transforms in the x and y direction. Definitions

of these transforms are

$$\Phi(x, y, z) = \frac{1}{2\pi} \iint_{-\infty}^{\infty} \bar{\Phi}(s, \beta, z; k) e^{isx + i\beta y} ds d\beta \quad (2.83)$$

$$\bar{\Phi}(s, \beta, z; k) = \frac{1}{2\pi} \iint_{-\infty}^{\infty} \Phi(x, y, z; k) e^{-isx - i\beta y} dx dy \quad (2.84)$$

$$P(x, y, z; k) = \frac{1}{2\pi} \iint_{-\infty}^{\infty} \bar{P}(s, \beta, z; k) e^{isx + i\beta y} ds d\beta \quad (2.85)$$

$$\bar{P}(s, \beta, z; k) = \frac{1}{2\pi} \iint_{-\infty}^{\infty} P(x, y, z; k) e^{-isx - i\beta y} dx dy \quad (2.86)$$

The relation between the Φ and P transforms is

$$\bar{\Phi} = \frac{i\bar{P}}{(s+k)} \quad (2.87)$$

Laplace's equation for Φ and P becomes an ordinary second-order differential equation for $\bar{\Phi}$ and \bar{P} , with z as the independent variable. The transform variables appear as parameters

$$\frac{d^2 \bar{P}}{dz^2} - (s^2 + \beta^2) \bar{P} = 0 \quad (2.88)$$

$$\frac{d^2 \bar{\Phi}}{dz^2} - (s^2 + \beta^2) \bar{\Phi} = 0 \quad (2.89)$$

The free surface boundary condition for \bar{P} is

$$-(k+s)^2 \bar{P} + \frac{1}{F^2} \frac{d\bar{P}}{dz} = 0 \quad @ z=0 \quad (2.90)$$

Also, as

$$z \rightarrow -\infty \quad \mathcal{P} \rightarrow 0 \quad (2.91)$$

The basic equations, as just derived, hold for general surfaces at arbitrary orientations below the free surface. To achieve clarity in presentation, we shall now restrict ourselves to lifting surfaces oriented parallel to the free surface.

We located the planar lifting surface at $z = -d$ below the free surface. The kernel function for this surface has the property that across $z = -d$, $P(x,y,z)$ experiences a jump of unit strength.

$$P(x,y,-d^-) - P(x,y,-d^+) = \delta(x-\xi, y-\eta) \quad (2.92)$$

The jump conditions on the transform of $P(x,y,z)$ are

$$\bar{\mathcal{P}}(\xi, \beta, -d^-) - \mathcal{P}^+(\xi, \beta, -d^+) = \frac{e^{-i\xi d - i\beta d}}{2\pi} \quad (2.93)$$

where $\bar{\mathcal{P}}$ is the Fourier transform for $z < -d$ and \mathcal{P}^+ is the Fourier transform for $z > -d$.

For a zero thickness lifting surface, the upwash is continuous across $z = -d$. This condition becomes a condition on $\mathcal{P}(\xi, \beta, z)$ of

$$\frac{d\bar{\mathcal{P}}}{dz}(\xi, \beta, -d^-) - \frac{d\mathcal{P}^+}{dz}(\xi, \beta, -d^+) = 0 \quad (2.94)$$

The two solutions to equation (2.80) are

$$\mathcal{P}^+ = A e^{-\sqrt{s^2 + \beta^2} z} + B e^{\sqrt{s^2 + \beta^2} z} \quad (2.95)$$

$$\mathcal{P}^- = C e^{\sqrt{s^2 + \beta^2} z} \quad (2.96)$$

To solve for A, B and C we apply the boundary conditions (2.90) at $z = 0$, and the jump conditions (2.93) and (2.94) at $z = -d$. In order to insure that $\mathcal{P}^- \rightarrow 0$, as $z \rightarrow -\infty$, the real part of the radical in \mathcal{P} must be taken as positive. Application of these conditions gives

$$\mathcal{P}^+ = - \frac{\exp(-i s \xi - i \beta \eta - \sqrt{s^2 + \beta^2} (z+d))}{4\pi} \quad (2.97)$$

$$+ \frac{\exp(-i s \xi - i \beta \eta + \sqrt{s^2 + \beta^2} (z-d))}{4\pi} \left[\frac{F^2 (s+k)^2 + \sqrt{s^2 + \beta^2}}{F^2 (s+k)^2 - \sqrt{s^2 + \beta^2}} \right]$$

$$\mathcal{P}^- = \frac{\exp(-i s \xi - i \beta \eta + \sqrt{s^2 + \beta^2} (z+d))}{4\pi}$$

$$+ \frac{\exp(-i s \xi - i \beta \eta + \sqrt{s^2 + \beta^2} (z-d))}{4\pi} \left[\frac{F^2 (s+k)^2 + \sqrt{s^2 + \beta^2}}{F^2 (s+k)^2 - \sqrt{s^2 + \beta^2}} \right]$$

(2.98)

For an oscillating pressure jump at $z = -d$ in an infinite fluid equation (2.97) reduces to:

$$\mathcal{P}^+ = - \frac{\exp(-i s \xi - i \beta \eta - \sqrt{s^2 + \beta^2} (z+d))}{4\pi} \quad (2.99)$$

$$\mathcal{P}^- = \frac{e^{-i\zeta z - i\beta x}}{4\pi} e^{\sqrt{s^2 + \beta^2}(z+d)} \quad (2.100)$$

For an oscillating pressure jump at $z = -d$ in a fluid at infinite Froude number, we have (2.99), (2.100) plus a correction term due to a positive image located at $z = +d$.

$$\mathcal{P}^+ = -\frac{e^{-i\zeta z - i\beta x}}{4\pi} \left(e^{-\sqrt{s^2 + \beta^2}(z+d)} - e^{-\sqrt{s^2 + \beta^2}(z-d)} \right) \quad (2.101)$$

$$\mathcal{P}^- = \frac{e^{-i\zeta z - i\beta x}}{4\pi} \left(e^{-\sqrt{s^2 + \beta^2}(z+d)} + e^{-\sqrt{s^2 + \beta^2}(z-d)} \right) \quad (2.102)$$

The normal upwash on the planar surface is

$$v(x, y) = \frac{\partial \Phi}{\partial z}(x, y, -d; k) \quad (2.103)$$

The expression for the velocity potential transform is

$$\Phi = \frac{i\mathcal{P}}{(k+s)} \quad (2.104)$$

The upwash due to a unit oscillating lift located at $x = \xi$, $y = \eta$, $z = -d$ on a planar surface parallel to the free surface is

$$v(x, y) = \lim_{z \rightarrow -d} \left\{ \frac{i}{2\pi} \iint \frac{d\mathcal{P}}{dz} \frac{e^{i\zeta x + i\beta y}}{(s+k)} ds d\beta \right\} \quad (2.105)$$

The resulting kernel function valid for $z > -d$ is found by applying equation (2.105) to the form of \mathcal{P}^+ in equation (2.97)

$$\chi = \lim_{z \rightarrow -d} \left\{ \frac{i}{8\pi^2} \iint_{-\infty}^{\infty} ds d\beta \left[\exp(is(x-s) + i\beta(y-\eta) + (z+d)\sqrt{s^2+\beta^2}) \cdot \frac{\sqrt{s^2+\beta^2}}{(s+k)} \right] + \frac{i}{8\pi^2} \iint_{-\infty}^{\infty} ds d\beta \left[\frac{F^2(s+k)^2 + \sqrt{s^2+\beta^2}}{F^2(s+k)^2 - \sqrt{s^2+\beta^2}} \right] \cdot \exp(is(x-s) + i\beta(y-\eta) + (z-d)\sqrt{s^2+\beta^2}) \frac{\sqrt{s^2+\beta^2}}{(s+k)} \right\} \quad (2.106)$$

The first integral in equation (2.106) is a well known expression for the upwash due to an oscillating pressure doublet (see Chapter I).

We will discuss the second integral and propose a method for numerical evaluation and an interpretation of the results. The complete correction including the image is

$$\chi_F = \frac{i}{8\pi^2} \iint_{-\infty}^{\infty} \exp((z-d)\sqrt{s^2+\beta^2} + is(x-s) + i\beta(y-\eta)) \cdot \left(\frac{\sqrt{s^2+\beta^2}}{s+k} \right) \left(\frac{F^2(s+k)^2 + \sqrt{s^2+\beta^2}}{F^2(s+k)^2 - \sqrt{s^2+\beta^2}} \right) ds d\beta \quad (2.107)$$

A change of variables which gives a striking comparison between the two and three-dimensional kernel functions is $s = s$, $\beta = \tau s$ where τ is a real number. Properties of this transformation are worked out in Appendix iii. General results are that if

$$\varphi(x, y, z) = \frac{1}{2\pi} \iint_{-\infty}^{\infty} \Phi(s, \beta; z) e^{isx + i\beta y} ds d\beta \quad (2.108)$$

Then

$$\varphi(x, y, z) = \frac{1}{2\pi} \iint_{-\infty}^{\infty} \Phi(s, \tau s; z) e^{is(x+\tau y)} |s| ds d\tau \quad (2.109)$$

With this transformation, the expression for the kernel due to a pressure jump in an infinite fluid is

$$\chi_{\infty} = \frac{i}{8\pi} \lim_{z \rightarrow -d^+} \left\{ \iint_{-\infty}^{\infty} \frac{|s| \sqrt{1+\tau^2}}{(s+k)} |s| \cdot \exp(i s(x-z) + i(\beta(y-\eta) - |s| \sqrt{1+\tau^2}(z+d))) ds d\tau \right\} \quad (2.110)$$

This may also be written

$$\chi_{\infty} = \frac{1}{8\pi} \lim_{z \rightarrow -d^+} \left\{ - \int_{-\infty}^{\infty} \frac{\partial}{\partial z} \int_{-\infty}^{\infty} \frac{i |s|}{(s+k)} \cdot \exp(i s(x-z) + \tau(y-\eta) - |s| \sqrt{1+\tau^2}(z+d)) ds d\tau \right\} \quad (2.111)$$

The expression for the equivalent two-dimensional kernel function for a pressure jump in an infinite fluid is

$$\chi_{2D}^{\infty} = \lim_{z \rightarrow -d^+} \left\{ \frac{1}{4\pi} \int_{-\infty}^{\infty} \frac{i |s|}{(s+k)} \exp(i s(x-z) - |s|(z+d)) ds \right\} \quad (2.112)$$

Comparing χ_{2D}^{∞} and χ_{∞} we notice that

$$\chi_{\infty} = -\frac{1}{2\pi} \left\{ \frac{\partial}{\partial z} \int_{-\infty}^{\infty} \chi_{2D}^{\infty} ((x-z) + \pi(y-\eta)) d\tau \right\} \quad (2.113)$$

We may write a similar expression for the upwash contribution of the free surface including the image. Equation (2.107) becomes

$$\chi^F = \frac{1}{8\pi} \lim_{z \rightarrow -d^+} \left\{ \int_{-\infty}^{\infty} \frac{\partial}{\partial z} \int_{-\infty}^{\infty} \frac{i |s|}{(s+k)} \left[\frac{F^2(s+k)^2 + |s| \sqrt{1+\tau^2}}{F^2(s+k)^2 - |s| \sqrt{1+\tau^2}} \right] \cdot \exp(i s(x-z) + s\tau(y-\eta) + |s|(z-d) \sqrt{1+\tau^2}) ds d\tau \right\} \quad (2.114)$$

As discussed in section 2.2, the equivalent expression for the two-dimensional kernel is

$$\chi_{2D}^F = \frac{1}{4\pi} \int_{-\infty}^{\infty} \frac{i|s|}{(s+k)} e^{i s(x-z) + |s|(z-d)} \left(\frac{F^2(s+k)^2 + |s|}{F^2(s+k)^2 - |s|} \right) \quad (2.115)$$

The expression for the three-dimensional kernel becomes

$$\chi^F = -\frac{1}{5\pi} \frac{\partial}{\partial z} \int_{-\infty}^{\infty} \chi_{2D}^F ((x-z) + \tau(y-z)) d\tau \quad (2.116)$$

An analytic closed form expression for χ_{2D} was derived in section 2.2. The advantage of an expression like (2.116) is that radiation conditions carefully worked out for the two-dimensional kernel can be applied to this form of the three-dimensional kernel. This gives a unique definition to the various contour integrals which are evaluated in solving for this three-dimensional kernel function. Equation (2.116) in addition to settling questions of incoming and outgoing waves, also gives a numerical technique for evaluating the three dimensional kernel function. Convergence properties can be checked by examining the asymptotic expansions of $\frac{\partial}{\partial z} \chi_{2D}^F$ for large τ .

The final result for the three-dimensional kernel function is reminiscent of an expansion in plane waves. First we note that the "apparent depth" of the equivalent two-dimensional disturbance grows as $d_{app.} = d_{actual} \cdot \sqrt{1 + \tau^2}$.

The apparent Froude number of the individual two-dimensional contributions decreases as

$$F_{app} = \frac{F_{actual}}{(1+\tau^2)^{1/4}} \quad (2.118)$$

For a given value of $|\tau|$, waves come from both the $x-\tau y$ and $x+\tau y$ directions. A better form to demonstrate the equivalence of the $x+\tau y$ and $x-\tau y$ directions would be

$$\chi^F(x-z, y-\eta) = \frac{-1}{-2\pi} \left\{ \frac{\partial}{\partial z} \int_0^\infty K_{2D}^F(x-z) + \tau(y-\eta) d\tau + \frac{\partial}{\partial z} \int_0^\infty K_{2D}^F(x-z) - \tau(y-\eta) d\tau \right\} \quad (2.119)$$

For hydrofoils operating at practical ranges of Froude numbers, it is felt that the numerical evaluation of these integrals would not be practical. In the two-dimensional finite Froude number solution, results of $F = 10$ were indistinguishable from infinite Froude number results for all practical purposes. The computation time required to carry out the evaluations of the kernel function necessary for a determination of the loads of a three-dimensional hydrofoil at finite Froude number could not be justified.

Extension to non-planar lifting surfaces can be made by noting that the nature of the singularity which gives a pressure jump across a surface is the normal derivative of a pressure source, the pressure doublet. Taking advantage of this, we derive the expression for a pressure source below a free surface and the expression for the upwash it produces.

We then take a derivative in any direction we choose to find the kernel function for an arbitrary nonplanar lifting surface.

The problem statement is essentially that for the planar kernel function. The jump conditions will be those associated with a pressure source which when differentiated in the y direction gives the unit pressure jump for a planar foil parallel to the free surface.

The jump conditions on pressure across this pressure source located at $z = \eta$, $x = \xi$, $y = \eta$ are

$$P^-(\xi, \eta, \eta) - P^+(\xi, \eta, \eta) = 0 \quad (2.120)$$

$$\frac{\partial P^-}{\partial z}(\xi, \eta, \eta) - \frac{\partial P^+}{\partial z}(\xi, \eta, \eta) = \delta(x-\xi) \delta(y-\eta) \quad (2.121)$$

In the transform variable \mathcal{P} the jump conditions are

$$\mathcal{P}^- - \mathcal{P}^+ = 0 \quad (2.122)$$

$$\frac{d\mathcal{P}^-}{dz} - \frac{d\mathcal{P}^+}{dz} = e^{-i s \xi - i \beta \eta} \quad (2.123)$$

These equations together with equations (2.88) to (2.91) give the solution for P^+ and P^- for this pressure source located at $z = \eta$

$$\begin{aligned} \mathcal{P}^+ = & - \exp(-i s \xi - i \beta \eta - \sqrt{s^2 + \beta^2} (z - \eta)) \frac{1}{4\pi \sqrt{s^2 + \beta^2}} \\ & + \frac{\exp(-i s \xi - i \beta \eta + \sqrt{s^2 + \beta^2} (z + \eta))}{4\pi \sqrt{s^2 + \beta^2}} \left[\frac{F^2 (s+k)^2 + \sqrt{s^2 + \beta^2}}{F^2 (s+k)^2 - \sqrt{s^2 + \beta^2}} \right] \end{aligned} \quad (2.124)$$

$$\begin{aligned}
 \mathcal{P}^- = & - \frac{\exp(-i s z - i \beta \eta + (z - \rho) \sqrt{s^2 + \beta^2})}{4\pi \sqrt{s^2 + \beta^2}} \\
 & + \frac{\exp(-i s z - i \beta \eta + (z + \rho) \sqrt{s^2 + \beta^2})}{4\pi \sqrt{s^2 + \beta^2}} \left[\frac{F^2(s+k)^2 + \sqrt{s^2 + \beta^2}}{F^2(s+k)^2 - \sqrt{s^2 + \beta^2}} \right]
 \end{aligned}
 \tag{2.125}$$

The velocity potential due to a pressure source under a free surface is

$$\begin{aligned}
 \varphi^+ = & - \frac{1}{8\pi} z \iint_{-\infty}^{\infty} \frac{\exp(i s(x-z) + i \beta(y-\eta) - \sqrt{s^2 + \beta^2}(z-\rho))}{\sqrt{s^2 + \beta^2} (s+k)} i ds d\beta \\
 & + \frac{1}{8\pi} z \iint_{-\infty}^{\infty} \frac{\exp(i s(x-z) + i \beta(y-\eta) + \sqrt{s^2 + \beta^2}(z+\rho))}{\sqrt{s^2 + \beta^2} (s+k)} \left[\frac{F^2(s+k)^2 + \sqrt{s^2 + \beta^2}}{F^2(s+k)^2 - \sqrt{s^2 + \beta^2}} \right] ds d\beta
 \end{aligned}
 \tag{2.126}$$

$$\begin{aligned}
 \varphi^- = & - \frac{1}{8\pi} z \iint_{-\infty}^{\infty} \frac{\exp(i s(x-z) + i \beta(y-\eta) + \sqrt{s^2 + \beta^2}(z-\rho))}{\sqrt{s^2 + \beta^2} (s+k)} i ds d\beta \\
 & + \frac{1}{8\pi} z \iint_{-\infty}^{\infty} \frac{\exp(i s(x-z) + i \beta(y-\eta) + \sqrt{s^2 + \beta^2}(z+\rho))}{\sqrt{s^2 + \beta^2} (s+k)} \left[\frac{F^2(s+k)^2 + \sqrt{s^2 + \beta^2}}{F^2(s+k)^2 - \sqrt{s^2 + \beta^2}} \right] ds d\beta
 \end{aligned}
 \tag{2.127}$$

To find the normal upwash at a point x, y, z of a surface due to a unit pressure jump at a point ξ, η, ρ of a surface, we follow a procedure similar to that of Chapter I for non-planar wings in an infinite fluid or at infinite Froude number below a free surface.

We derive the kernel function for three-dimensional finite Froude number by the following operation on the velocity potential due to the pressure source.

$$\chi_{3D}(x-z, y-\eta, z-\rho) = \frac{\partial}{\partial \eta_1} \frac{\partial}{\partial \eta_2} \varphi(x-z, y-\eta, z-\rho)
 \tag{2.128}$$

where as in Chapter I.

$$\frac{\partial}{\partial n_1} = \cos \psi(\eta) \frac{\partial}{\partial z} - \sin \psi(\eta) \frac{\partial}{\partial y} \quad (2.129)$$

$$\frac{\partial}{\partial n_2} = -\cos \psi(\eta) \frac{\partial}{\partial z} + \sin \psi(\eta) \frac{\partial}{\partial y} \quad (2.130)$$

The configuration for a nonplanar surface is sketched in Fig. 1.1

If the kernel function described in equation (2.123) could be evaluated either analytically or numerically, it would replace the kernel function used in Chapter I if free surface effects were desired. When the Froude number F is infinity, the kernel function described by equation (2.128) reduces to the simple pressure doublet plus image doublet.

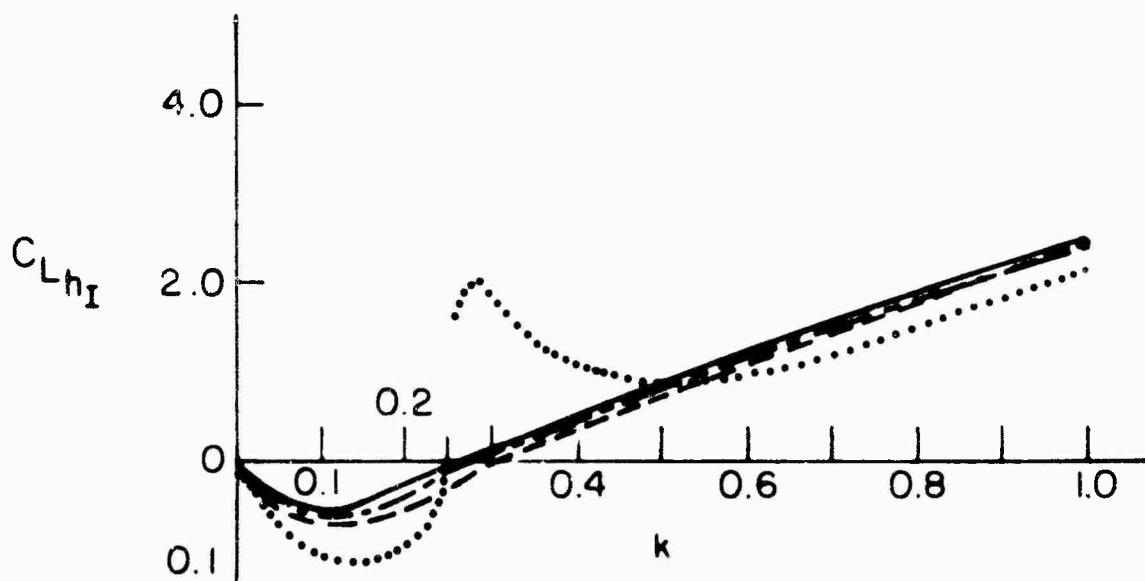
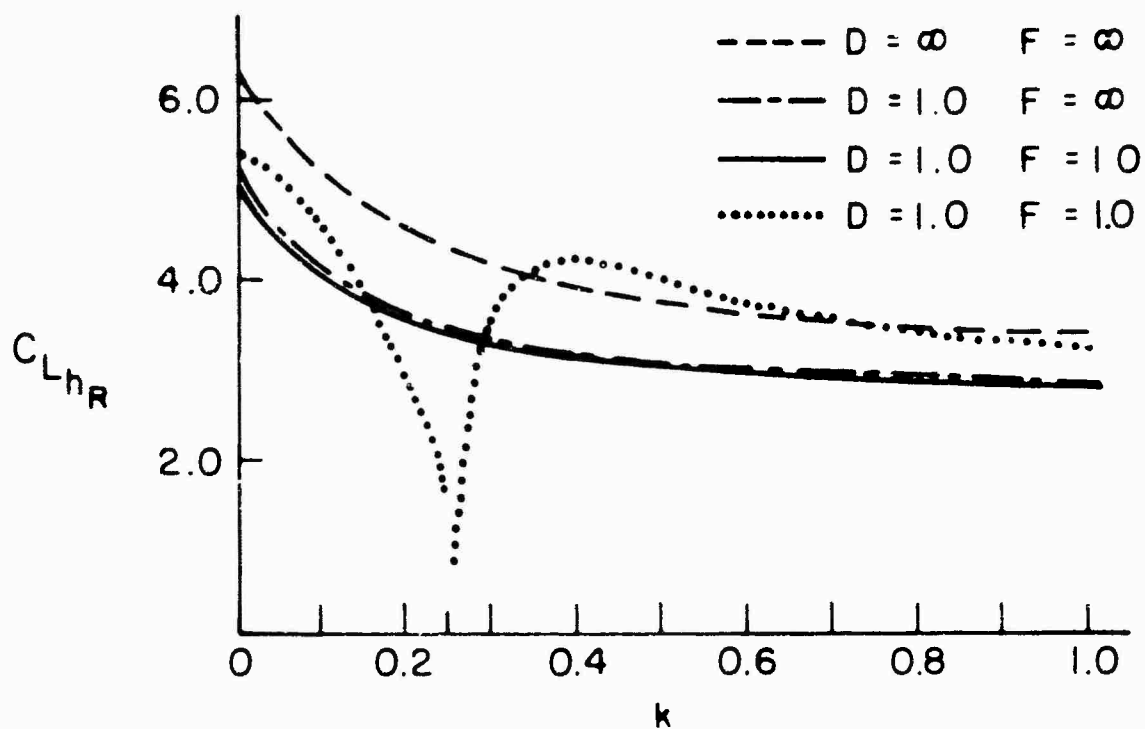


FIG.2.2 LIFT COEFFICIENT DUE TO HEAVE VS k FOR A TWO DIMENSIONAL HYDROFOIL

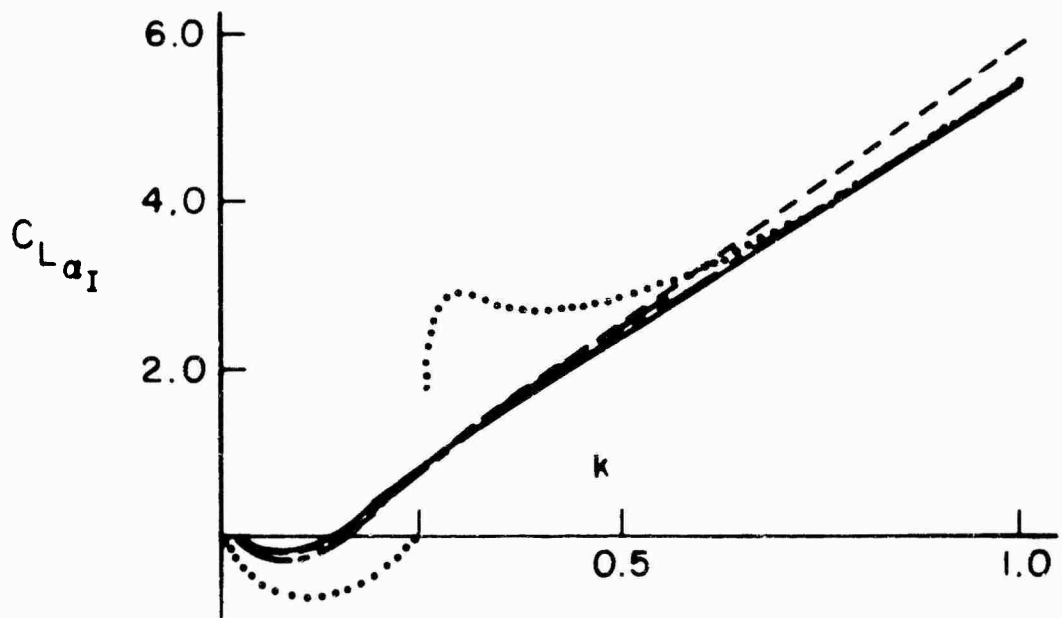
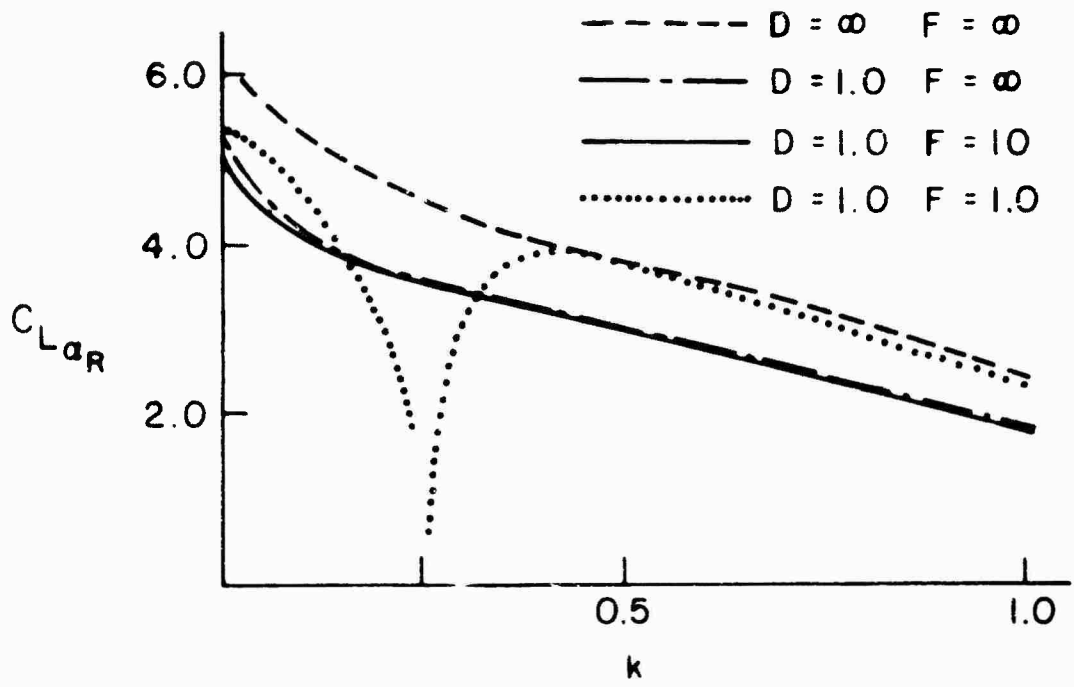


FIG. 2.3 LIFT COEFFICIENT DUE TO PITCH VS k FOR A TWO DIMENSIONAL HYDROFOIL

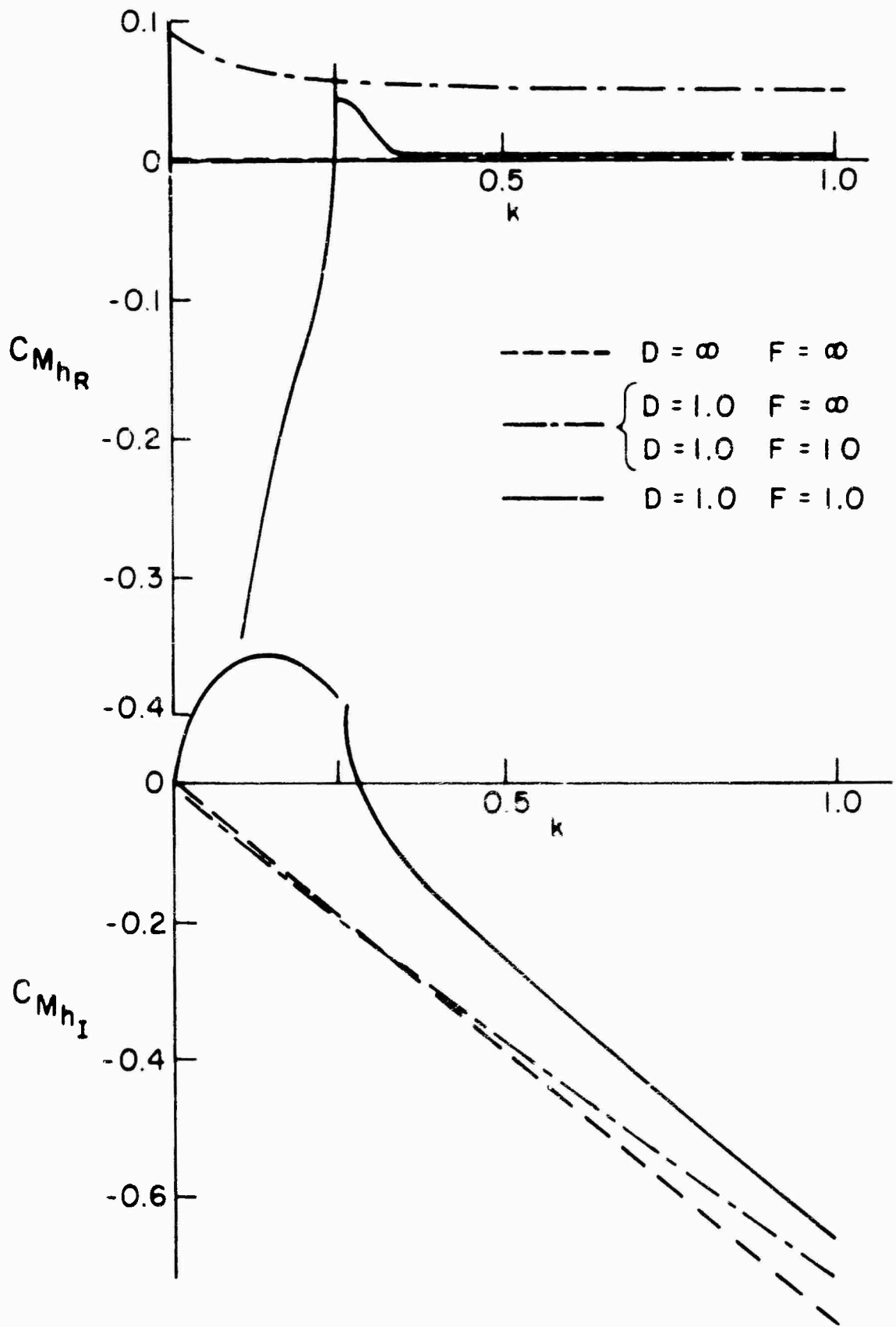


FIG. 2.4 MOMENT COEFFICIENT ($1/4 C$) DUE TO HEAVE VS k FOR A TWO DIMENSIONAL HYDROFOIL

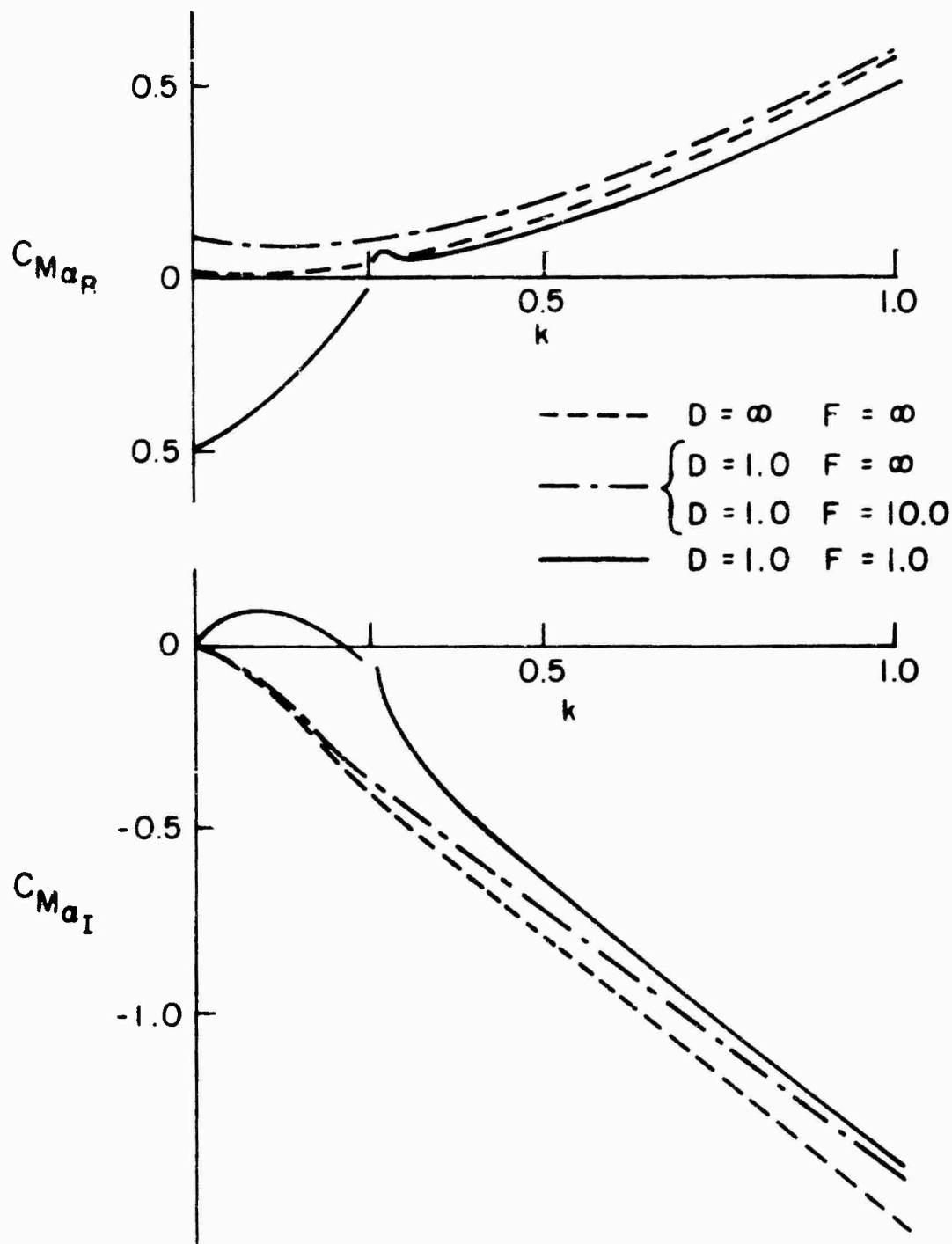


FIG. 2.5 MOMENT COEFFICIENT (1/4 C) DUE TO PITCH VS k FOR A TWO DIMENSIONAL HYDROFOIL

CHAPTER III
UNSTEADY LOADS ON SUPERCAVITATING
THREE DIMENSIONAL HYDROFOILS

3.1 Introduction

A hydrofoil traveling at high speed will experience cavitation if the pressure on the foil falls below some critical value. If the cavity extends over the complete upper surface of the foil, the foil is said to be supercavitating. The pressure in the cavity may be the vapor pressure or in the case of operation close to the free surface, it may be atmospheric pressure. The latter condition is often called ventilation. If a cavitation bubble forms, it will have a constant pressure on its surface equal to this critical value. To solve mathematical problems of cavity flows, it is usually assumed that this critical pressure is given.

Problems of finite cavitating bodies such as vertical flat plates in two-dimensional steady flow have been solved using complex variable techniques. A review of these problems and the mathematical techniques used is given by Gilbarg, Ref. (26). Some new developments in two dimensional cavitation theory are contained in papers of Ref. (27).

For thin, two-dimensional hydrofoils in steady and unsteady motion, linearized theories have been studied by Tulin (28), Woods (29), Parkin (30), Timman (31) and Guerst (32).

In his doctoral desertation, Guerst has discussed the relation between the two-dimensional linearized theory for a cavitating wedge and the nonlinear models for a cavitating wedge, the Riabouchinsky model and the re-entrant jet model. He shows that "linearized cavity theory is a first order approximation to both nonlinear models for small wedge angle."

The two-dimensional linearized theory for steady flow have shown good agreement with experiment for thin supercavitating hydrofoils. Therefore, we feel that a three-dimensional linearized theory will give accurate predictions for the loads on steady and unsteady supercavitating foils of finite span.

3.2 Linearized Theory for Three-dimensional Supercavitating Hydrofoils

The coupled linearized integral equations for cavitating hydrofoils can be put into the general framework of lifting surface theory using the pressure or acceleration potential and Green's theorem. For linearized incompressible irrotational flow, the nondimensional perturbation pressure and the perturbation velocity potentials satisfy Laplaces equation.

$$\nabla^2 \hat{p} = 0 \quad (3.1)$$

$$\nabla^2 \phi = 0 \quad (3.2)$$

In the application of Green's theorem to the present problem we will use as the surface S enclosing the fluid, the wetted surface of the foil and the cavity surface plus a surface at infinity. Defining the unit normal \vec{n} as pointing into the fluid from the closed surface we then obtain

$$\hat{p}(x, y, z) = \frac{1}{4\pi} \iint_S \hat{p} \nabla \left(\frac{1}{R} \right) \cdot \vec{n} \, dS' - \frac{1}{4\pi} \iint_S \frac{\nabla \hat{p} \cdot \vec{n}}{R} \, dS \quad (3.3)$$

where

R = radius vector from field point x, y, z to point ξ, η, ζ on S .

The surface at infinity does not contribute to the value of $P(xyz)$, since one of the boundary conditions is that the perturbation pressure must vanish at infinity.

For the velocity potential, Green's theorem gives

$$\phi(x, y, z) = \frac{1}{4\pi} \iint_S \phi \nabla \left(\frac{1}{R} \right) \cdot \vec{n} \, dS' - \frac{1}{4\pi} \iint_S \frac{\nabla \phi \cdot \vec{n}}{R} \, dS \quad (3.4)$$

We shall consider both steady flow and simple harmonic time-dependent perturbations. The steady flow case can be found by setting the reduced frequency k equal to

zero. The linearized relationship between the complex amplitude of $P(xyz)$ and $\phi(xyz)$ for simple harmonic motion is

$$-P = \epsilon k \phi + \frac{\partial \phi}{\partial x} \quad (3.5)$$

The inverse relation is

$$\phi(x,y,z) = - \int_{-\infty}^x P(\lambda,y,z) e^{ik(\lambda-x)} d\lambda \quad (3.6)$$

A sketch of the foil-cavity surface S is shown in fig. 3.1.

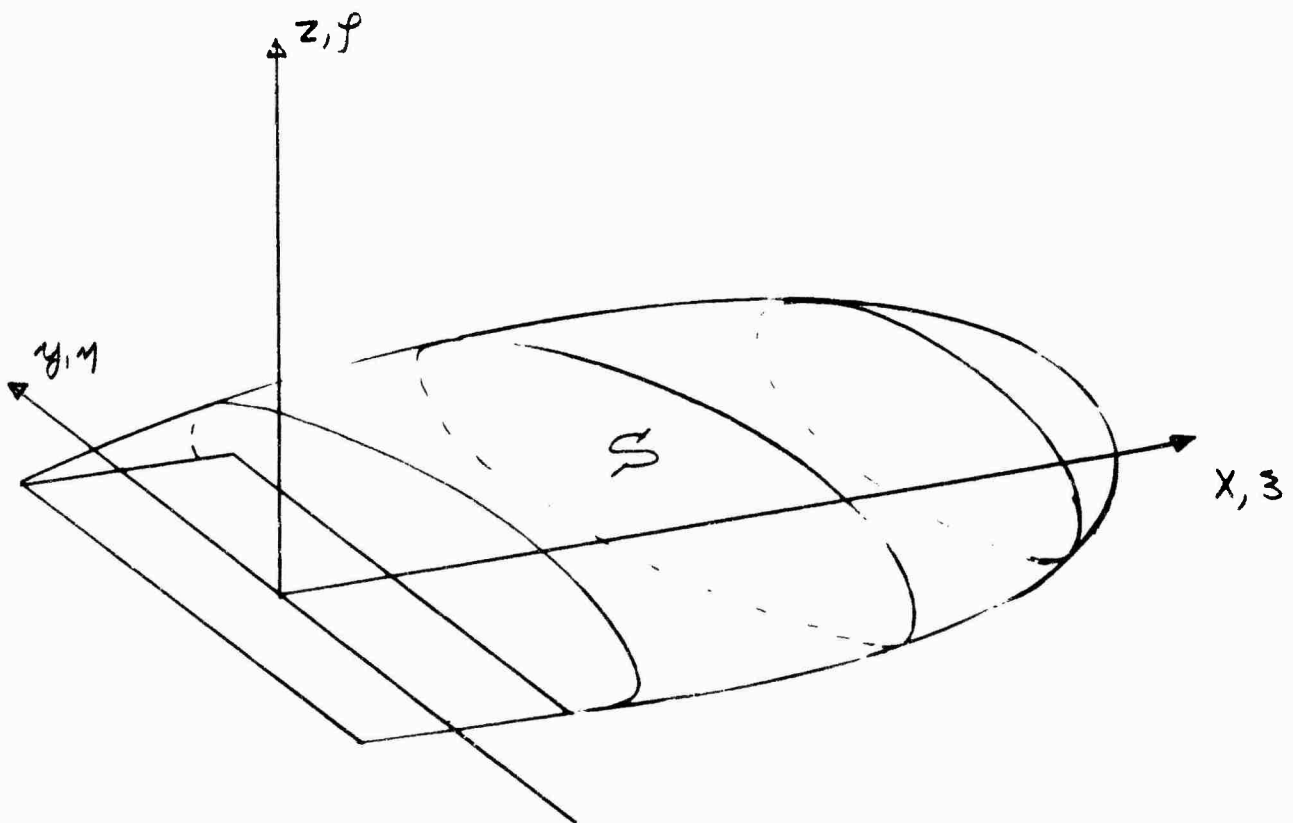


Fig. 3.1 Closed Surface of Cavity and Foil

As in the linearized theory for fully wetted flow, we satisfy boundary condition not S but on the projection of S in the x, y plane.

The boundary condition on the cavity surface is that the perturbation pressure is a constant. The cavitation number σ is defined

$$\sigma = \frac{P_\infty - P_c}{\frac{1}{2} \rho V^2} \quad (3.7)$$

P_c = pressure in the cavity

P_∞ = free stream pressure

The nondimensional perturbation pressure on the cavity surface is

$$\hat{p} = -\frac{\sigma}{2} \quad (3.8)$$

Linearized theory is valid only if $\sigma \ll 1$.

On the wetted surface of the foil the boundary condition is that there is no flow through the surface.

The foil-cavity surface collapses to become a region in the x, y plane as sketched in fig. 3.2. The projection of the foil surface is denoted as S_w , the projection of the cavity surface as S_c . When it is necessary to distinguish between the top and bottom of S_c or S_w , we will use the notation S_c^+ , S_c^- , S_w^+ and S_w^- .

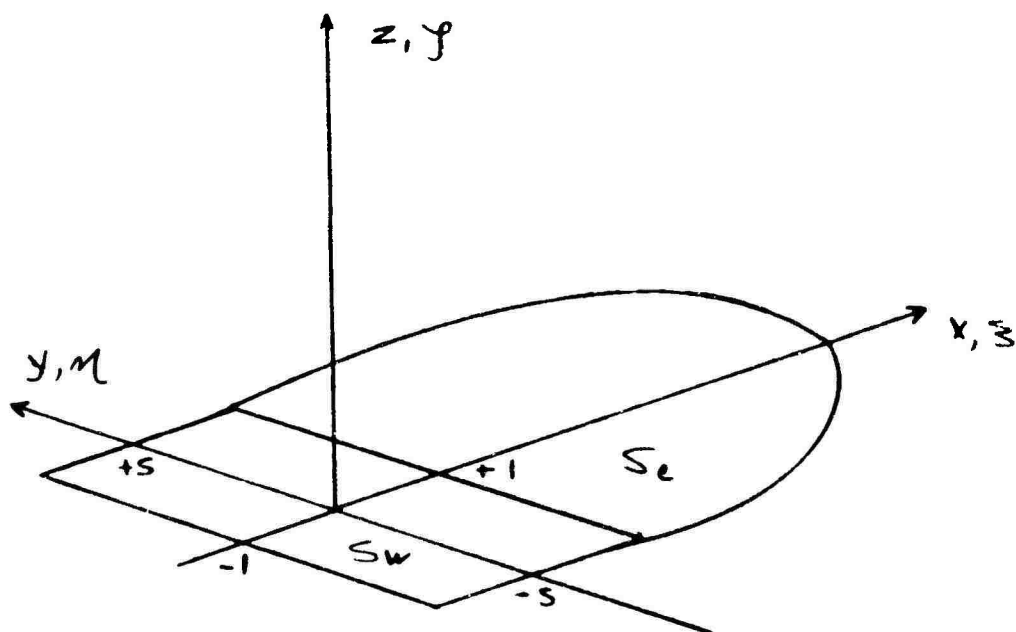


Fig. 3.2 The projection of S on to the x, y plane

The linearized boundary conditions are

$$\hat{P}_{\text{on } S_w^+} = -\frac{b}{N} \quad (3.9)$$

$$\hat{P}_{\text{on } S_e} = -\frac{b}{N} \quad (3.10)$$

$$\frac{\partial \psi}{\partial z}_{\text{on } S_w^-} = v(x, y) \quad (3.11)$$

where $v(x, y)$ = upwash on the wetted surface.

Using the relation $\frac{\partial}{\partial z} \left(\frac{1}{R} \right) = -\frac{\partial}{\partial \rho} \left(\frac{1}{R} \right)$, the closed surface in eq. (3.3) and (3.4) are rewritten as open surface integrals over S_w and S_c . The pressure perturbation at any point xyz is given by

$$\hat{p}(xyz) = \frac{1}{4\pi} \iint_{S_w + S_c} \left\langle \frac{\partial \hat{p}}{\partial \rho}(z, \eta) \right\rangle \frac{d\xi d\eta}{R} \quad (3.12)$$

$$+ \frac{1}{4\pi} \iint_{S_w} \Delta \hat{p}(z, \eta) \frac{\partial}{\partial z} \left(\frac{1}{R} \right) d\xi d\eta$$

where $\left\langle \frac{\partial \hat{p}}{\partial \rho}(z, \eta) \right\rangle$ is the notation for the jump in $\frac{\partial \hat{p}}{\partial \rho}$ across S and $\Delta \hat{p}$ denotes the jump in \hat{p} across S .

$$\left\langle \frac{\partial \hat{p}}{\partial \rho}(z, \eta) \right\rangle = \frac{\partial \hat{p}^-(z, \eta)}{\partial \rho} - \frac{\partial \hat{p}^+(z, \eta)}{\partial \rho} \quad (3.13)$$

$$\Delta \hat{p}(z, \eta) = \hat{p}^-(z, \eta) - \hat{p}^+(z, \eta) \quad (3.14)$$

The $1/R$ singularities are called pressure sources. It can be seen from the z momentum equation that their strength is related to the local curvature of the streamlines. The

$\frac{\partial}{\partial \rho} \left(\frac{1}{R} \right)$ singularities are called pressure doublets. A pressure doublet causes a unit lift to act at the point ξ, η, ρ , in the ρ direction. For this reason, no pressure doublets can appear off the solid foil surface.

The expression for the upwash velocity perturbation caused by this distribution of pressure sources and doublets is found by the application of eq. (3.6) which upon interchanging of the order of integration gives

$$\begin{aligned} \varphi(x,y,z) = & -\frac{1}{4\pi} \iint_{S_w+S_c} \left\langle \frac{\partial P}{\partial y} \right\rangle \int_{-\infty}^{x-3} \frac{d\lambda}{R(\lambda)} e^{ik(\lambda-(x-3))} dz dy \\ & - \frac{1}{4\pi} \iint_{S_w} \Delta P \int_{-\infty}^{x-3} \frac{d}{\partial z} \left(\frac{1}{R(\lambda)} \right) e^{ik(\lambda-(x-3))} d\lambda dz dy \quad (3.15) \end{aligned}$$

The expression for the upwash on the wetted foil surface is

$$\begin{aligned} v(x,y) = \lim_{z \rightarrow 0^-} \left\{ \frac{1}{4\pi} \iint_{S_w+S_c} \left\langle \frac{\partial P}{\partial y} \right\rangle \left(-\frac{1}{4\pi} \frac{d}{\partial z} \int_{-\infty}^{x-3} \frac{e^{ik(\lambda-(x-3))}}{R(\lambda)} d\lambda \right) dz dy \right. \\ \left. + \iint_{S_w} \Delta P \left(-\frac{1}{4\pi} \frac{d^2}{\partial z^2} \int_{-\infty}^{x-3} \frac{e^{ik(\lambda-(x-3))}}{R(\lambda)} d\lambda \right) dz dy \right\} \quad (3.16) \end{aligned}$$

The limit as $z \rightarrow 0^-$ of the expressions under the integral sign are the Kernel functions of the problem.

Physically they represent the upwash at a point x, y on the foil wetted surface caused by a pressure source or pressure doublet of oscillating strength located at ξ, η . The analytical expressions for these kernel functions are evaluated in Appendix 1. Starting from the definitions

$$\chi_1(x-\xi, y-\eta) = -\frac{1}{4\pi} \lim_{z \rightarrow 0^-} \left\{ \frac{\partial}{\partial z} \int_{-\infty}^{x-\xi} \frac{d\lambda}{R(\lambda)} e^{ik(\lambda-(x-\xi))} \right\} \quad (3.17)$$

$$\chi_2(x-\xi, y-\eta) = -\frac{1}{4\pi} \lim_{z \rightarrow 0^-} \left\{ \frac{\partial^2}{\partial z^2} \int_{-\infty}^{x-\xi} \frac{d\lambda}{R(\lambda)} e^{ik(\lambda-(x-\xi))} \right\} \quad (3.18)$$

The results of appendix 1 give

$$\chi_1 = -\frac{1}{2} e^{ik(x-\xi)} \delta(y-\eta) H(x-\xi) \quad (3.19)$$

$$\begin{aligned} \chi_2 = & \frac{e^{-ik(x-\xi)}}{4\pi(y-\eta)^2} \left\{ ik|y-\eta| + k|y-\eta| K_1(k|y-\eta|) \right. \\ & + \frac{i\pi}{2} k|y-\eta| [I_1(k|y-\eta|) - L_1(k|y-\eta|)] + \frac{(x-\xi) e^{ik(x-\xi)}}{\sqrt{(x-\xi)^2 + (y-\eta)^2}} \\ & \left. - ik|y-\eta| \int_0^{\frac{x-\xi}{|y-\eta|}} \frac{\tau e^{ik(x-\xi)}}{\sqrt{1+\tau^2}} d\tau \right\} \quad (3.20) \end{aligned}$$

The kernel function K_2 is used for fully wetted flow. A discussion of the singularities of K_2 is given in Chapter 1.

For steady flow it becomes

$$K_2 = \frac{1}{4\pi(y-\eta)^2} \left[1 + \frac{x-\xi}{\sqrt{(x-\xi)^2 + (y-\eta)^2}} \right] \quad (3.21)$$

The boundary condition on perturbation pressure is applied by taking suitable limits of eq. (3.12).

$$\begin{aligned} -\frac{\sigma}{2} = \hat{p}(x, y, 0^+) &= \frac{1}{4\pi} \iint_{S_w + S_0} \left\langle \frac{\partial \hat{p}}{\partial y} \right\rangle \frac{d\xi d\eta}{\sqrt{(x-\xi)^2 + (y-\eta)^2}} \\ &+ \frac{1}{4\pi} \iint_{S_w} \Delta \hat{p}(\xi, \eta) \lim_{z \rightarrow 0^+} \left\{ \frac{\partial}{\partial z} \left(\frac{1}{\sqrt{(x-\xi)^2 + (y-\eta)^2 + z^2}} \right) \right\} \quad (3.22) \end{aligned}$$

We define a third kernel function

$$\chi_3 = \lim_{z \rightarrow 0^+} \frac{\partial}{\partial z} \left(\frac{1}{\sqrt{(x-\xi)^2 + (y-\eta)^2 + z^2}} \right) \quad (3.23)$$

In appendix 1 this is shown to be

$$\chi_3 = -2\pi \delta(y-\eta) \delta(x-\xi)$$

With this substitution eq. (3.22) simplifies to

$$-\frac{\sigma}{2} = \frac{1}{4\pi} \iint_{S_w + S_c} \left\langle \frac{\partial \hat{p}}{\partial y} \right\rangle \frac{dz d\eta}{\sqrt{(x-z)^2 + (y-\eta)^2}} - \frac{\Delta \hat{p}}{2}(x,y) \quad (3.24)$$

The second integral equation, for the complex amplitude of the upwash distribution on the wetted foil surface becomes

$$v(x,y) = -\frac{e}{2} \int_{-1}^x \left\langle \frac{\partial p}{\partial y} \right\rangle e^{ikz} dz + \iint \Delta p(z,\eta) K_2(x-z, y-\eta) dz d\eta \quad (3.25)$$

where $\hat{p} = p e^{ikt}$, $\hat{v} = v e^{ikt}$

These two equations must be solved for a complete description of the linearized supercavitating hydrofoil. The unknowns are the distribution of pressure source strength $\left\langle \frac{\partial \hat{p}}{\partial y} \right\rangle$ on the foil and cavity surfaces, and the lift distribution $\Delta \hat{p}$ on the foil surface.

For steady flow at a given cavitation number σ , we obtain the following equations:

$$\hat{v}(x,y) = -\frac{1}{2} \int_{-1}^x \left\langle \frac{\partial \hat{p}}{\partial y} \right\rangle dz + \frac{1}{4\pi} \iint \frac{\Delta \hat{p}(z,\eta)}{(y-\eta)^2} \left(1 + \frac{x-z}{\sqrt{(x-z)^2 + (y-\eta)^2}} \right) dz d\eta \quad (3.26)$$

$$-\frac{\sigma}{2} = \frac{1}{4\pi} \iint_{S_w + S_c} \left\langle \frac{\partial \hat{p}}{\partial y} \right\rangle \frac{dz d\eta}{\sqrt{(x-z)^2 + (y-\eta)^2}} - \frac{\Delta \hat{p}}{2} \quad (3.27)$$

"For calculation of forces and moments, we assume that the unsteady motion is of small amplitude so that the cavity pressure remains unchanged from its steady value. The following integral equations for the complex amplitude of the unsteady perturbation then result:

$$v(x,y) = -\frac{e^{-ikx}}{2} \int_{-1}^x \left\langle \frac{\partial p}{\partial f}(s,\eta) \right\rangle e^{iks} ds \quad (3.28)$$

$$+ \iint \Delta p(s,\eta) \mathcal{K}_2(x-s, y-\eta) ds d\eta$$

(3.29)

$$0 = \frac{1}{4\pi} \iint_{S_u + S_c} \left\langle \frac{\partial p}{\partial f}(s,\eta) \right\rangle \frac{ds d\eta}{\sqrt{(x-s)^2 + (y-\eta)^2}} - \frac{\Delta p(x,y)}{2}$$

3.3 Numerical Method for three-dimensional supercavitating Hydrofoils

The coupled integral equation for the flow around a three-dimensional supercavitating hydrofoil were discussed in section 3.1. In the present section, we shall describe a numerical method similar to that used for fully wetted foils, to determine the lift distribution for steady and unsteady motion for cavities longer than the chord.

Equation (3.26) and (3.27) on (3.28) and (3.29) will be solved approximately by assuming a series of functions for both Δp and $\langle \frac{dp}{dy} \rangle$. The unknown coefficients are found by satisfying the upwash and cavity pressure boundary conditions at collocation points on the foil-cavity surface. For fully wetted flows as discussed in Chapter 1, the assumed chordwise functions for Δp were solutions to two-dimensional linearized thin airfoil problems including the solution for a flat plate in steady flow with a square root leading edge singularity. The assumed spanwise functions were elliptical with Δp going to zero at the tip. For an accurate determination of the lift distribution, it is important to choose a set of functions for Δp which approximate the physical behavior as closely as possible. The solution by linearized two-dimensional theory for supercavitating flow past a flat plate has a quarter root leading edge singularity in the distribution of Δp . We choose this function as one of the modes of Δp , in place of the function

for a fully wetted flat plate. The integrations of these assumed modes time the kernel function relating upwash to Δp are performed numerically.

Because of the very simple form of the kernel function relating pressure in the cavity to the pressure source strength distribution, we chose functions for $\langle \frac{\partial p}{\partial y} \rangle$ for which the integrals in eq. (3.27) and (3.29) can be evaluated analytically.

Since the Δp distribution is affected by the $\langle \frac{\partial p}{\partial y} \rangle$ distribution only through the coupled integral equations, we should be able to obtain an accurate prediction of lift and moment with only an approximate pressure source strength distribution. Rather than select as streamwise modes of the distributions of $\langle \frac{\partial p}{\partial y} \rangle$ from linearized two-dimensional solutions for supercavitating flows, we use a simpler set of functions which replaces the actual singularities of these solutions with simple delta functions and gives a piecewise linear approximation to $\langle \frac{\partial p}{\partial y} \rangle$.

The two-dimensional linearized solution for a supercavitating flat plate has a $5/4$ root leading edge singularity. The correct definition of integrals over this singularity is the Hadamar "finite part" (ref. (11)). Since the velocities and pressures produced by this non-integrable singularity have only a quarter root leading edge singularity, we feel that the boundary conditions can be satisfied and an accurate prediction of Δp obtained by approximating the effect of this singularity of $\langle \frac{\partial p}{\partial y} \rangle$ with a piecewise linear function plus a delta function.

Both the supercavitating flat plate and symmetric wedge solutions have a square root singularity in $\langle \frac{\partial p}{\partial y} \rangle$ at the trailing edge. We hope to approximate the effect of these singularities of $\langle \frac{\partial p}{\partial p} \rangle$ on the lift distribution by locating delta function of arbitrary strength at the leading and trailing edges. Although this is admittedly a very crude procedure, it is felt that it would be sufficiently accurate at the present exploratory stage.

In the two-dimensional non-linear theories of finite cavity flows, various artifices have been used to account for the trailing edge of the cavity. The constant pressure condition on the cavity prevents the occurrence of a stagnation point with smooth flow off the trailing edge.

Two models which have been used for finite cavities are the re-entrant jet model and the modified Riabouchinsky model which terminates the cavity with a fictitious vertical flat plate.



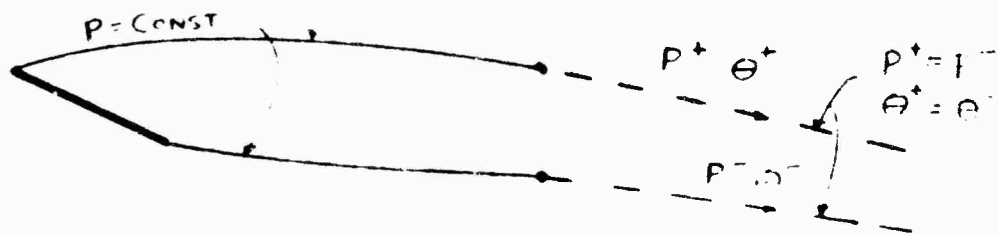
Re-entrant jet model



Modified Riabouchinsky model

Linearized theory derived from both of these models replaces the trailing edge of the cavity with a singularity and imposes a cavity closure condition.

Another non-linear model which has been studied is the smooth wake termination model.



Smooth wake termination model

The linearized theory based on this model does not require cavity closure, but only that the vertical velocity is continuous in the wake.

Fabula (ref. (35)) has compared the lift and moment computed by these linearized theories derived from these two types of cavity models. For cavities at least twice as long as the chord, that is for $\tau_\alpha < 1$, the numerical results differ by less than 2%.

In terms of pressure source strength, the cavity closure condition would require

$$\int_{-1}^{x_E} \int_{-1}^z \left\langle \frac{\partial P}{\partial p}(z') \right\rangle d_3' = 0$$

The smooth wake termination would require

$$\int_{-1}^{x_E} \left\langle \frac{\partial P(z)}{\partial f} \right\rangle d_3 = 0$$

Either of these conditions could be incorporated into the numerical method by adding a cavity termination constraint. Further research should be done to determine the effect of closure conditions at the trailing edge. It is not expected that the actual conditions used will effect the prediction of lift and moment for cavities longer than the chord.

In the present method, we terminate the cavity by requiring the pressure source strength to go to zero beyond the cavity trailing edge.

Further refinements could be made to account for the actual singularities by choosing as the chordwise modes of $\langle \frac{\partial p}{\partial x} \rangle$ the solutions from linearized two-dimensional theory. The integrations would then be performed by numerical quadrature. The present discussion merely suggests a simple numerical technique for three-dimensional supercavitating foils. The success of the approximations can be judged by the accuracy of the prediction of lift and moment on the foil.

3.3a Numerical Calculations for a Steady Symmetric Wedge

We shall begin our discussion of numerical techniques for three-dimensional supercavitating flows by considering the special case of a symmetric wedge.

For this special case, the integral equations (3.26) and (3.27), uncouple. Since Δp is zero for symmetric wedge flow, equation (3.26) becomes simply

$$v(x, y) = -\frac{1}{2} \int_{-1}^1 \left\langle \frac{dP}{df}(z, y) \right\rangle dz \quad (3.30)$$

The solution for a wedge of half angle α is

$$\left\langle \frac{dP}{df}(z, y) \right\rangle = 2\alpha f(z+1) \quad (3.31)$$

The second integral equation, (3.27) becomes

$$\begin{aligned} -\frac{\sigma}{2} &= \frac{\alpha}{2\pi} \operatorname{arctan} \left(\frac{(z-y) + \sqrt{(z-y)^2 + (x+1)^2}}{\sqrt{(s+y)^2 + (x+1)^2} - (s+y)} \right) \\ &= \frac{1}{4\pi} \iint_{S_c} \left\langle \frac{dP}{df}(z, y) \right\rangle \frac{dz d\eta}{\sqrt{(x-z)^2 + (y-\eta)^2}} \end{aligned} \quad (3.32)$$

The only unknown is the distribution of $\left\langle \frac{dP}{df}(z, y) \right\rangle$ on S_c .

One additional problem in cavity flows is that the shape and length of the cavity is not known in advance. To proceed with a numerical method, however, we must make some assumptions about cavity length and shape. We then test our numerical results to determine the sensitivity to these assumptions. For a valid linearized theory we require the cavitation number to be small. In the exact

linearized solution for two dimensional cavity flows, long cavities are consistent with small cavitation numbers. Thus, any effects due to cavity length and end conditions should produce minor effects on the foil itself.

We assume that the cavity surface is a rectangle equal in span to the foil and of some length X_E . For a given foil and a given cavitation number σ , we would test the numerical results for sensitivity to the assumed value of X_E . Fig. 3.3 shows the configuration for the linearized solution of a supercavitating symmetric wedge of constant chord equal to two, and of aspect ratio S . In the linearized problem, both the foil and cavity surfaces are located in the x, y plane ($z = 0$).

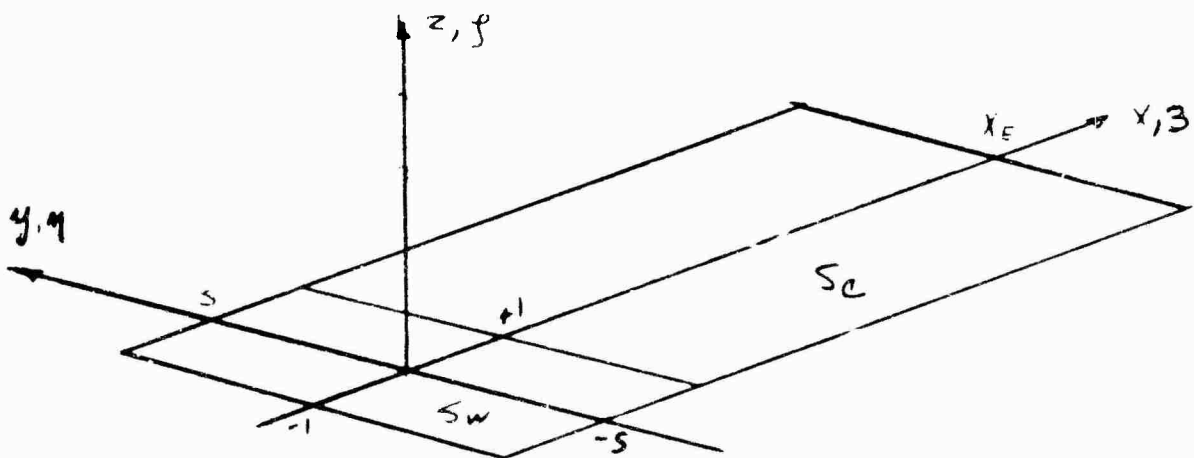


Fig. 3.3 Model for a supercavitating wedge

For this problem, the source distribution $\left\langle \frac{dP}{d\beta} \right\rangle$ is a symmetric function about the η axis.

As in the numerical solution for fully wetted three dimensional flows, we pick a set of n functions for the source distribution with unknown coefficients. These functions will be symmetric in η . The n coefficients are found by satisfying eq. (3.37) at collocation points on the cavity surface.

We define a set of spanwise functions $h(\eta, \eta_1, \eta_2)$ to have the following properties:

$$h(\eta, \eta_1, \eta_2) = \begin{cases} 0 & \left\{ \begin{array}{l} \eta < -\eta_2 < -\eta_1 < \eta_1 < \eta_2 \\ -\eta_2 < \eta_1 < \eta < \eta_1 < \eta_2 \\ -\eta_2 < \eta_1 < \eta_1 < \eta_2 < \eta \end{array} \right. \\ 1 & \left\{ \begin{array}{l} -\eta_2 < \eta_1 < -\eta_1 < \eta_1 < \eta_2 \\ -\eta_2 < -\eta_1 < \eta_1 < \eta_2 < \eta \end{array} \right. \end{cases}$$

(3.38)

The function $h(\eta, \eta_1, \eta_2)$ is sketched in Fig. 3.4

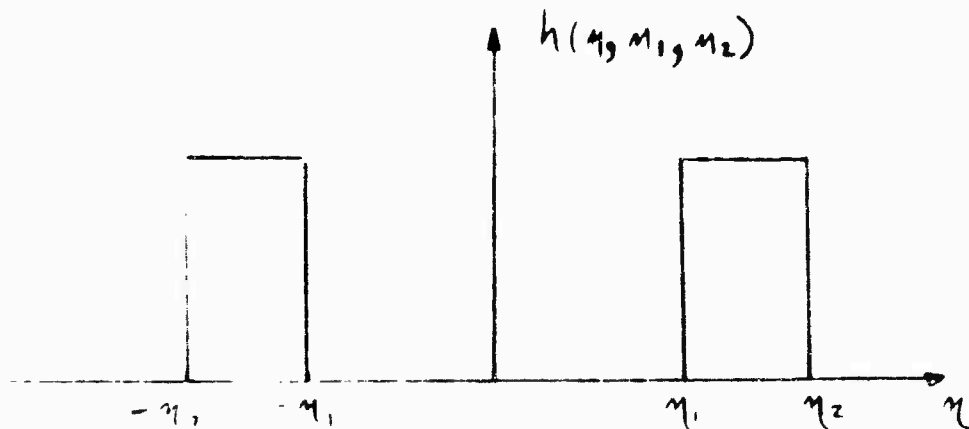


Fig. 3.4 The function $h(\eta, \eta_1, \eta_2)$ vs η

The rectangular cavity area, S_c , is divided into $2m$ rectangles of width $\Delta\eta$ and length Δz . We let I be the number of rectangles in the z direction and J be the number of rectangles in the η direction. Then

$$\Delta z = (X_E - 1) / I$$

$$\Delta \eta = S / J \quad (3.39)$$

The following set of functions for $\langle \frac{\partial P}{\partial \eta}(z, \eta) \rangle$ are chosen:

$$\langle \frac{\partial P}{\partial \eta}(z, \eta) \rangle = \sum_{j=1}^J \hat{a}_j h(\eta, \eta_j, \eta_{j+\Delta\eta}) \cdot f(z) \quad (3.40)$$

where

$$f(z) = \delta(z-1) + \sum_{i=2}^{I+2} \tilde{a}_i f_i(z) \quad (3.41)$$

The functions $f_i(z)$ are sketched in Fig. 3.5.

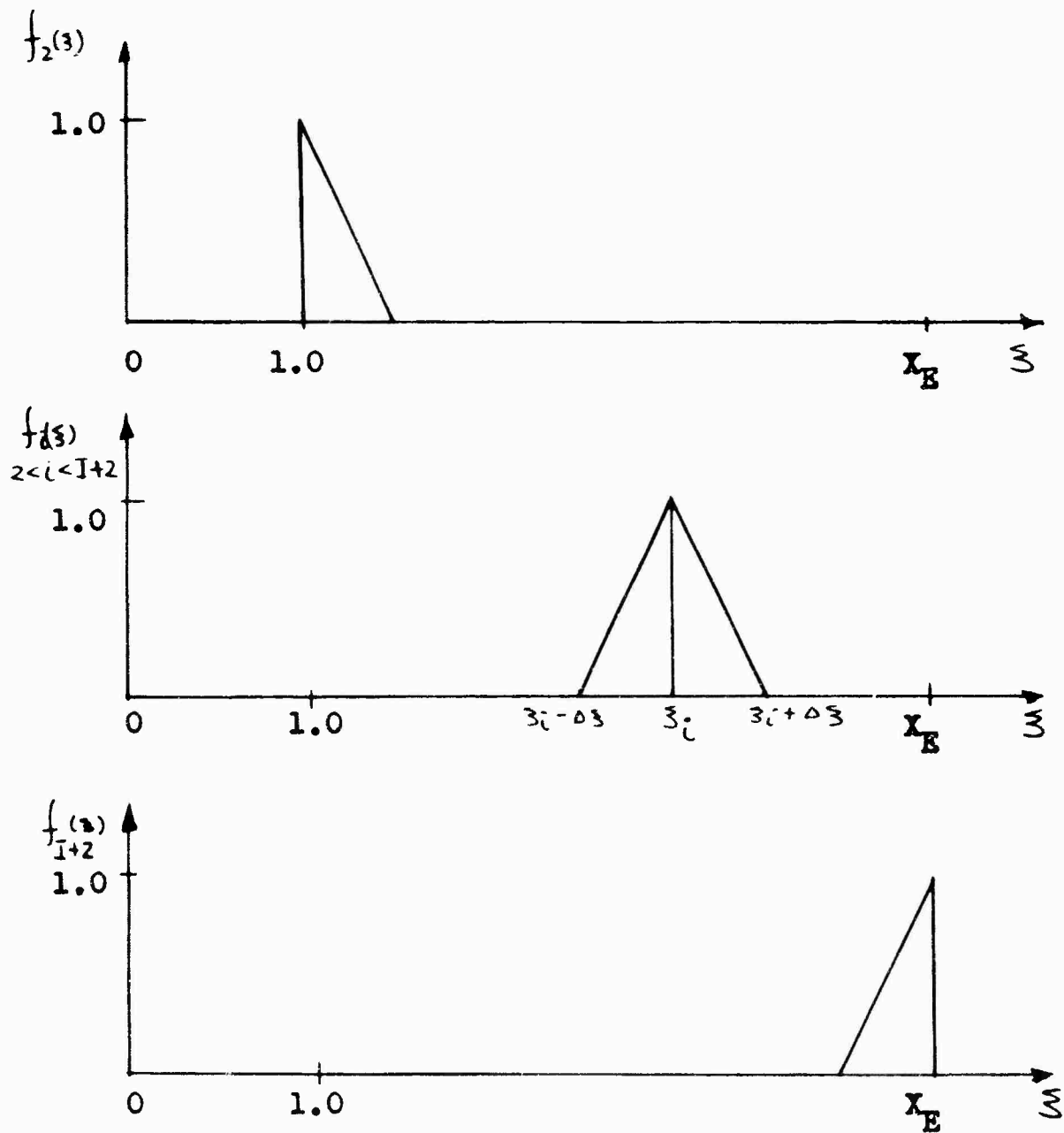


Fig. 3.5 The Set of Functions $f_i(z)$

The function $f(\xi)$ has the following properties:

1. Unit delta function behavior at the trailing edge.
where the two dimensional linearized solution has a square root singularity.
2. Piecewise linear and continuous variation in ξ from the trailing edge to the end of the cavity.

For a typical set of \tilde{a}_i 's, the function $f(\xi)$ is sketched in Fig. 3.6.

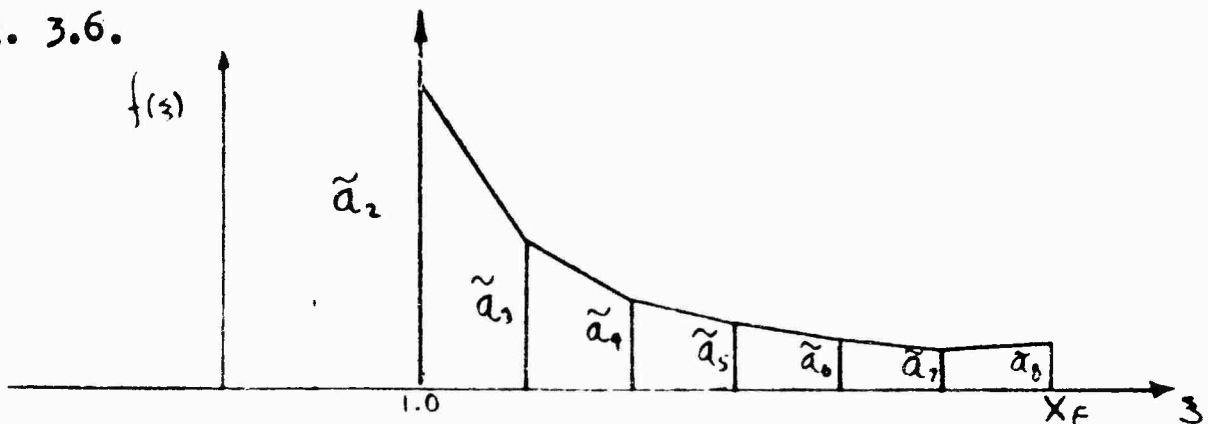


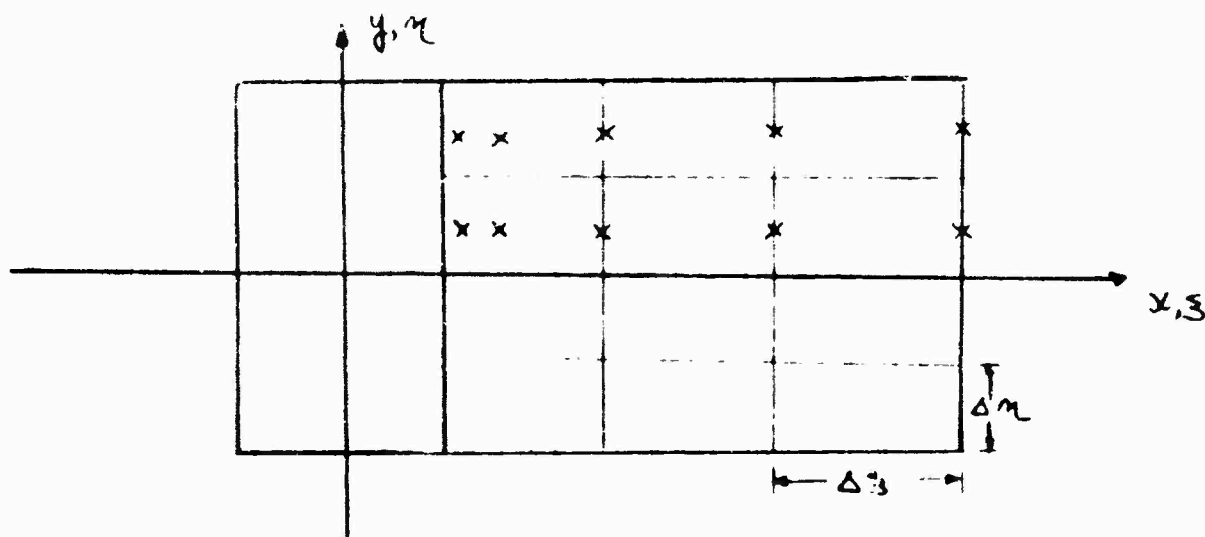
Fig. 3.6 Typical $f(\xi)$

The assumed set of functions for $\left\langle \frac{\partial P(\xi, \eta)}{\partial f} \right\rangle$ has the following properties.

1. Symmetric in η , constant in each $\Delta\eta$ rectangle.
2. Symmetric delta function rows of unknown strength at the trailing edge in each $\Delta\eta$ rectangle.
3. Piecewise linear and continuous in ξ .

The total number of unknown coefficients is $(1+2) \times J$, which is also the number of collocation points required. We put two control points in each rectangle closest to the trailing edge to allow for accurate determination of the delta function strength and to satisfy boundary conditions close to the trailing edge. The remaining control points are located at the ξ coordinates in the center of the $\Delta\eta$ rectangles.

(See Fig. 3.7)



3.7 Control point locations on S_c for a symmetric wedge solution

These simple assumed distributions allow the integral in (3.37) to be evaluated analytically. For the n collocation points, we thus obtain:

$$\left\{ -\frac{\sigma}{2} \right\} - \left\{ W_k \right\} = \left[P_{kn} \right] \left\{ a_n \right\} \quad (3.42)$$

where

$$W_k = \frac{\alpha}{2\pi} \ln \left(\frac{s - y_k + \sqrt{(s - y_k)^2 + (x_k + 1)^2}}{\sqrt{(s + y_k)^2 + (x_k + 1)^2} - (s + y_k)} \right)$$

x_k, y_k are coordinates of the k th control point and P_{kn} is the pressure at the k th control point caused by the n th assumed $\left\langle \frac{\partial P}{\partial y} \right\rangle$ mode.

Solution of equation (3.42) gives the a_n 's, the coefficients of the source distribution modes. The pressure at any point on the wedge may be found from

$$p(x, y) = \sum_n P_n(x, y) a_n + W(x, y)$$

where $P_n(xy)$ is the pressure at a point x, y due to the n th source mode, and $W(xy)$ is the pressure at a point x, y due to the leading edge delta function source of strength 2α .

3.3b Numerical Results for Symmetric Wedge

The numerical method has been programmed for the IBM 7090. We will present a few numerical results. A useful comparison can be made between numerical results obtained for pressure and source strength distributions on the center section of a large aspect ratio wedge and results of two dimensional linearized theory for cavitating wedges.

Two dimensional linearized theory for supercavitating wedges at zero cavitation number gives the following results (see Guerst ref. (32))

The pressure distribution along a symmetric wedge of semichord unity is:

$$P(x) = \frac{\alpha}{\pi} \log \left(\frac{1 + \sqrt{1-x}}{1 - \sqrt{1-x}} \right) \quad (3.43)$$

where $x = -1$ is the leading edge

$x = +1$ is the trailing edge

and α is the wedge half angle in radians.

The pressure source distribution is zero on the wedge except for a delta function of strength 2α at the leading edge. In the cavity the distribution of source strength is

$$\left\langle \frac{dP(x)}{dx} \right\rangle = - \left\langle \frac{dV(x)}{dx} \right\rangle = \frac{2\alpha}{\pi} \frac{1}{\left(\frac{x-1}{2} + 1 \right) \left(\frac{x-1}{2} \right)^{1/2}} \quad (3.44)$$

Results were computed for an aspect ratio 6 wedge with half angle $\alpha = .1$ radians. The calculations were done for cavity lengths, X_E , of 11, 7, 5 and 3 at a cavitation number of zero.

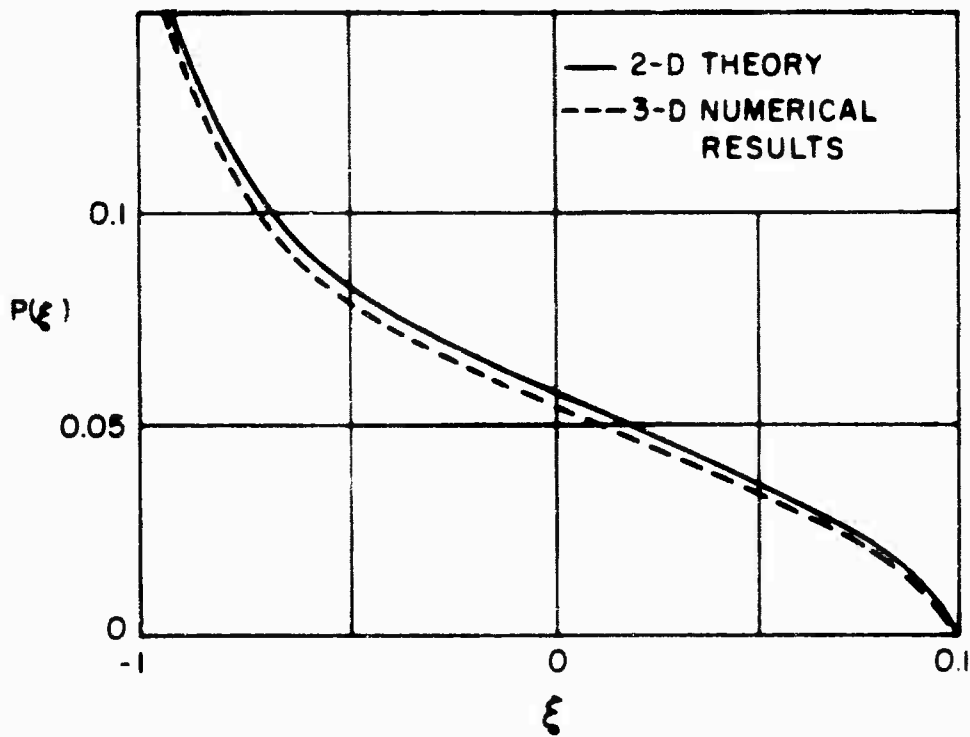


FIG. 3.8 COMPARISON OF CHORDWISE PRESSURE DISTRIBUTION ON A SYMMETRIC WEDGE BY TWO-DIMENSIONAL THEORY AND THREE-DIMENSIONAL NUMERICAL RESULTS ON THE CENTER SECTION OF AN ASPECT RATIO 6 WEDGE $\sigma = 0$ $\alpha = 0.1$

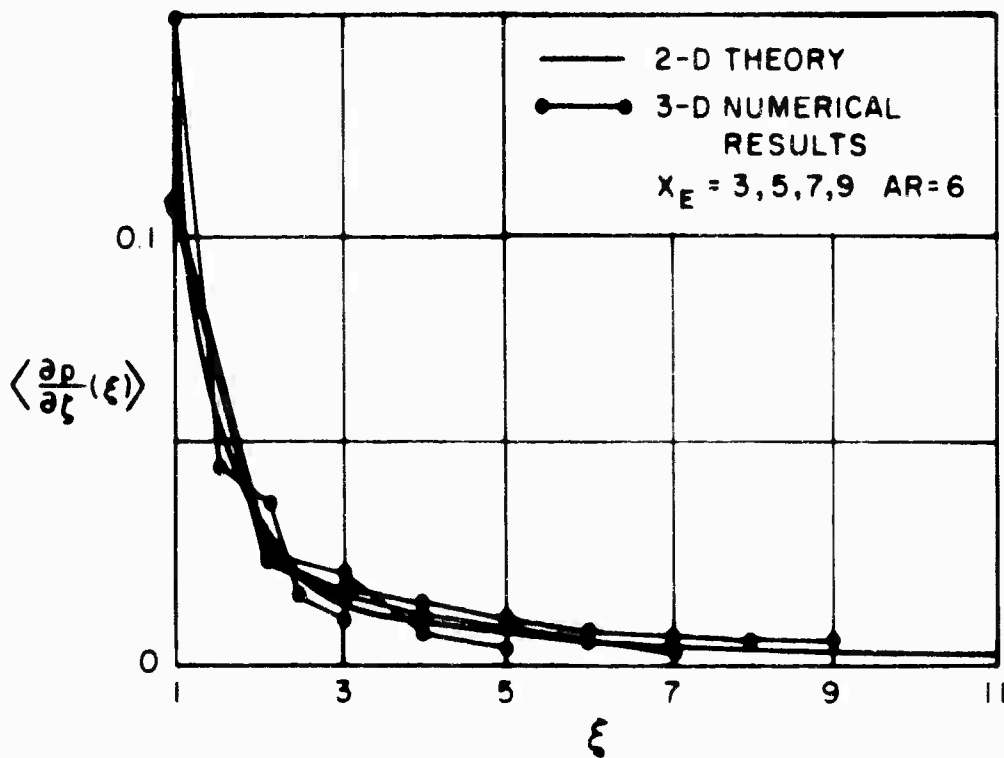


FIG. 3.9 COMPARISON OF PRESSURE SOURCE DISTRIBUTION IN THE CAVITY BEHIND A SYMMETRIC WEDGE BY TWO-DIMENSIONAL THEORY AND THREE-DIMENSIONAL NUMERICAL RESULTS $\sigma = 0$ $\alpha = 0.1$

Fig. 3.8 shows a comparison between the pressure distribution on the center section and the two dimensional theoretical result. The numerically calculated curves for various cavity lengths fall on top of one another, and thus are very insensitive to assumed cavity length.

Fig. 3.9 gives a comparison between the source strength on the cavity surface of the center section as calculated numerically for various assumed cavity lengths and the two dimensional result.

3.3c Numerical Method for a Supercavitating Flat Plate

The numerical approach to the supercavitating flat plate is similar to that described for the symmetric wedge. In this case, however, the integral equations do not uncouple and must be solved simultaneously.

The cavity shape is again taken as a rectangle on the $Z = 0$ plane of some length X_E and of span equal to that of the foil.

In this problem, there are two unknown distribution of singularities, a pressure doublet distribution on the foil only and a pressure source distribution on the foil and cavity surfaces. For each of these distributions, we pick a set of functions with unknown coefficients. The boundary conditions on both upwash and cavity pressure are then satisfied at an equivalent number of appropriate control points on foil and cavity surface. Results will yield lift distribution on the foil and pressure source distribution of foil and cavity.

The assumed series for $\Delta p(\xi, \eta)$ was that used for fully wetted flow. This series allows the possibility of a square root singularity at the leading edge. Two dimensional solutions for supercavitating flat plates show a quarter root singularity at the leading edge. From the numerical standpoint, it is a simple matter to substitute this function for the square root singularity. For steady flow solutions, we consider only functions which are symmetric in η . For oscillation about a steady cavity solution, we consider both symmetric and antisymmetric solutions. The form of $\Delta p(\xi, \eta)$, as in chapter 1, is taken to be

$$\Delta p(\xi, \eta) = \sum_{n=0}^N \sum_{m=0}^M a_{m+M-n} f_m(\xi) \quad (3.45)$$

where $\xi = -\cos \theta$

$$f_0(\xi) = \left(\frac{1 - (\frac{\xi+1}{3})^{1/2}}{(\frac{\xi+1}{3})^{1/2}} \right)^{1/2} \quad (3.46)$$

$$f_n(\theta) = \frac{4}{2^{2n}} \sin(n\theta) \quad (3.47)$$

the symmetric functions are

$$f_n(\eta) = \eta^{2n} \sqrt{1-\eta^2} \quad (3.48)$$

the antisymmetric functions are

$$f_n(\eta) = \eta^{2n+1} \sqrt{1-\eta^2} \quad (3.49)$$

The integrals in equation (3.33) and (3.35) involving $\Delta P(z, \eta)$ are treated numerically by the same technique used in the numerical method of chapter 1 for fully wetted flow.

The assumed set of functions for the pressure source distribution $\langle \frac{\partial P}{\partial s}(s, \eta) \rangle$ on the foil and cavity surfaces is similar to that chosen for the symmetric wedge solution. Both the foil and the cavity surfaces are divided into rectangular areas of width $\Delta \eta$ and length Δs_f on the foil and Δs_c on the cavity. Δs_f and Δs_c are not necessarily equal in length. The form of $\langle \frac{\partial P}{\partial s}(z, \eta) \rangle$ is chosen as follows:

For steady flow cavity solutions, or for a symmetric oscillation about a steady flow solution $\langle \frac{\partial P}{\partial s}(z, \eta) \rangle$ is symmetric in η .

$$\langle \frac{\partial P}{\partial s}(z, \eta) \rangle = \sum_{j=1}^N c_j h(\eta, \eta_j, \eta_j + \Delta \eta) \quad (3.50)$$

where $h(\eta, \eta_j, \eta_j + \Delta \eta)$ was defined in equation (3.38).

For antisymmetric oscillations about a steady cavity flow, $\langle \frac{\partial P}{\partial s}(z, \eta) \rangle$ is antisymmetric in η . We therefore set

$$\langle \frac{\partial P}{\partial s}(z, \eta) \rangle = \sum c_j \text{sgn}(\eta) h(\eta, \eta_j, \eta_j + \Delta \eta) \quad (3.51)$$

where

$$\text{sgn}(\eta) = \frac{\eta}{|\eta|}$$

Since the two dimensional linearized solution for a supercavitating flat plate has singularities in $\left(\frac{dP}{dz}\right)$ at both the leading and trailing edges, the function $f(\xi)$ is chosen to have the following properties:

1. unit delta function at the leading edge
2. arbitrary strength delta function at trailing edge
3. piecewise linear and continuous on both foil and cavity surfaces, may be discontinuous at the trailing edge.

If the number of rectangles in the ξ direction is I_f on the foil and I_c on the cavity, the total number of modes in $f(\xi)$ is $(I_f + 2) + (I_c + 2)$. These modes of $f(\xi)$ are sketched in Fig. 3.11.

$$f(\xi) = \delta(\xi + 1) + d_{I_f+3} \delta(\xi - 1) + \sum_{i=2}^{I_f+2} d_i f_i(\xi) + \sum_{i=I_f+4}^{I_f+I_c+4} J_i f_i(\xi) \quad (3.52)$$

For a set of d_i 's, a typical $f(\xi)$ is sketched in Fig. 3.10.

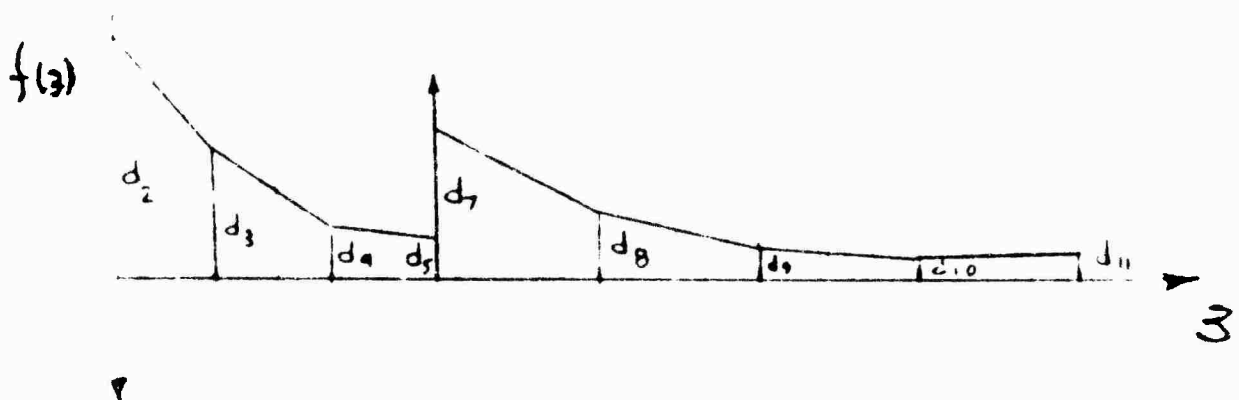


Fig. 3.10 Typical $f(\xi)$ for supercavitating plate.

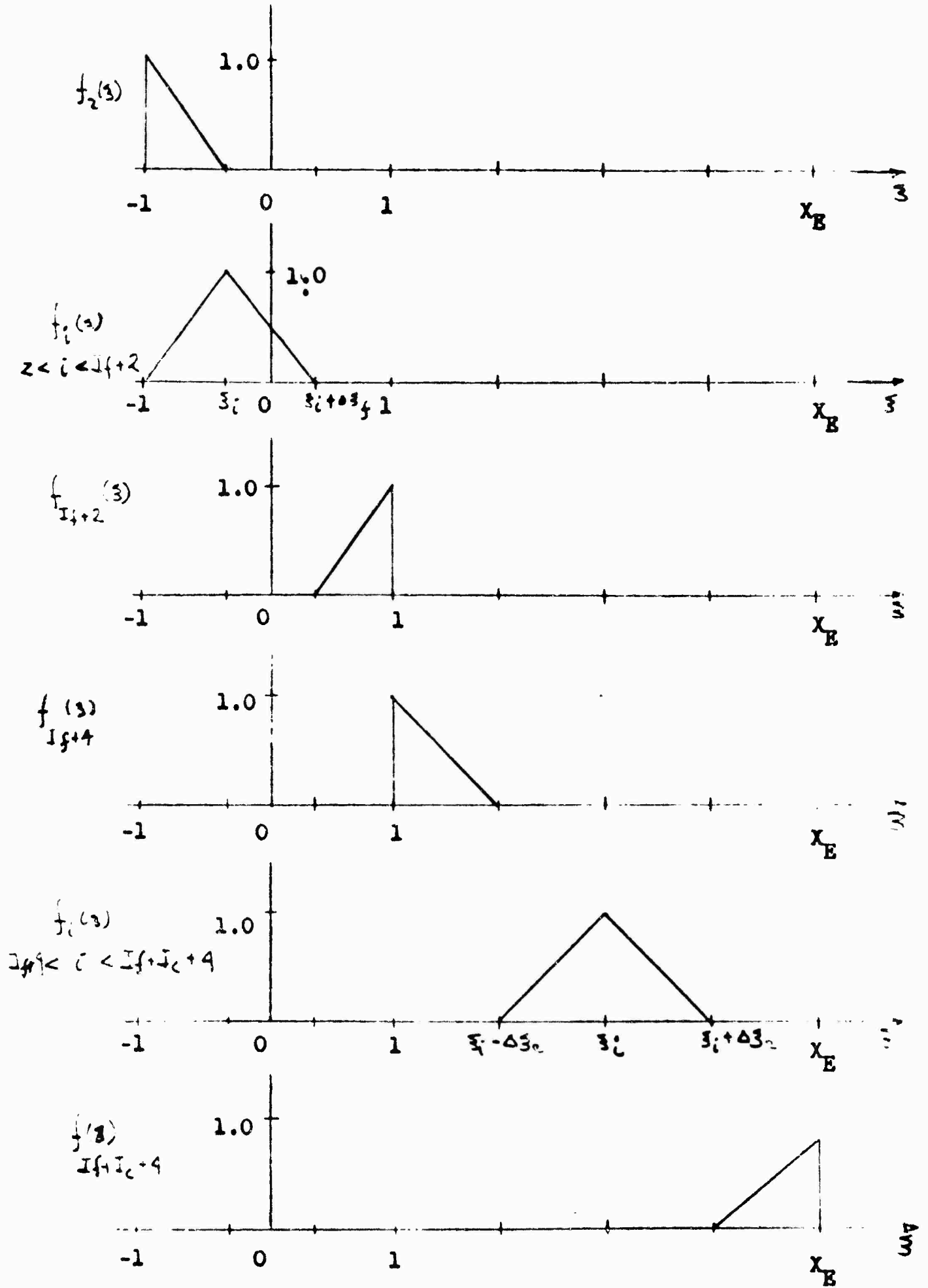


Fig. 3.11 Modes of $f(z)$

The integrals of $\left\langle \frac{\partial P}{\partial f} \right\rangle$ in equations (3.33) to (3.35) can be done analytically for this set of modes.

The total number of rectangular areas on S_c and S_w is $2N * (I_f + I_c)$. The total number of unknown coefficients for the pressure source modes is $N * (I_f + 2 + I_c + 2)$. For numerical simplicity, we choose N spanwise modes and $I_f + 2$ chordwise modes for Δf on the foil surface. We then satisfy both the upwash condition and the cavity pressure condition at the same control points on the foil. We need $N * (I_f + 2)$ control points on the foil for either the symmetric or antisymmetric case. The condition on cavity pressure behind the foil on S_c is satisfied at $N * (I_c + 2)$ control points. This collocation gives a complete set of linear algebraic equations whose unknowns are the coefficients of the Δf modes and the $\left\langle \frac{\partial P}{\partial f} \right\rangle$ modes.

The set of control points used in the numerical method is sketched in Fig. 3.12. The philosophy on control point location is to select an even distribution with special emphasis on sensitive areas such as leading or trailing edges. For either symmetric or antisymmetric cases, control points are located on only half of S_w and S_c .

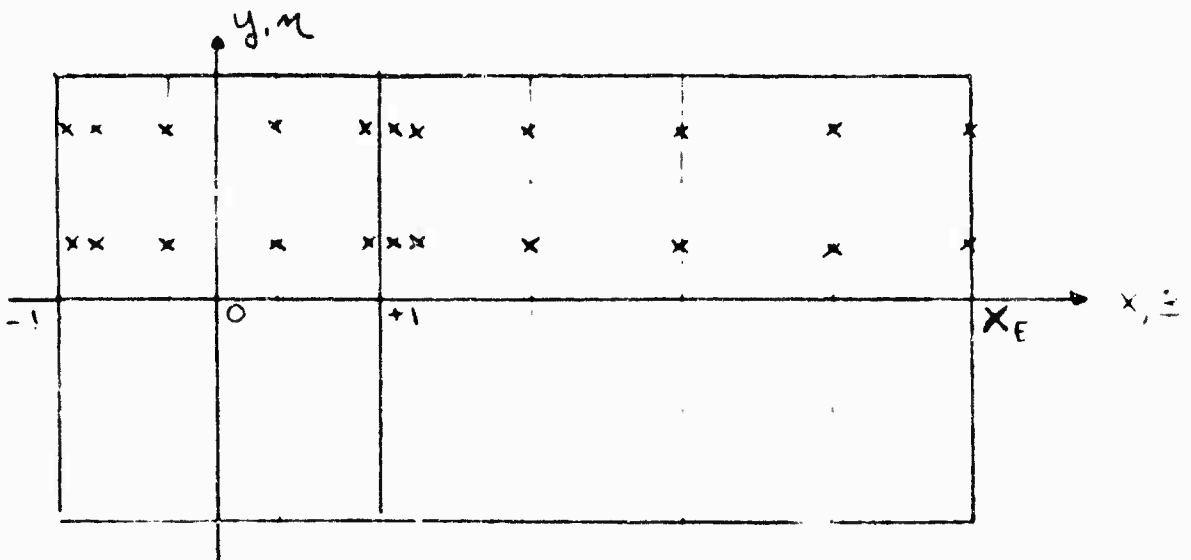


Fig. 3.12 Configuration for numerical solution for supercavitating flat plate showing control point locations, x_k, y_k

In matrix notation, equations (3.33) and (3.34) on (3.35) and (3.36) take the following form after the integrals have been evaluated either numerically or analytically for the assumed set of $\Delta p(z, \eta)$ and $\langle \frac{\partial P}{\partial p}(z, \eta) \rangle$ modes.

$$\begin{bmatrix} V_k \\ \vdots \\ -\frac{D}{2} \\ \vdots \\ \frac{D}{2} \end{bmatrix} = \begin{bmatrix} DW_{kn} & | & DWW_{kn} & | & 0 \\ \hline DPM_{kn} & & & & \\ \hline 0 & & P_{kn} & & \end{bmatrix} \begin{bmatrix} b_n \\ \vdots \\ a_n \\ \vdots \\ a_n \\ \vdots \end{bmatrix} \begin{matrix} \text{on foil} \\ \\ \text{on cavity} \end{matrix} \quad (3.53)$$

where b_n is the coefficient of the n th Δp mode on the foil and a_n is the coefficient of the n th $\langle \frac{\partial P}{\partial p} \rangle$ mode.

The matrix has been partitioned to show the relationship to equations (3.33) and (3.34) or (3.35) and (3.36). For the latter set of equations (i.e., in unsteady flow) this matrix set is complex. The elements of the partition DW are the upwash at the k th control point from the n th Δp mode. For a fully wetted flow, an inversion of this matrix alone gives the complete solution for the lift distribution.

$$\begin{bmatrix} V_k \end{bmatrix} = \begin{bmatrix} DW_{kn} \end{bmatrix} \begin{bmatrix} b_n \end{bmatrix} \quad (3.54)$$

The elements of the DDW matrix are found from the integral on $\langle \frac{\partial P}{\partial y}(z, y) \rangle$ in equation (3.33) or (3.35)

$$DDW_{kn} = -\frac{1}{2} \int_{-1}^x f_n(z) e^{-ik(x_k - z)} dz \quad (3.55)$$

Only those \bar{z} points directly ahead of the control point contribute to the elements of DDW. The elements of the DPM are just the Δp modes evaluated at the control points of the foil.

$$DPM_{kn} = -\frac{1}{2} \Delta p(x_k, y_k) \quad (3.56)$$

where Δp_n denotes the n th pressure mode.

The elements of the P matrix are the pressures at the control points on both the cavity and foil surface due to the various assumed modes of $\langle \frac{\partial P}{\partial y}(z, y) \rangle$.

$$P_{kn} = \frac{1}{4\pi} \iint_{S_n} \langle \frac{\partial P}{\partial y}(z, y) \rangle_n \frac{dz dx}{\sqrt{(x-z)^2 + (y-y)^2}} \quad (3.57)$$

where $\langle \frac{\partial P}{\partial y}(z, y) \rangle_n$ denotes the n th source mode and S_n is the appropriate area for the n th source mode.

The two matrices with zero elements appear in the complete matrix for two reasons: first the pressure source distribution on the cavity surface does not affect the upwash on the foil surface, second the function $\Delta p(z, y)$ is zero on the cavity surface.

The matrix in eq. (3.53) is inverted to give the coefficients b_n 's and a_n 's for a given cavitation number σ

and upwash distribution $v(xy)$ on the wetted surface of the foil. Hence:

$$\begin{bmatrix} b_n \\ \vdots \\ a_n \end{bmatrix} = \begin{bmatrix} \text{I} & | & \text{II} \\ \hline & \text{C} & \\ \text{III} & | & \text{IV} \end{bmatrix} \begin{bmatrix} v_k \\ \vdots \\ b'_n \end{bmatrix}$$

(3.58)

where the $[C]$ matrix is the inverse of the square matrix in (3.53). For a flat plate, the upwash, $v(x,y)$ is equal to $-\alpha$. We rewrite equation (3.58) to show the dependence of the a_n 's and b_n 's on α and σ

$$\{a_n\} = \left[-\frac{C_{IV}}{2} \right] \{ \sigma \} + \left[-C_{III} \right] \{ \alpha \} \quad (3.59)$$

$$\{b_n\} = \left[-C_I \right] \{ \alpha \} + \left[-\frac{C_{II}}{2} \right] \{ \sigma \} \quad (3.60)$$

$C_{I,II,III,IV}$ denote the partitions of the C matrix. For a given assumed cavity length, X_p , the coefficients are linear in α and σ with coefficients proportional to the sum of row elements of $[C]$.

$$a_n = a_{n\sigma} \cdot \sigma + a_{n\alpha} \cdot \alpha \quad (3.61)$$

$$b_n = b_{n\alpha} \cdot \alpha + b_{n\sigma} \cdot \sigma$$

where

$$\begin{aligned}
 a_{n\alpha} &= \sum_j (-C_{III nj}) \\
 a_{n\sigma} &= \sum_j (-C_{IV nj}) \\
 b_{n\alpha} &= \sum_j (-C_{I nj}) \\
 b_{n\sigma} &= \sum_j (-C_{II nj})
 \end{aligned}$$

The lift and moment on the foil may be obtained from a linear operation on the b_n 's as in the case for a fully wetted surface.

$$C_L = L \quad C_{Ln} \quad J \left\{ b_n \right\} \quad (3.62)$$

$$C_m = L \quad C_{mn} \quad J \left\{ b_n \right\} \quad (3.63)$$

where C_{Ln} and C_{mn} are row matrices; C_{Ln} , C_{mn} are the contributions to the lift and moment coefficients of the n th Δp mode. The lift and moment coefficients are then linear in both α and σ .

$$\begin{aligned}
 C_L &= C_{L\alpha} \cdot \alpha + C_{L\sigma} \cdot \sigma \\
 C_m &= C_{m\alpha} \cdot \alpha + C_{m\sigma} \cdot \sigma
 \end{aligned} \quad (3.64)$$

where

$$\begin{bmatrix} C_{L\alpha} & C_{L\sigma} \\ C_{m\alpha} & C_{m\sigma} \end{bmatrix} = \begin{bmatrix} C_{Ln} \\ C_{mn} \end{bmatrix} \begin{bmatrix} b_{n\alpha} & b_{n\sigma} \end{bmatrix} \quad (3.65)$$

For any given foil, the coefficients $C_{L\alpha}$ and $C_{L\tau}$ may be calculated for various values of the assumed cavity length X_E to determine the sensitivity of the predicted loads to cavity length. As in the case of the non-lifting wedge, the results for the lifting flows considered below were, fortunately, found to be very insensitive to cavity length, provided X_E is longer than about twice the foil chord. Results of two dimensional linearized theory and the experiments of Kermeen (ref (20)) indicate that the cavity is long compared to the chord for $\sigma/\alpha < 1$. This must be kept in mind when applying the numerical method.

The numerical method described in this section has been programmed for the IBM 7090 for both steady and unsteady flow. We will present a few numerical results and comparisons with both theory and available experiments.

3.3d Comparison with Steady Two Dimensional Linearized Theory

A useful comparison can be made between two dimensional linearized theory and some numerical results for the center section of a large aspect ratio supercavitating foil, in this case an aspect ratio 6 foil.

Two dimensional linearized theory gives the following results for lift distribution on a steady supercavitating flat plate at a cavitation number of zero (Ref. 32).

$$\Delta p(x) = \alpha \left(\frac{1 - \left(\frac{x+1}{2}\right)^{1/2}}{\left(\frac{x+1}{2}\right)^{1/2}} \right)^{1/2}$$

(3.66)

where α is the angle of attack

$x = -1$ is the leading edge

and $x = +1$ is the trailing edge

The expression for the pressure source strength on this foil is:

$$\left\langle \frac{\partial P}{\partial y} \right\rangle = - \frac{\rho U \alpha}{8} \left(\frac{1}{\left(1 + \left(\frac{x+1}{2}\right)^{1/2}\right)^{1/2} \left(\frac{x+1}{2}\right)^{5/4}} \right) \quad (3.67)$$

where the "finite part" must be taken of integrals over the $5/4$ root singularity.

The source strength on the cavity is

$$\left\langle \frac{\partial P}{\partial y} \right\rangle = - \frac{\rho U \alpha}{8} \left(\frac{\left(\left(\frac{x+1}{2}\right)^{1/2} - 1\right)^{1/2} + \left(1 + \left(\frac{x+1}{2}\right)^{1/2}\right)^{1/2}}{\left(\frac{x+1}{2} - 1\right)^{1/2} \left(\frac{x+1}{2}\right)^{5/4}} \right) \quad (3.68)$$

These expressions are plotted in Fig. 3.13 and 3.14 for $\alpha = .1$.

Calculations using the present method were made for a rectangular flat-plate foil of aspect ratio 6 at $\tau = 0$. Results for the chordwise lift and pressure source distribution at the center section are included in Figures 3.13 and 3.14. For these calculations, a cavity length equal to 3 times the chord was chosen.

Calculations were done with both a square root and quarter root leading edge singularity in the assumed form of $\Delta p(3.9)$. Fig. 3.13 and 3.14 also compare the results from these two methods. The difference-in predicted lift

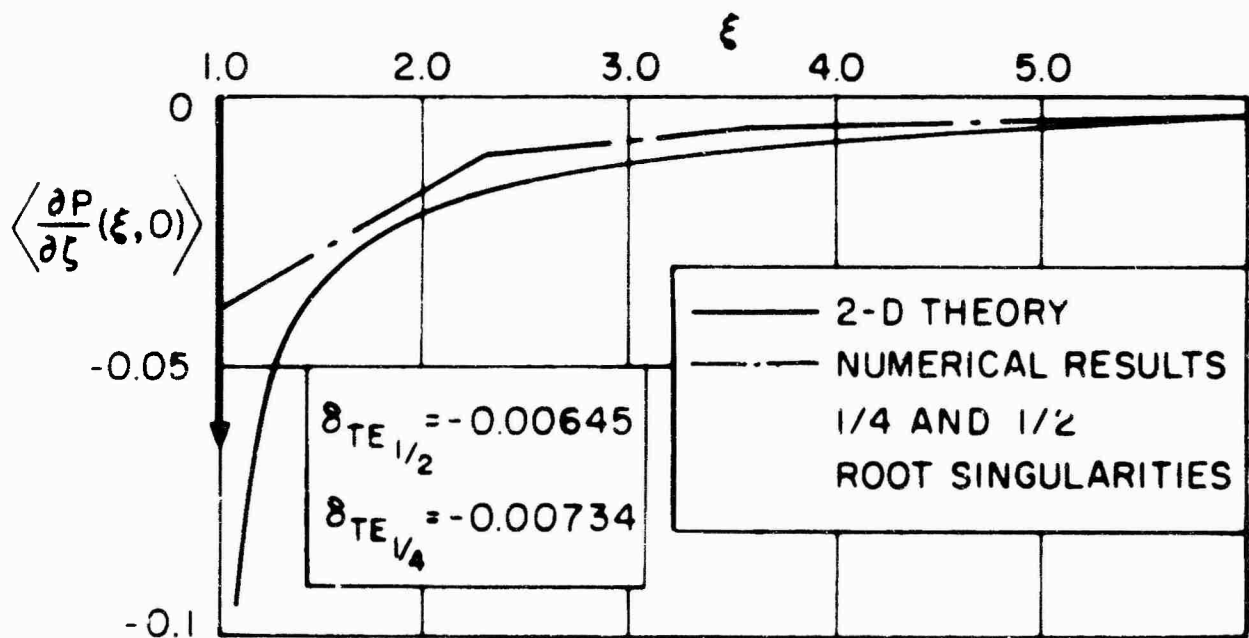
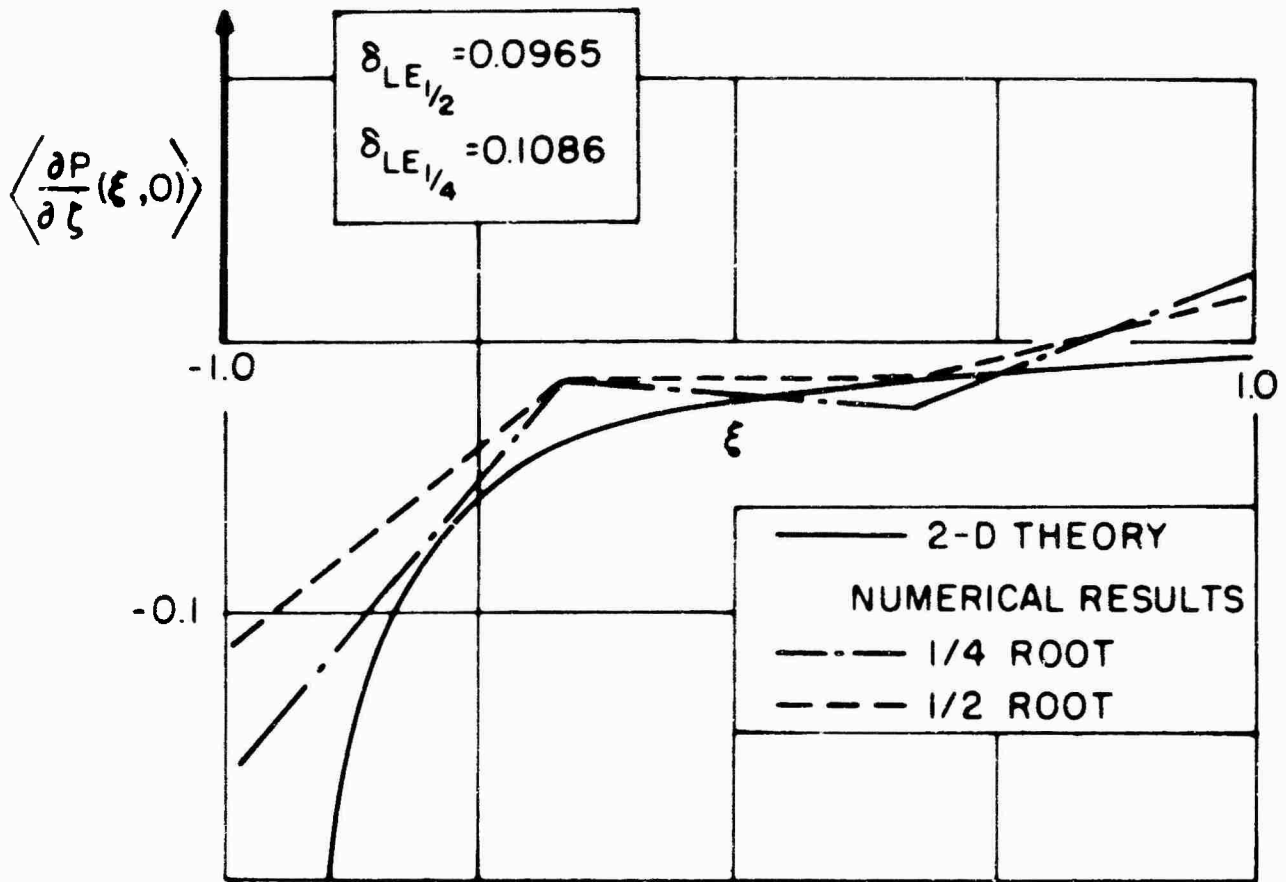


FIG. 3.13 NUMERICAL RESULTS FOR THE PRESSURE SOURCE DISTRIBUTION ON THE CENTER SECTION OF AN ASPECT RATIO 6 SUPERCAVITATING FLAT PLATE, COMPARISON WITH TWO-DIMENSIONAL LINEAR THEORY.
 $\alpha = 0.1, \sigma = 0, x_E = 5$

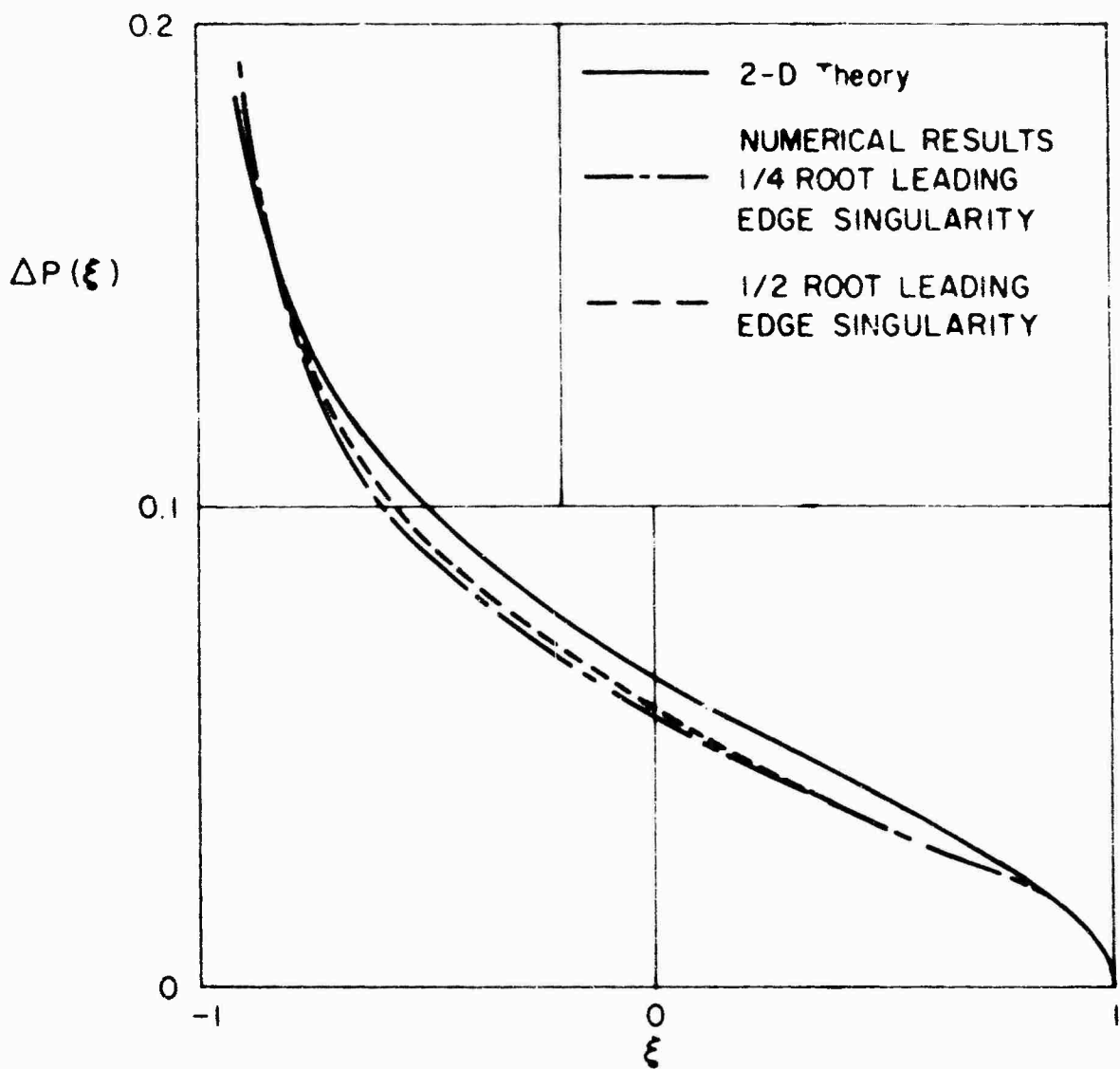


FIG. 3.14 NUMERICAL RESULTS FOR THE LIFT DISTRIBUTION ON THE CENTER SECTION OF AN ASPECT RATIO 6 FLAT PLATE, COMPARISON WITH TWO-DIMENSIONAL THEORY $\alpha = 0.1, \sigma = 0, X_E = 5.0$

TABLE 3.1 NUMERICAL RESULTS FOR THE CENTER SECTION OF AR=6 FLAT PLATE, COMPARISON WITH 2-D THEORY

| | 2-D | NUMERICAL 1/4 root sing. | NUMERICAL 1/2 root sing. |
|---------------|--------|-----------------------------|-----------------------------|
| $C_{L\alpha}$ | 1.5707 | 1.52 | 1.6055 |
| X_{CP} | 0.32 | 0.29 | 0.275 |

coefficient is about 5%. The variation in the center of pressure location is also about 5%. The prediction of source strength is very crude, but seems adequate for load calculations.

Two dimensional linearized (Ref. 32) theory gives the following results for lift and moment coefficient and cavity length.

$$\tan \gamma_0 = \left(\frac{\sigma}{2\alpha} \right) \quad (3.69)$$

$$C_{L_{2D}} = \frac{\alpha \pi}{2} (\cos \gamma_0)^{-1} (1 + \cos \gamma_0)^{-1} \quad (3.70)$$

$$C_{M_{2D}} = \frac{\pi \alpha}{8} \left(\frac{4 + \cos \gamma_0}{(\cos \gamma_0 (1 + \cos \gamma_0)^2)} \right) \quad (3.71)$$

$$X_{E_{2D}} = 1 + \frac{2}{(\sin \gamma_0)^2} \quad (3.72)$$

where γ_0 is a parameter

The expressions for C_L and C_m for $\alpha = .1$ are plotted vs. σ in Fig. 3.15 .. The numerical results obtained for the C_L and C_m on the center section of the aspect ratio 6 foil are also plotted vs. σ . As discussed in section 3.3c, the numerical technique gives a linear relation for C_L and C_m

$$C_L = C_{L_\alpha} \cdot \alpha + C_{L_\sigma} \cdot \sigma \quad (3.73)$$

$$C_m = C_{m_\alpha} \cdot \alpha + C_{m_\sigma} \cdot \sigma \quad (3.74)$$

The non-linear character of the $C_{L_{2D}}$ and $C_{m_{2D}}$ vs σ curves predicted by two dimensional theory comes from the dependence of cavity length on σ .

The three dimensional results have shown a very small variation of these coefficients with assumed cavity length.

Table 3.2 gives $C_{L_{3D}}$, $C_{m_{3D}}$, $C_{m_{\sigma}}$ and $C_{L_{\sigma}}$ tabulated vs. assumed cavity length X_E .

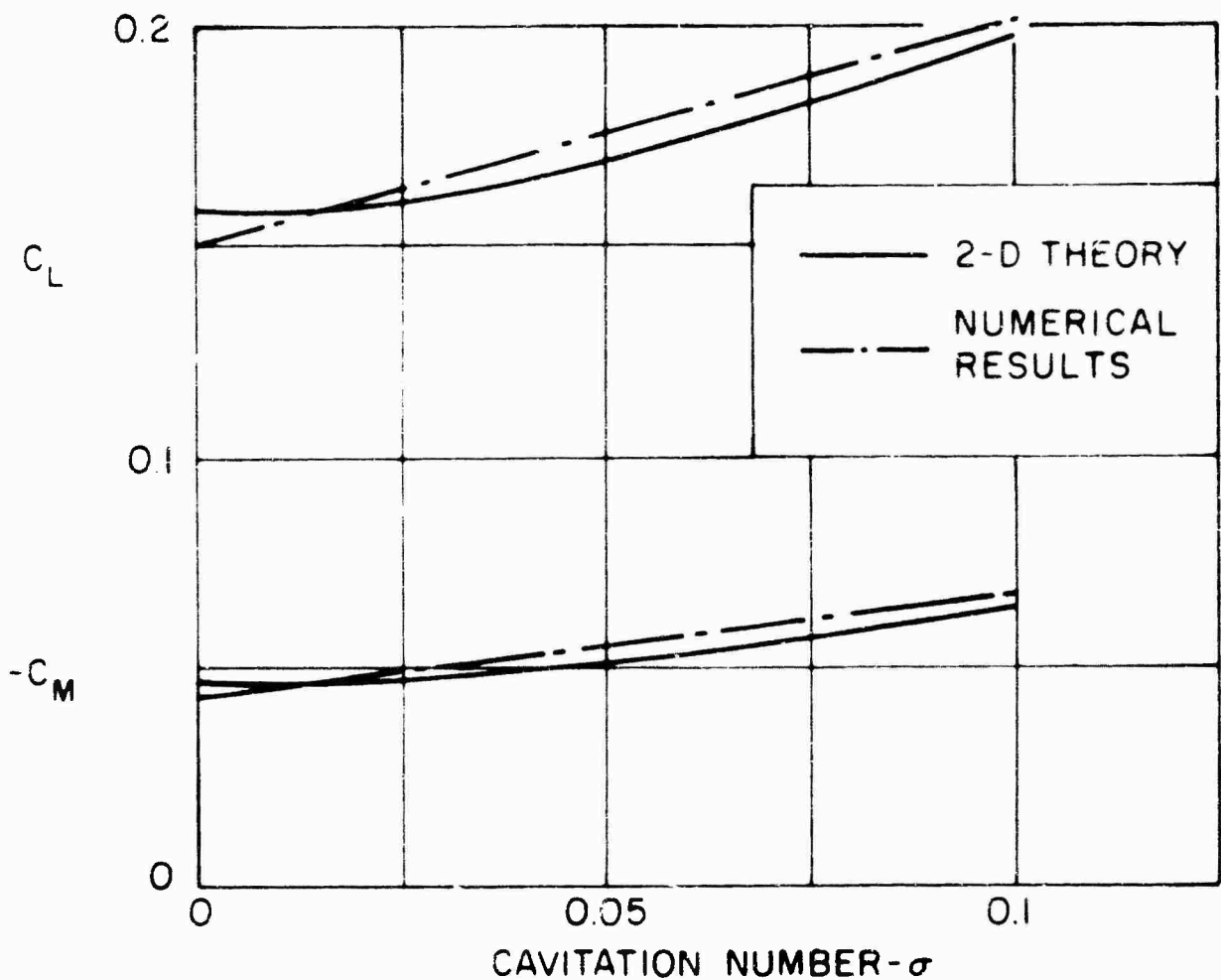
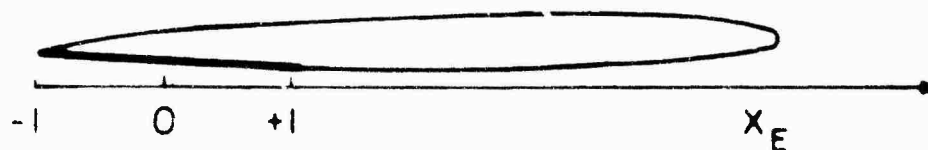


FIG. 3.15 LIFT AND MOMENT COEFFICIENTS VS σ . ($\alpha = 0.1$)
 NUMERICAL RESULTS FOR THE CENTER SECTION OF
 AN AR=6 FOIL; TWO-DIMENSIONAL THEORY

TABLE 3.2 NUMERICAL RESULTS, TABULATED FOR ASSUMED
 CAVITY LENGTH X_E

| X_E | $C_{L\alpha}$ | $C_{L\sigma}$ | $C_{M\alpha}$ | $C_{M\sigma}$ |
|-------|---------------|---------------|---------------|---------------|
| 5.0 | 1.5131 | .4019 | -.44159 | -.1485 |
| 7.0 | 1.5097 | .3783 | -.44058 | -.1385 |
| 9.0 | 1.5080 | .3629 | -.4300 | -.1337 |



3.3e Comparison with Other Three-Dimensional Theories and Experiment

Johnson (ref. (21), (22)) has developed a method for calculating lift and drag on a supercavitating hydrofoil at a cavitation number of zero. This theory is based on the assumption that the "influence of finite span on the two-dimensional lift coefficient is due to the effects of the trailing vorticity". For fully wetted flow, this assumption forms the basis of lifting line theory and its various refinements.

The results of this assumption in fully wetted flow give the following form for the lift coefficient. (see; e.g., Jones Ref. (24)).

$$C_L = 2\pi (\alpha - \alpha_i) \quad (3.74)$$

where α_i is the induced angle due to the trailing vorticity. Johnson assumes that for a supercavitating hydrofoil, the lift coefficient takes the same form with 2π , the lift curve slope for two-dimensional fully wetted flow replaced by $\pi/2$, the lift curve slope for supercavitating two-dimensional flow at a cavitation number of zero.

$$C_L = \frac{\pi}{2} (\alpha - \alpha_i) \quad (3.75)$$

α_i evaluated from lifting line theory for elliptical loading is

$$\alpha_i = \frac{C_L}{\pi R} \quad (3.76)$$

Glauerts modification (Ref. (25)) to α_i is used for rectangular planforms.

$$\alpha_i = \frac{C_L}{\pi AR} (1 + T) \quad (3.77)$$

where T is a planform correction. A correction for lift due to crossflow around the tips is also included

$$C_L = \frac{1}{A^2 + 1} \cdot BE \sin^2 \alpha \cos \alpha \quad (3.78)$$

The second theory for steady supercavitating foils was developed by Cumberbatch Ref. (23). This theory is valid for large aspect ratio foils at cavitation numbers for which the cavity length is of the order of the chord. ($-1 \cdot X_E \leq 1.5$). The model developed for this theory is a large aspect ratio foil with two-dimensional supercavitating flow over the foil except at the tips. At the tips, the wing tip vortices cause conical wing tip cavities. These wing tip cavities are treated by slender-body theory. The effect of the wing tip vortices on the flow away from the tips is handled by an induced angle correction.

$$C_L = C_{L_{2D}}(\sigma, \alpha - \alpha_i) \quad (3.79)$$

where α_i is the induced angle created by the two trailing cavitating vortices. $C_{L_{2D}}(\sigma, \alpha - \alpha_i)$ is the two-dimensional lift coefficient at cavitation number σ and local angle of attack $\alpha - \alpha_i$.

A few steady flow calculations were performed to compare with the experiments of Scheibe and Wetzel (Ref. 19) and with those of Kermeen (Ref. 20). The first set of experiments measured lift coefficients on flat plate supercavitating foils of aspect ratio 2.5, 4.0, and 6.0. The cavities were artificially created by injecting air on to the upper surface of the foil. The range of σ obtained in these tests was from about .05 to .3. In the second set of experiments, lift coefficients were measured for supercavitating flat plate foils of aspect ratio 4, 2, 1 and 1/2. The cavities on the foils were obtained naturally by pumping down the ambient tunnel pressure. Two values of σ were obtained for each test, σ_v calculated from the vapor pressure of water at the test conditions and the actual σ_k measured in the test.

Photographs included in both of these references reinforce our choice of a model for the cavity. The cavities are rectangular in shape, bounded by the cavities created by the trailing vortices. The trailing edge of the cavity is not sharply defined, but disappears in a region of turbulence and bubbles. Our neglect of a strong trailing edge singularity seems justified by these photographs.

Experimental results of cavity length v.s. (σ/α) are shown in Fig. 3.16 . If the cavity length is about three times that of the chord, our numerical method is valid.

Fig. 3.17 shows the results of numerical calculations for an aspect ratio 6 flat plate supercavitating foil, as compared to experiment. Two cavity lengths were assumed, as cavity of three times the chord, and a cavity of five times the chord. The results of the calculation for $\alpha = .148$ show the insensitivity of the load prediction to assumed cavity length. The lift coefficients for $\sigma = 0$ as predicted by the method outlined by Johnson are also shown on this figure. Since this method is based on linearized theory, both α and σ should be small; the disagreement at high α and σ is not unexpected.

Calculations were done for an aspect ratio 4 supercavitating foil at an angle of attack of 10° ($\alpha = .175$ rad.) with assumed cavity length three times the chord. Fig. 3.18 shows lift coefficient vs cavitation number for the numerical results obtained by this method as compared to the theory of Cumberbatch (ref.(23)) and with the experiments of Ref. (19) and (20). The $\sigma = 0$ point as predicted by the method of Johnson is also shown. The numerical method is in good agreement with the available theories, the agreement with experiment is rather poor.

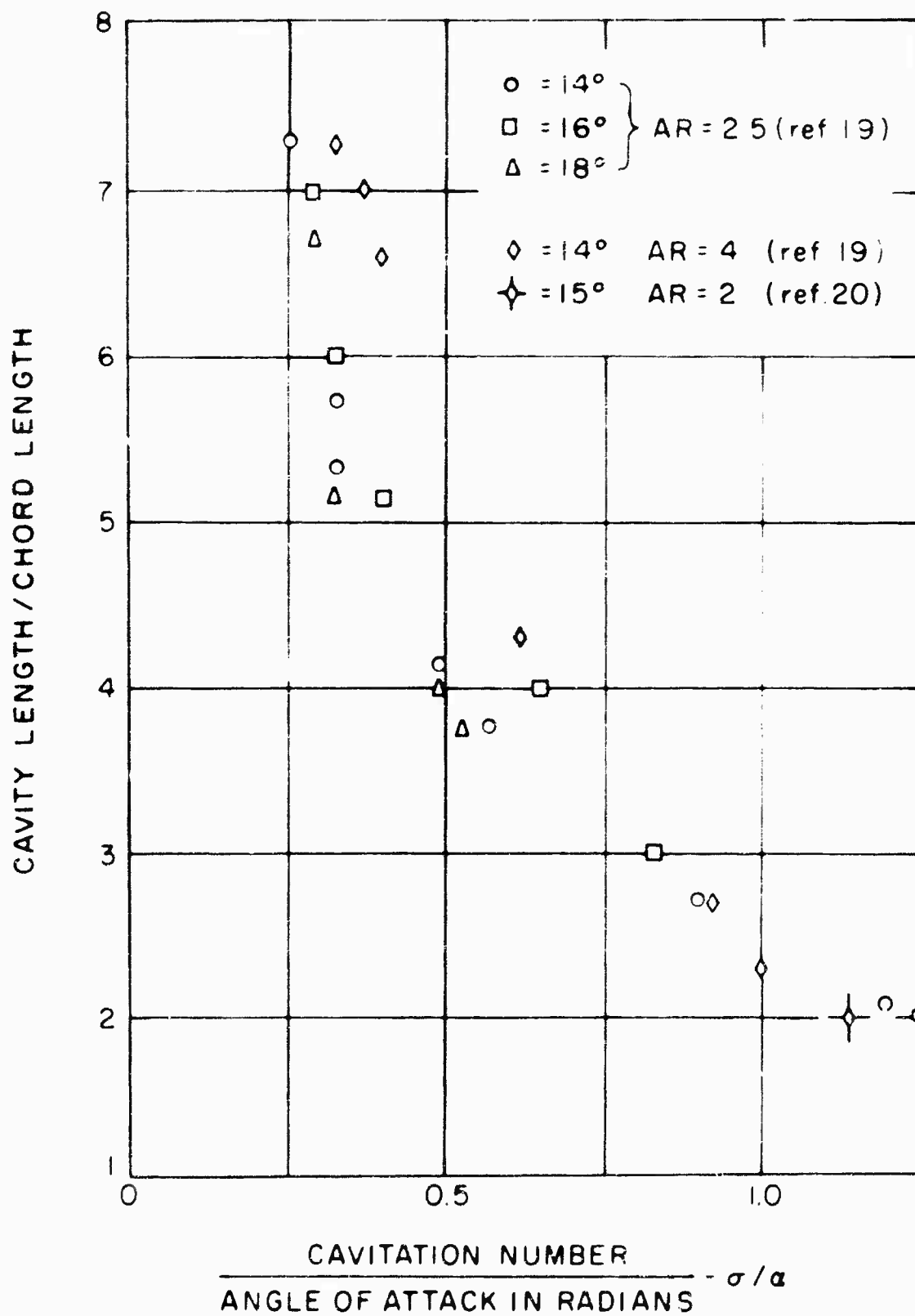


FIG. 3.16 EXPERIMENTAL RESULTS FOR CAVITY LENGTH VS σ/α

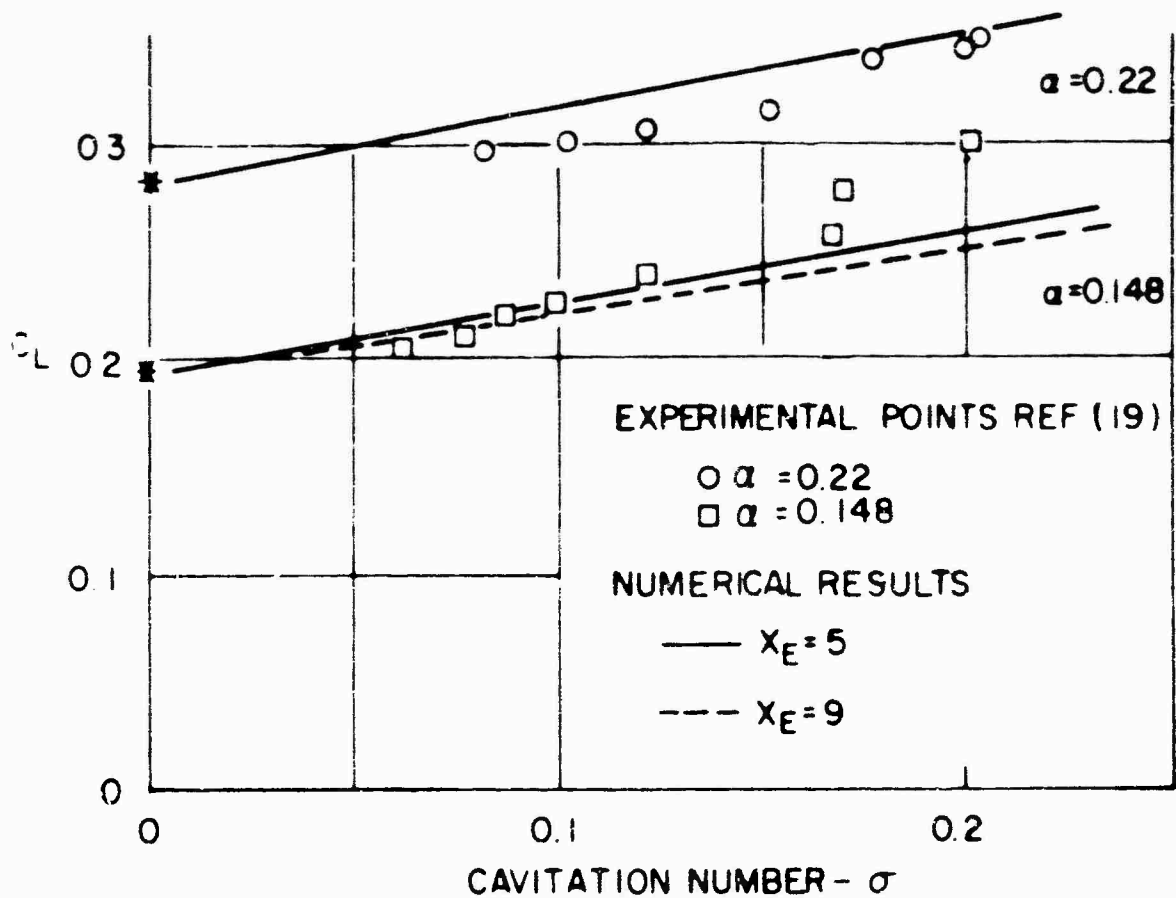


FIG 3.17 COMPARISON BETWEEN NUMERICAL RESULTS AND EXPERIMENT FOR AN ASPECT RATIO 6 FOIL LIFT COEFFICIENT VS CAVITATION NUMBER σ

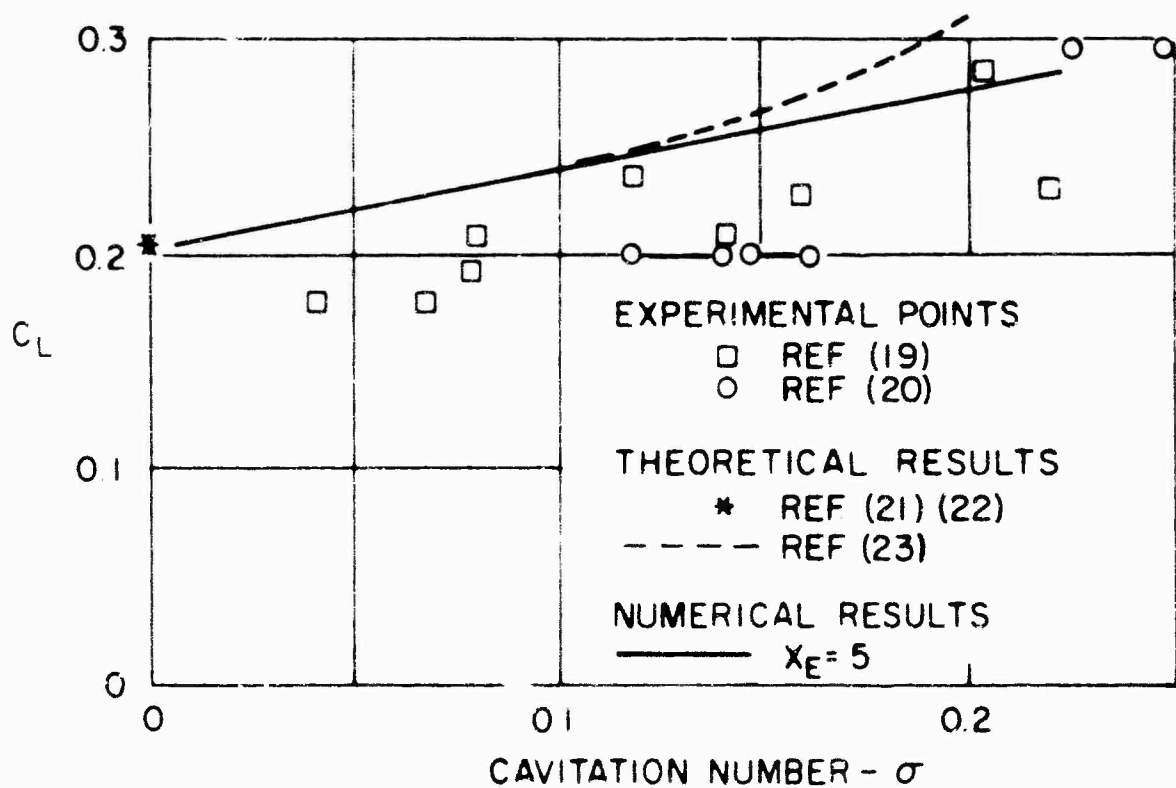


FIG 3.18 LIFT COEFFICIENT VS CAVITATION NUMBER FOR AN ASPECT RATIO 4 FOIL ($\alpha = 10^\circ$); COMPARISON WITH EXPERIMENT AND OTHER THEORIES

3.3f Lift and Moment on an Oscillating Supercavitating Hydrofoil of Finite Span

The lift and moment coefficients for an oscillating supercavitating hydrofoil were calculated using the numerical method described previously. For these cases, the boundary conditions on the complex amplitude of upwash on the wetted surface was satisfied at 15 control points, the boundary condition on the pressure in the cavity was satisfied at 33 control points. Results for assumed cavity lengths of two and three times the chord differed by about 2%. Computation time for a case with two assumed cavity lengths was under three minutes on the IBM7090.

The unsteady aerodynamic coefficients for the center section of an aspect ratio six foil in heave and pitch about the leading edge are compared with the two-dimensional coefficients as predicted by Woods (ref. 29). These coefficients are plotted vs reduced frequency k in Fig. 3.19 to 3.22 by use of the following definitions:

$$C_{L_{hr}} + i C_{L_{hi}} = \frac{\text{lift due to heave}}{\rho V^2 b_0 i k h_0}$$

$$C_{L_{\alpha r}} + i C_{L_{\alpha i}} = \frac{\text{lift due to pitch about L.E.}}{\rho V^2 b_0 \alpha_0}$$

$$C_{M_{hr}} + i C_{M_{hi}} = \frac{\text{moment about L.E. due to heave}}{2\rho V^2 b_0^2 i k h_0}$$

$$C_{M_{\alpha r}} + i C_{M_{\alpha i}} = \frac{\text{moment about L.E. due to pitch}}{2\rho V^2 b_0^2 \alpha_0}$$

The total value of the unsteady aerodynamic coefficients are shown in Fig. 3.19 to 3.22 for an aspect ratio six foil and in Fig. 3.23 to 3.26 for an aspect ratio one foil.

The general behavior of the coefficients with reduced frequency is the same for the two-dimensional foil and the foils of finite aspect ratio. The magnitudes are of course less for the finite aspect ratio foils.

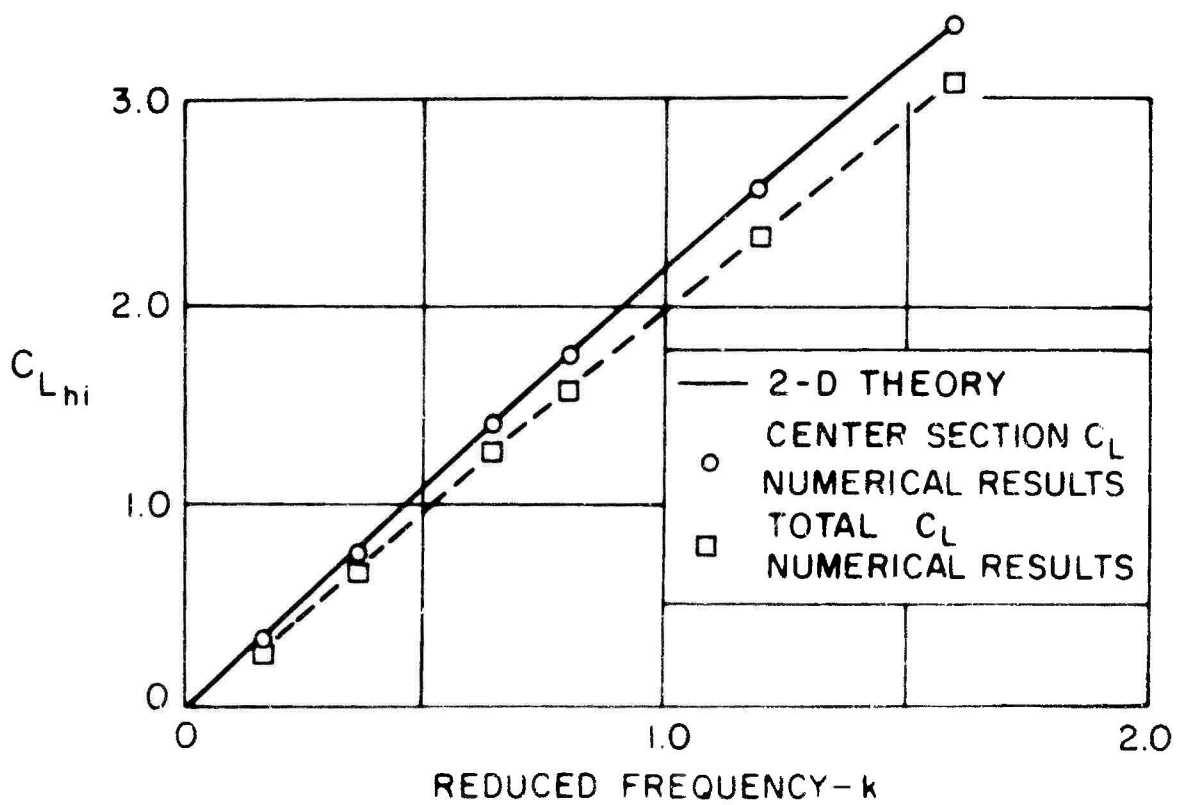
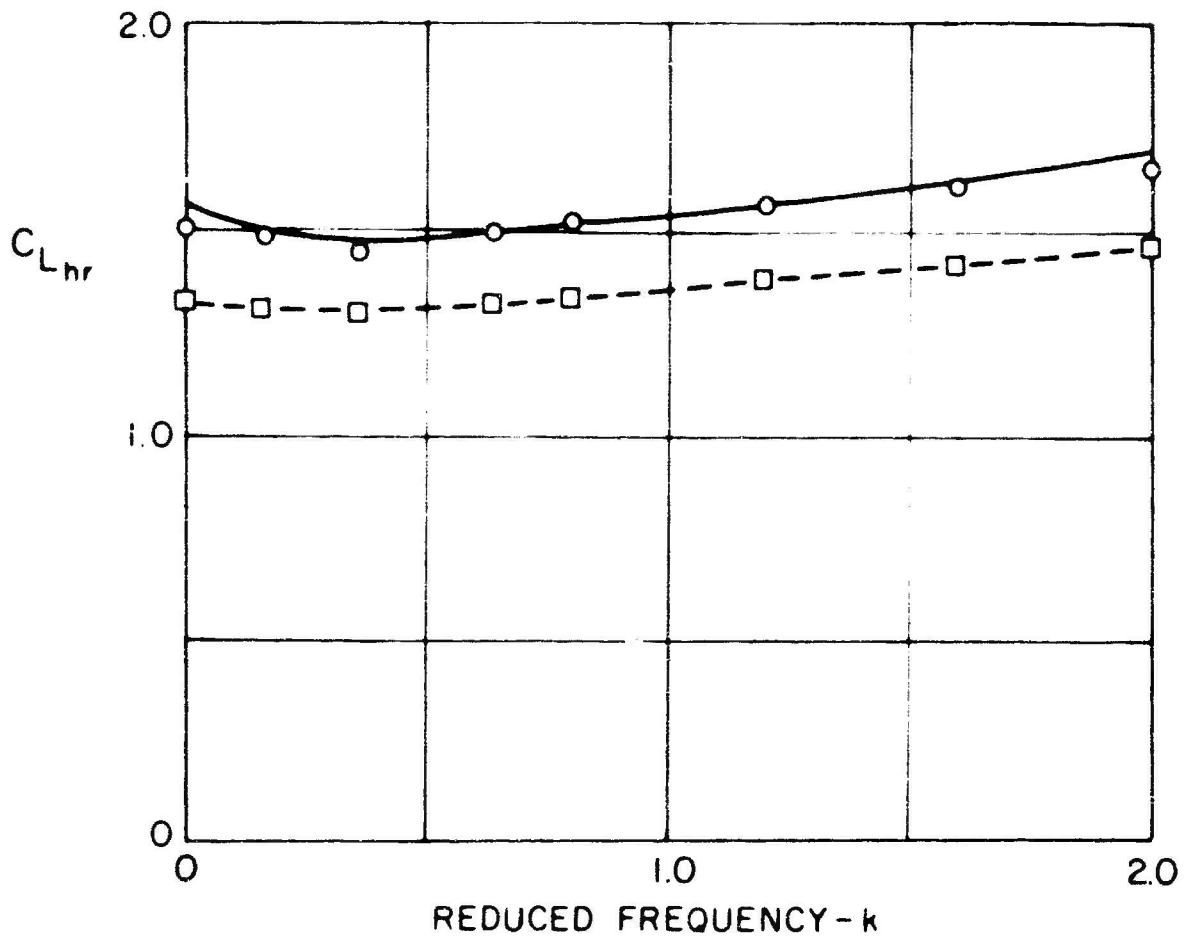


FIG. 3.19 LIFT COEFFICIENT DUE TO HEAVE FOR AN ASPECT RATIO 6 SUPECAVITATING FOIL COMPARISON WITH TWO-DIMENSIONAL THEORY

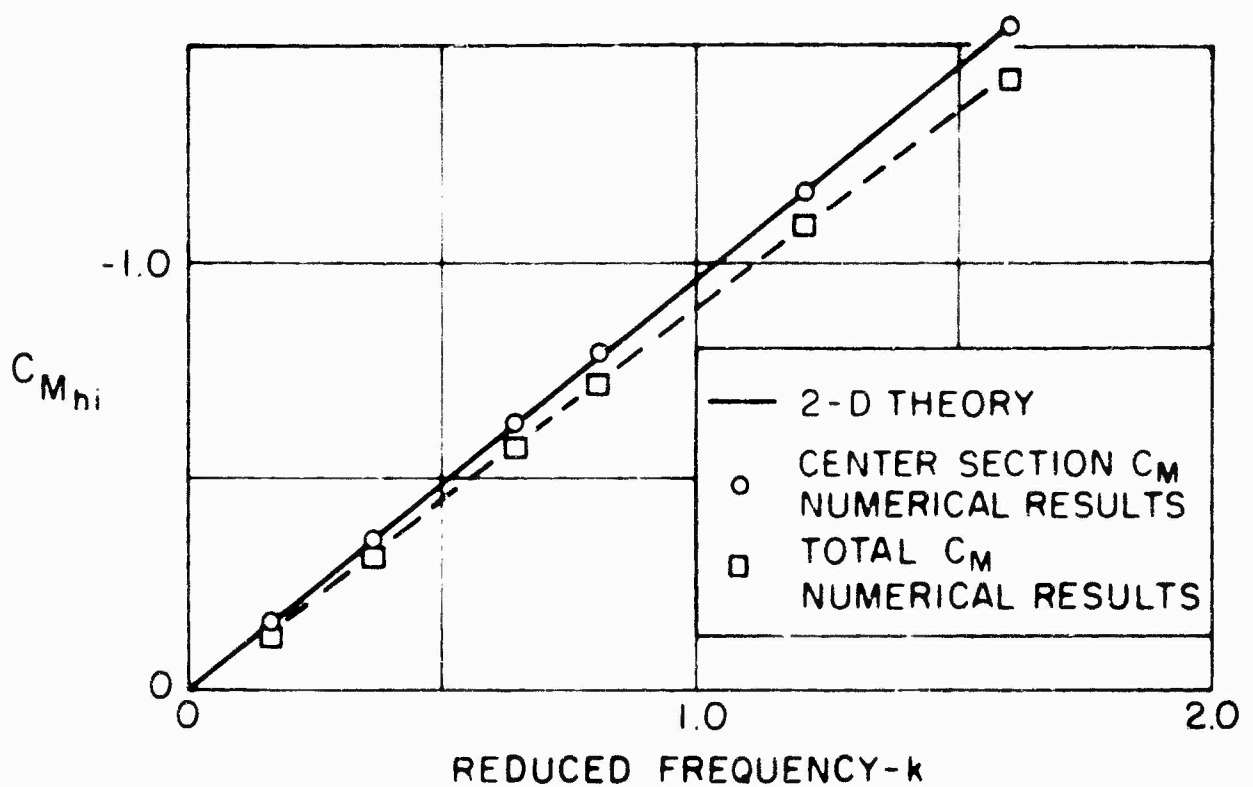
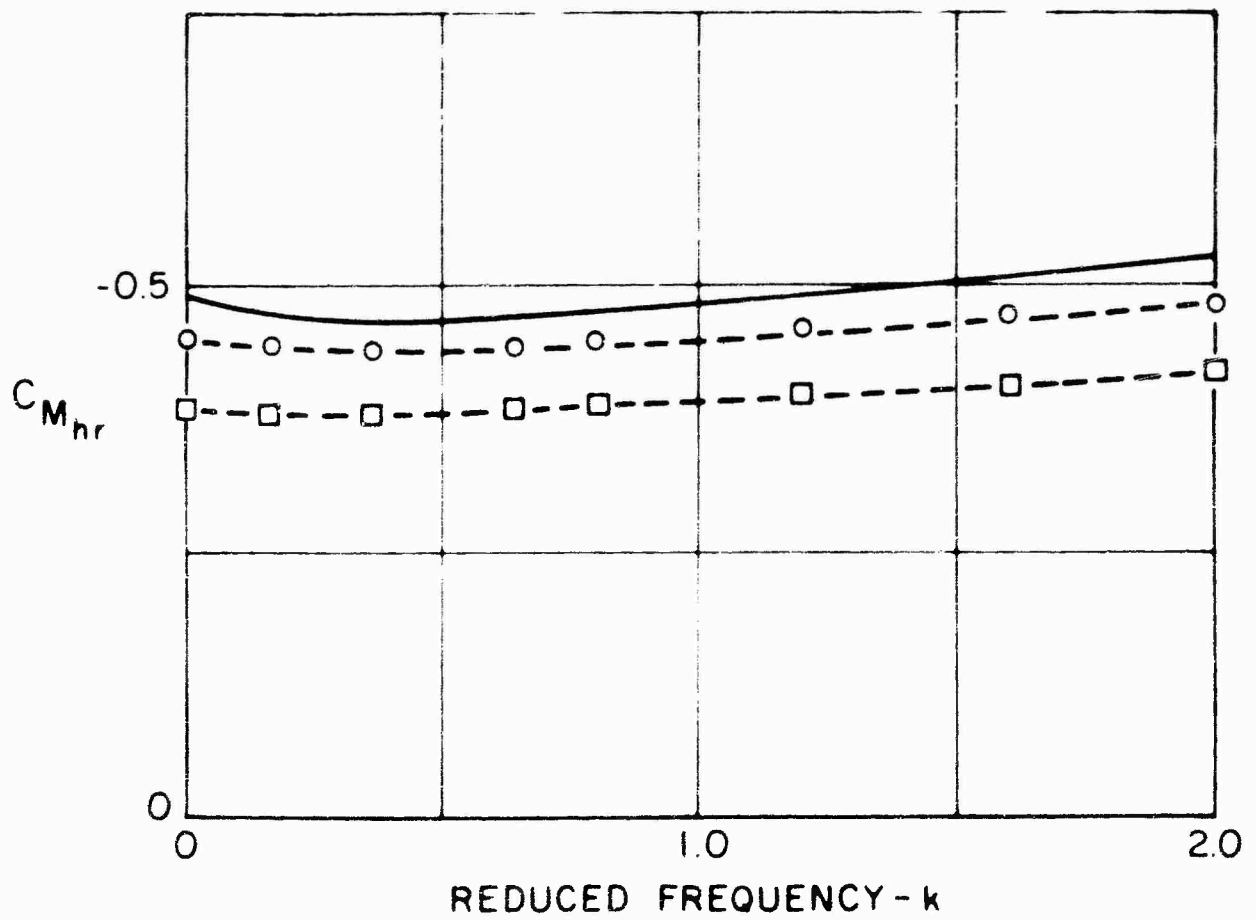


FIG. 3.20 MOMENT COEFFICIENT DUE TO HEAVE FOR AN ASPECT RATIO 6 SUPERCAVITATING FOIL COMPARISON WITH TWO-DIMENSIONAL THEORY

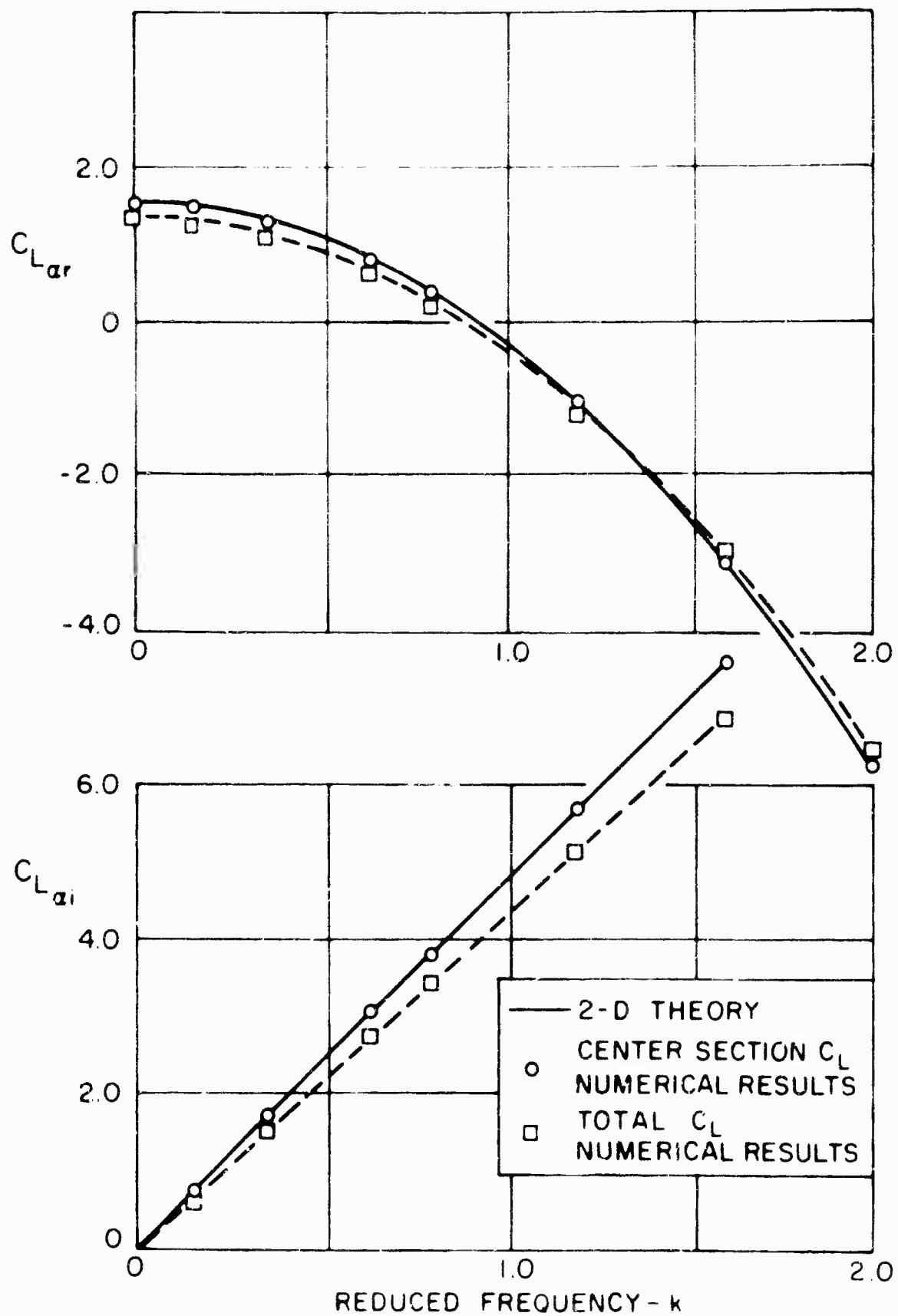


FIG. 3.21 LIFT COEFFICIENT DUE TO PITCH FOR AN ASPECT RATIO 6 SUPERCAVITATING FOIL COMPARISON WITH TWO-DIMENSIONAL THEORY

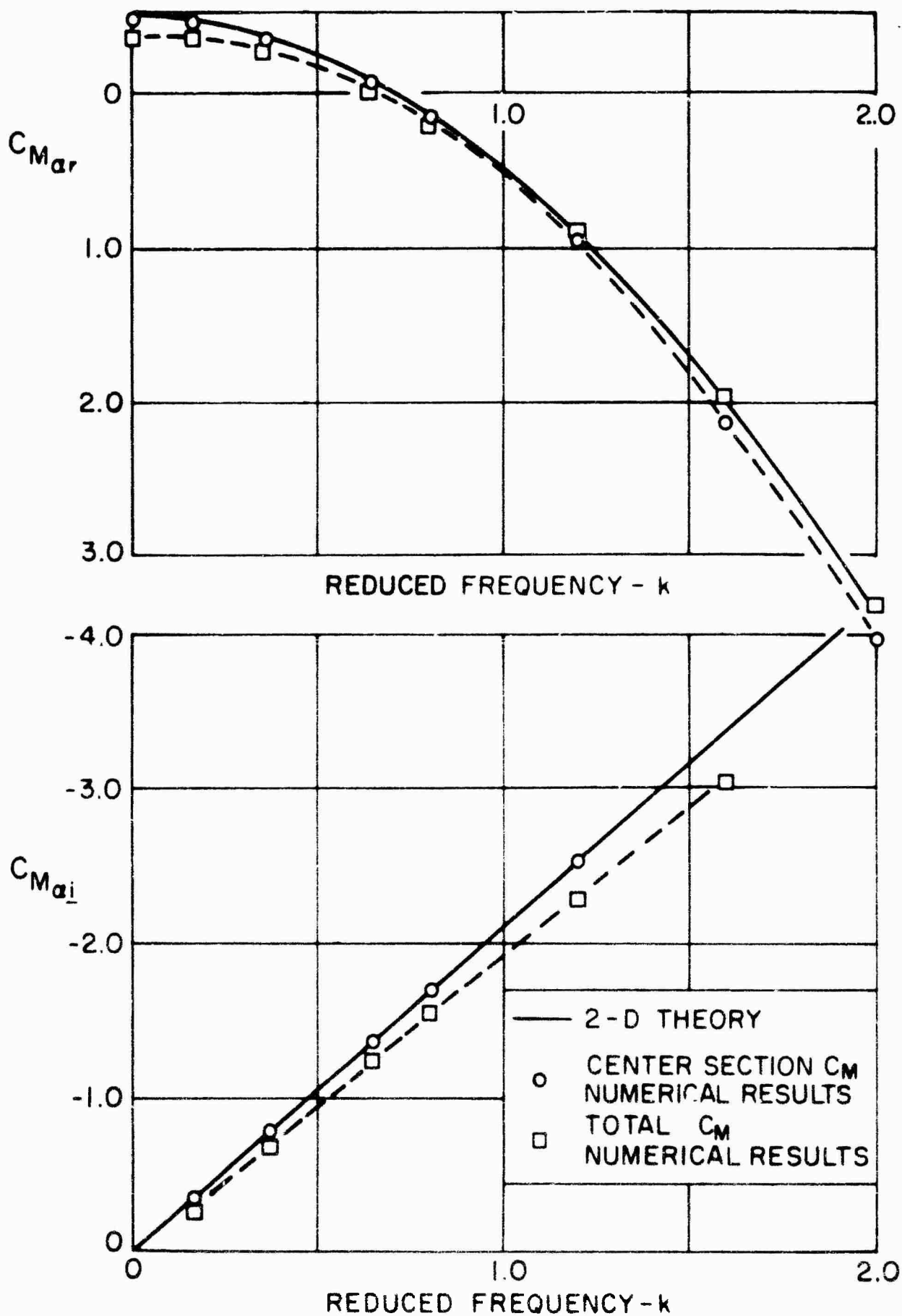


FIG. 3.22 MOMENT COEFFICIENT DUE TO PITCH FOR AN ASPECT RATIO 6 SUPERCAVITATING FOIL COMPARISON WITH TWO-DIMENSIONAL THEORY

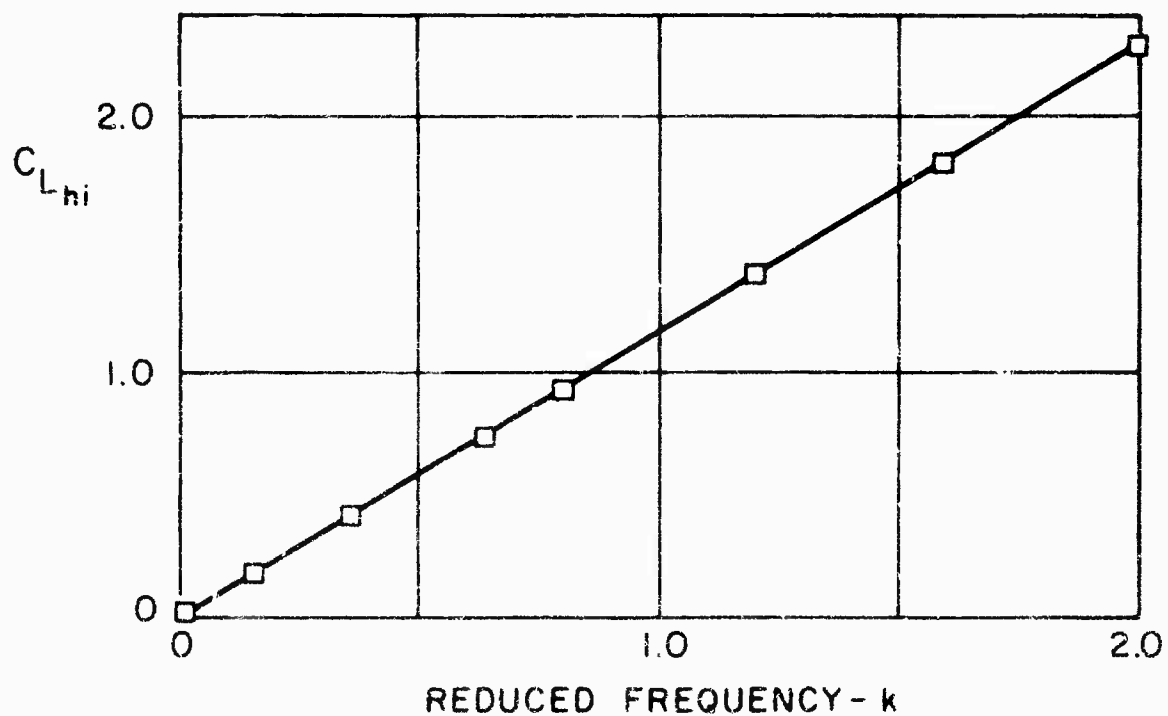
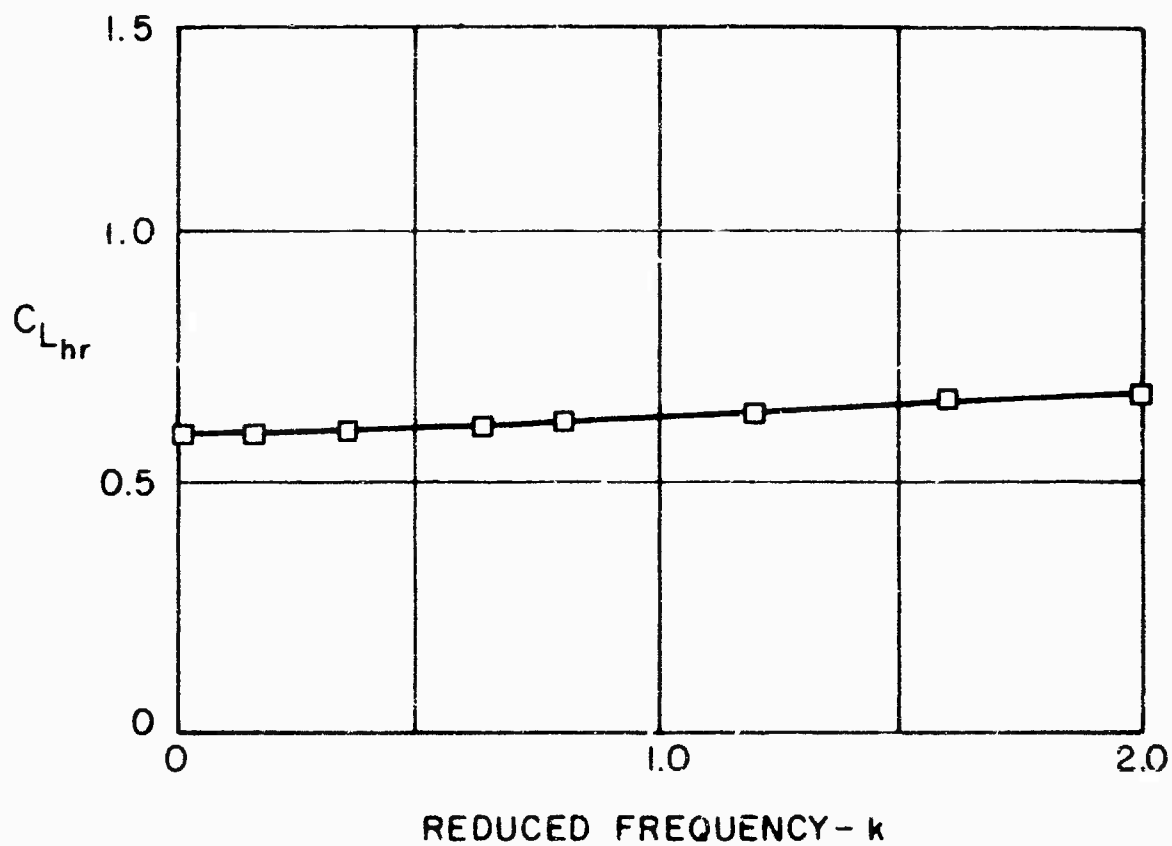


FIG. 3.23 LIFT COEFFICIENT DUE TO HEAVE FOR AN ASPECT RATIO ONE SUPERCAVITATING FOIL

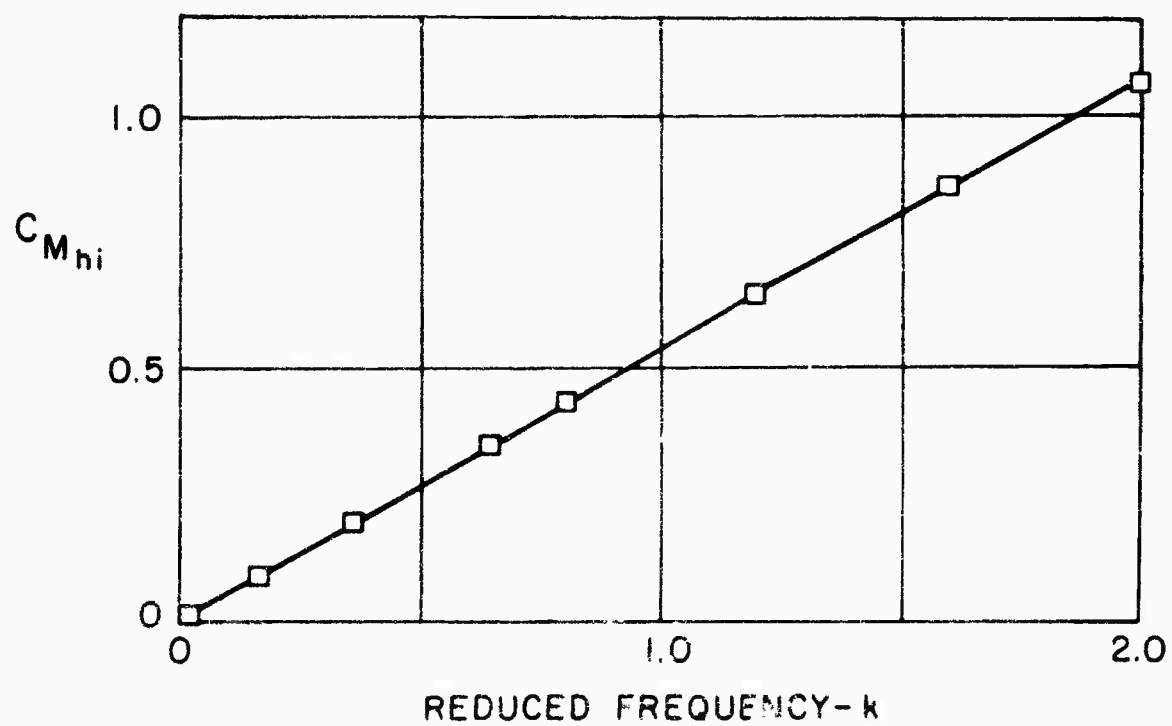
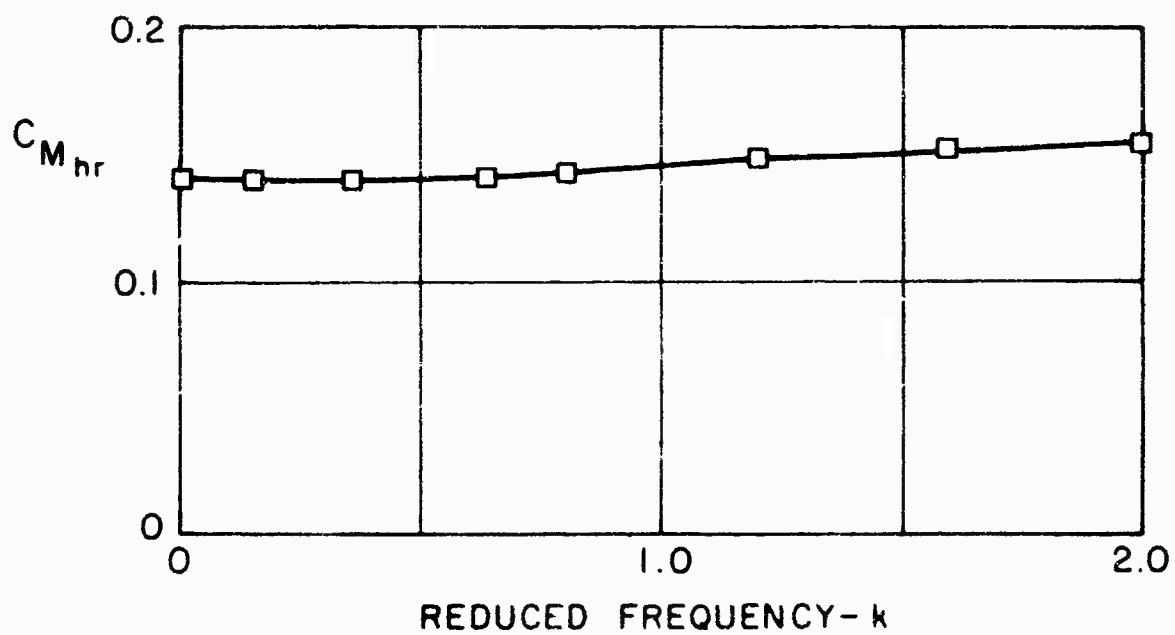


FIG. 3.24 MOMENT COEFFICIENT DUE TO HEAVE FOR A ASPECT RATIO ONE SUPERCAVITATING FOIL

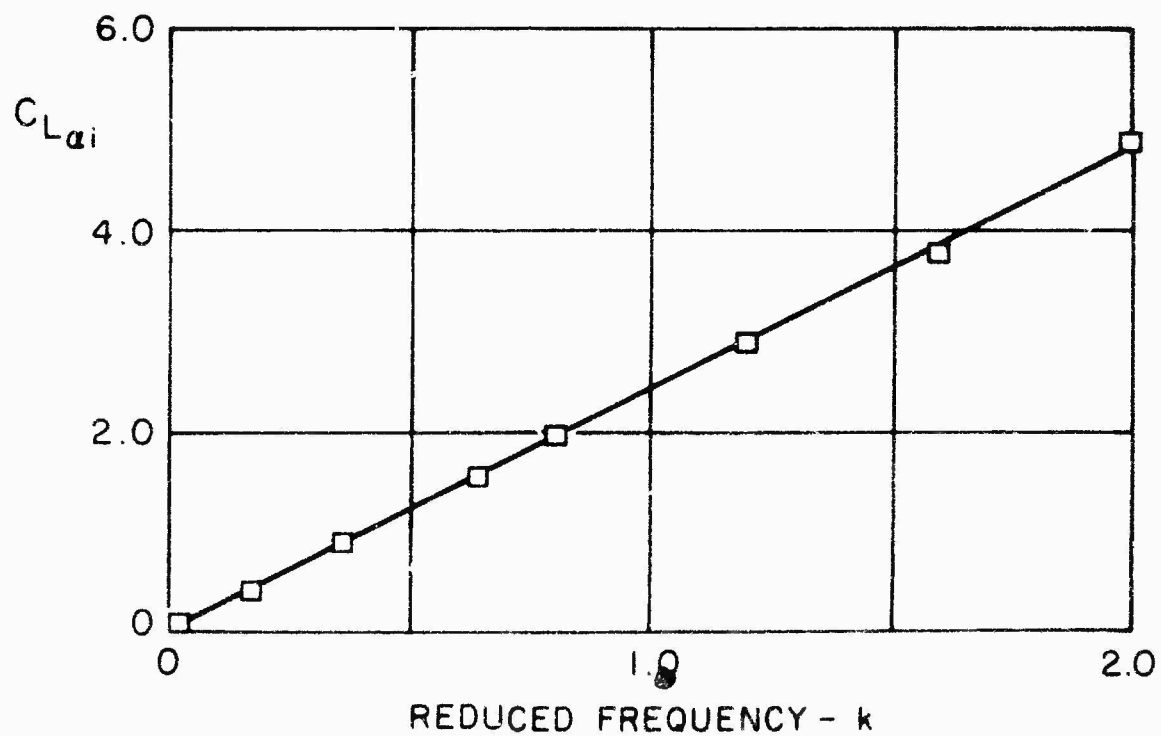
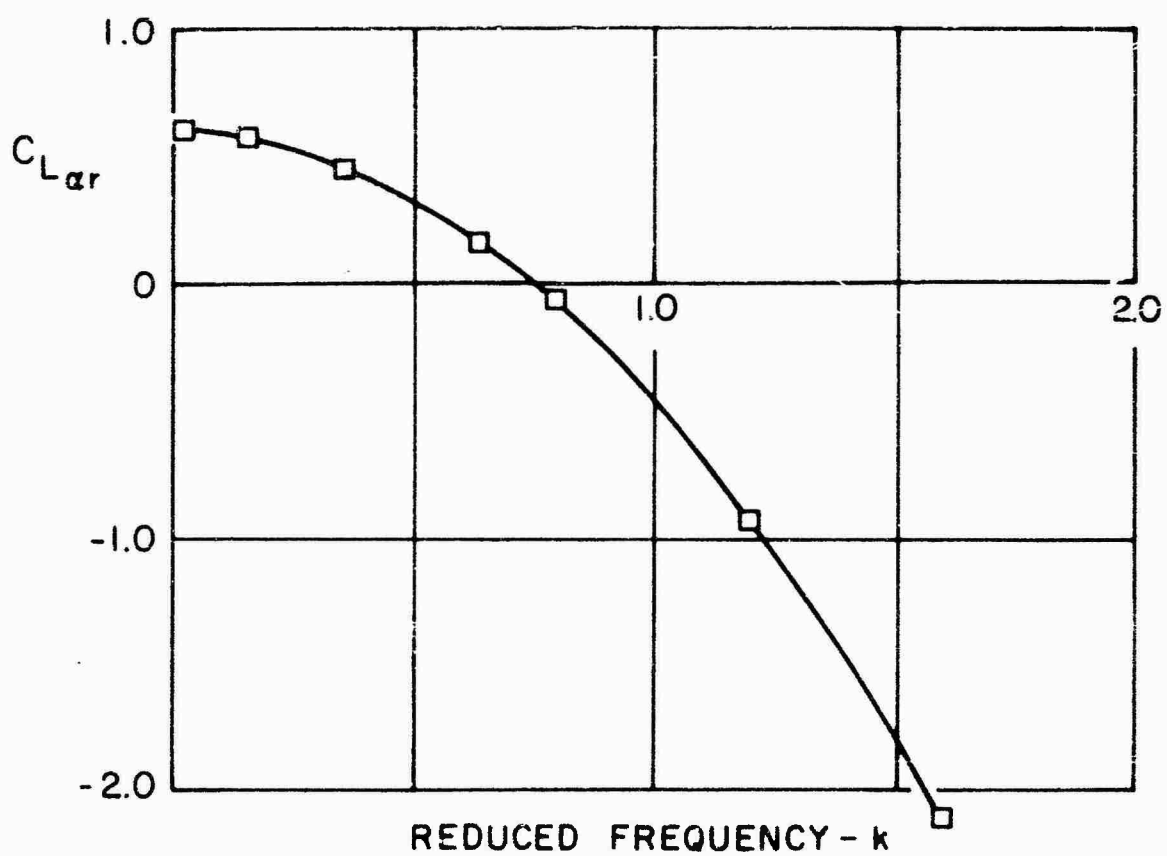


FIG. 3.25 LIFT COEFFICIENT DUE TO PITCH FOR AN ASPECT RATIO ONE SUPERCAVITATING FOIL

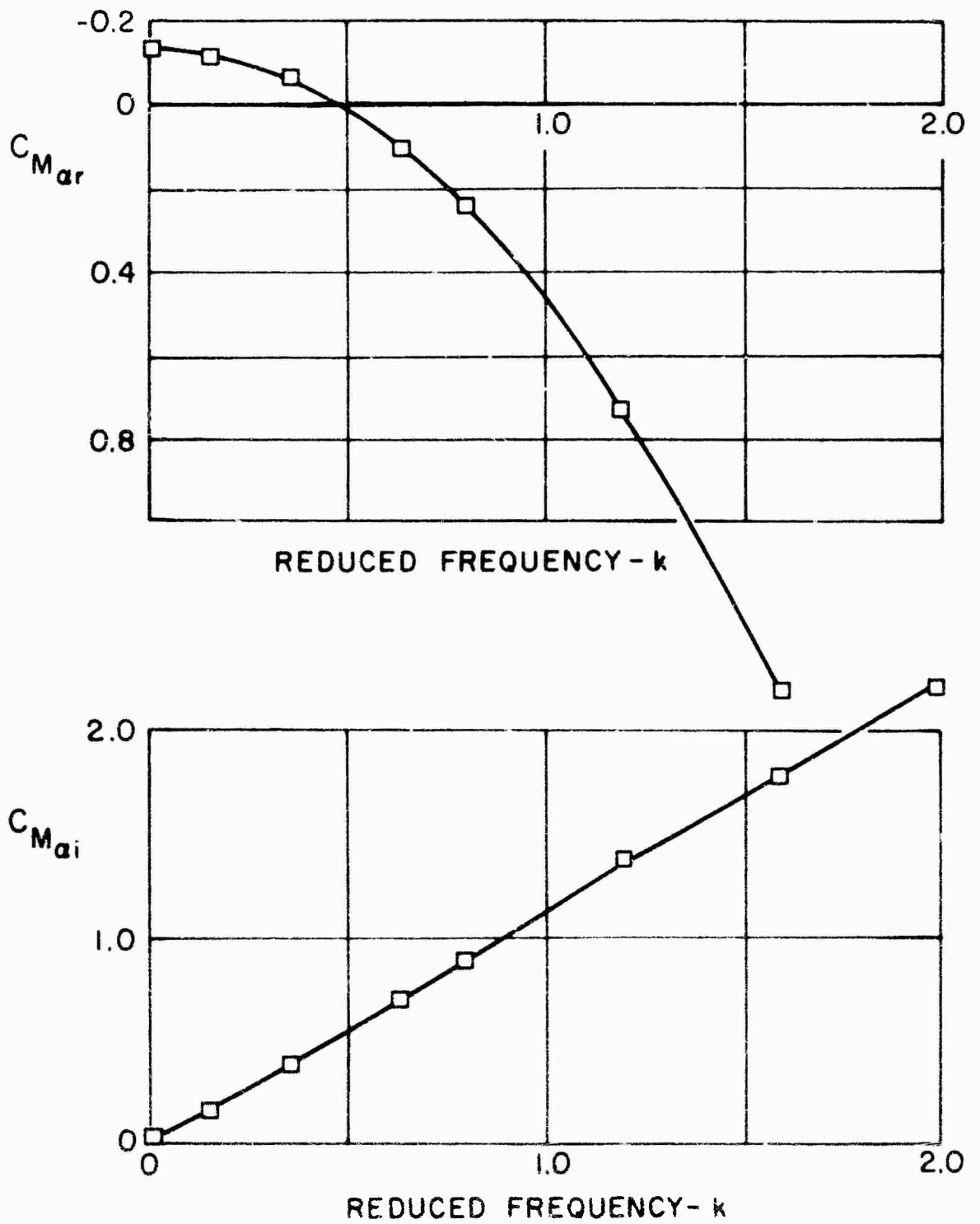


FIG.3.26 MOMENT COEFFICIENT DUE TO PITCH FOR AN ASPECT RATIO ONE SUPERCAVITATING FOIL

CHAPTER IV

CONCLUSIONS AND RECOMMENDATIONS

Numerical solution of the linearized integral equation for a sheet of pressure singularities has been shown to constitute a powerful tool in dealing with steady and unsteady problems of thin lifting surfaces moving through a liquid. The general technique of deriving the kernel function analytically and solving the resulting integral equations numerically by assumed modes results in an efficient procedure. It is felt that these techniques and further extensions and refinements constitute the best linearized solutions available for a wide variety of lifting-surface problems.

Certain comparison with experiments made in water fail because of effects which are outside the scope of an inviscid linearized theory. The apparent inadequacy of the Kutta condition at high reduced frequencies, noted in Chapter I, is an example. The disagreement between experiments and numerical calculations for steady supercavitating foils at finite angles of attack could also be mentioned. As yet, there are no loading measurements on oscillating hydrofoils of large aspect ratio running parallel to the free surface at low values of kF^2 . Experiments on supercavitating foils of finite span in unsteady vibration are currently being performed by Acosta at the California Institute of Technology.

The method for fully wetted nonplanar surfaces has wide applicability to interference problems. Experiments on steady and unsteady motion of nonplanar surfaces such as T tails would be very valuable to check the accuracy of the load predictions. After investigation of the kernel functions for helical motion, this approach could also be used for the more complicated problems of thin lifting propellor and helicopter blades. The treatment of the effect of gravity waves on an oscillating foil could be extended to compute "gust loads" on a foil running beneath waves. The three-dimensional kernel function can be evaluated numerically without difficulty if finite-span effects are of interest. The influence of cavity closure conditions on the predicted steady and unsteady loads on a supercavitating foil should be investigated further. Also more refined models for supercavitating foils could be developed with continuous functions, which have the proper singularities, assumed for the pressure source modes. The kernel functions for a supercavitating foil traveling close to a free surface at infinite Froude number can be derived straightforwardly by means of images and the numerical technique extended to cover this case.

1. Thwaites, B., Editor; Incompressible Aerodynamics, Clarendon Press, Oxford (1960).
2. Theodorsen, Theodore; General Theory of Aerodynamic Instability and The Mechanism of Flutter; NACA Report 496, (1935).
3. Schade, T.H., and Krienes, K., "The Oscillating Circular Airfoil on the Basis of Potential Theory"; NACA TM 1098 (1947).
4. Kochin, N.E.; "Steady Vibration of Wing of Circular Plan Form Theory of Wing of Circular Plan Form"; NACA TM 1324, (1953).
5. Stratton, J.A.; Electromagnetic Theory; McGraw-Hill Book Co., (1941).
6. Watkins, C.E., Runyan, H.L., and Woolston, D.S.; On the Kernel Function of the Integral Equation Relating the Lift and Downwash Distributions of Oscillating Finite Wings at Subsonic Speeds; NACA Report 1234, (1955).
7. Watkins, C.E., Woolston, D.S. and Cunningham, H.J.; A Systematic Kernel Function Procedure for Determining Aerodynamic Forces on Oscillating or Steady Finite Wings at Subsonic Speeds; NASA Report R-48, (1959).
8. Landahl, M.T., Ashley, H., and Widnall, S., "Some Free Surface Effects on Unsteady Hydrodynamic Loads and Hydroelasticity"; Preprints of the Fourth Symposium on Naval Hydrodynamics; Washington, D.C., August, 1962; Office of Naval Research ACR-73, Vol. II, pp. 490-518 (proceedings in preparation).

9. Ashley, H., Widnall, S., and Landahl, M.T., New Directions In Lifting Surface Theory; Aero Space Sciences Meeting, AIAA, New York, New York, January 20-22, 1964; preprint No. 64-1.
10. Dwight, H.B., Tables of Integrals and Other Mathematical Data; The MacMillian Company, 1961.
11. Mangler, K.W. "Improper Integrals in Theoretical Aerodynamics;" Aeronautics Research Council, RAE, Report No. Aero 2424, London, 1951.
12. Ransleben, G.E., Jr., and Abramson, H.N.; Experimental Determination of Oscillatory Lift and Moment Distributions on Fully Submerged Flexible Hydrofoils; Southwest Research Institute, Report No. 2, Contract No. Nonr-3335(00), (1962).
13. Bateman Manuscript Project, California Institute of Technology, "Integral Transforms"; Vol. I; McGraw-Hill Book Company, Inc., (1954).
14. Stoker, J.J.; Water Waves; Interscience Publishers, Inc., New York, (1957).
15. Tan, H.S.; "Waves Produced by a Pulsating Source Traveling Beneath a Free Surface"; Quarterly of Applied Math; Vol 15, (1957-58).
16. Kaplan, Paul; "The Waves Produced by the Forward Motion of an Oscillatory Pressure Distribution"; Midwest Conference of Solid and Fluid Mechanics; April 1957.
17. Kaplan, Paul; "Comments on the Paper--Waves Produced by a Pulsating Source Traveling Beneath a Free Surface"; Quarterly of Applied Math, Vol. 1, 16, (1958)

18. Crimi, P., and Statler, I.H.; "Forces and Moments on an Oscillating Hydrofoil"; Preprints of the Fourth Symposium on Naval Hydrodynamics; Washington, D.C., August 1962; Office of Naval Research ACR-73, Vol. II, pp. 447-466 (proceedings in preparation).
19. Schiepe, E.R. and Wetzel, J.M.; Ventilated Cavities on Submerged Three-Dimensional Hydrofoils; University of Minnesota, St. Anthony Falls Hydrolic Laboratory Technical Paper No. 36, Series B., December 1961).
20. Kermeen, R.W.; Experimental Investigations of Three-Dimensional Effects on Cavitating Hydrofoils; Engineering Division, California Institute of Technology; Rep. 47-14, September 1960.
21. Johnson, Virgil E., Jr.; Theoretical and Experimental Investigation of Supercavitating Hydrofoils Operating Near the Free Water Surface; NASA Technical Report R-93, 1961.
22. Johnson, V.E., Jr.; "Supercavitating Hydrofoils at Zero Cavitation Numbers"; Second Symposium on Naval Hydrodynamics, Washington, D.C., August 1958.
23. Cumberbatch, E., Cavitating Flow Past a Large Aspect-Ratio Hydrofoil; Engineering Division, California Institute of Technology, Rep. 47-12, May 1960.
24. Jones, R.T.; "Correction of Lifting-Line Theory for the Effect of the Chord"; NACA TN 817, 1941.
25. Glauert, H.; The Elements of Airfoil and Airscrew Theory; Second Edition; Cambridge University Press, 1947, (reprinted 1948).

26. Gilbarg, David; "Jets and Cavities"; Hanbuch Der Physik, Vol. IX, Fluid Dynamics III, Editor C. Truesdell, 1960.
27. Proc. Second ONR Symposium on Naval Hydrodynamics, Washington, D.C., August 1958; Government Printing Office.
28. Tulin, M.P., and Burkark, M.P.; Linearized Theory for Flows about Lifting Foils at Zero Cavitation Number; David Taylor Model Basin, Dept. C-638, February, 1955.
29. Woods, L.C.; Aerodynamic Forces on an Oscillating Airfoil Fitted with a Spoiler; Proceedings of the Royal Society, Series A., Vol. 239, 1957; pp. 328-337.
30. Parkin, B.R.; Fully Cavitating Hydrofoils in Non-Steady Motion; Engineering Division, California Institute of Technology; Rep. 85-2, July 1957.
31. Timman, R.; "A General Linearized Theory for Cavitating Hydrofoils in Non-Steady Flow"; Second Symposium on Naval Hydrodynamics; Washington, D.C., August 1958.
32. Guerst, J.A.; Linearized Theory of Two-Dimensional Cavity Flows; Doctoral Disertation. Techn. Hogeschool Deift, May 1961.
33. Tulin, M.P.; "Cavitation", Handbook of Fluid Dynamics, Chapter 12; Editor V.L. Streeter, McGraw-Hill Book Co.
34. Kaplan, Paul and Henry, C.J.; "A Study of the Hydroelastic Instabilities of Supercavitating Hydrofoils"; Journal of Ship Research, Vol. 4, No. 3, December 1960.
35. Fabula, A.; "Thin Airfoil Theory Applied to Hydrofoils with Single Finite Cavity and Arbitrary Free Streamline Detachment"; Journal of Fluid Mechanics, Vol. 12, pt. 2, Feb. 1962.

APPENDIX 1

**EVALUATION OF KERNEL FUNCTIONS
FOR STEADY AND UNSTEADY
THREE DIMENSIONAL FLOW**

We wish to evaluate the following functions:

$$K_1 = -\lim_{z \rightarrow 0^{\pm}} \left\{ \frac{e^{-iK(x-z)}}{4\pi} \frac{\partial}{\partial z} \int_{-\infty}^{x-z} \frac{e^{iK\lambda} d\lambda}{\sqrt{\lambda^2 + (y-y_0)^2 + z^2}} \right\} \quad (1)$$

$$K_1 = -\lim_{z \rightarrow 0^{\pm}} \left\{ \frac{1}{4\pi} \frac{\partial}{\partial z} \int_{-\infty}^{x-z} \frac{d\lambda}{\sqrt{\lambda^2 + (y-y_0)^2 + z^2}} \right\} \quad (2)$$

$$K_2 = -\lim_{z \rightarrow 0^{\pm}} \left\{ \frac{e^{-iK(x-z)}}{4\pi} \frac{\partial^2}{\partial z^2} \int_{-\infty}^{x-z} \frac{e^{iK\lambda} d\lambda}{\sqrt{\lambda^2 + (y-y_0)^2 + z^2}} \right\} \quad (3)$$

$$K_2 = -\lim_{z \rightarrow 0^{\pm}} \left\{ \frac{1}{4\pi} \frac{\partial^2}{\partial z^2} \int_{-\infty}^{x-z} \frac{d\lambda}{\sqrt{\lambda^2 + (y-y_0)^2 + z^2}} \right\} \quad (4)$$

$$K_3 = \lim_{z \rightarrow 0^{\pm}} \left\{ \frac{\partial}{\partial z} \left(\frac{1}{\sqrt{(x-z)^2 + (y-y_0)^2 + z^2}} \right) \right\} \quad (5)$$

Evaluation of K_1

$$K_1 = \lim_{z \rightarrow 0^{\pm}} \left\{ \frac{-1}{4\pi} \frac{z}{z} \int_{-\infty}^{x-3} \frac{d\lambda}{\sqrt{\lambda^2 + (y-\eta)^2 + z^2}} \right\}$$

$$K_1 = \lim_{z \rightarrow 0^{\pm}} \left\{ \frac{+z}{4\pi} \int_{-\infty}^{x-3} \frac{d\lambda}{(\lambda^2 + (y-\eta)^2 + z^2)^{3/2}} \right\}$$

$$= \lim_{z \rightarrow 0^{\pm}} \left\{ \frac{1}{4\pi} \frac{z}{(y-\eta)^2 + z^2} \left(\frac{x-3}{\sqrt{(x-3)^2 + (y-\eta)^2 + z^2}} + 1 \right) \right\}$$

The expression

$$\lim_{z \rightarrow 0^{\pm}} \left\{ \frac{-z}{z^2 + (y-\eta)^2} \right\}$$

is a generalized function defining the delta function except for a constant of proportionately, A . This constant is determined by requiring

$$A \lim_{z \rightarrow 0^{\pm}} \left\{ -z \int_{-\infty}^{\infty} \frac{dx}{z^2 + (y-\eta)^2} \right\} = 1$$

such that

$$\lim_{z \rightarrow 0^{\pm}} \frac{-Az}{z^2 + (y-\eta)^2} = \delta(y-\eta)$$

$$-\int_{-\infty}^{\infty} \frac{z}{z^2 + (y-\eta)^2} d\eta = \frac{-z}{|z|} \pi$$

and

$$\lim_{z \rightarrow 0^{\pm}} \left\{ \frac{-z}{z^2 + (y-\eta)^2} \right\} = \mp \pi \delta(y-\eta)$$

The expression for K_1 becomes

$$K_1^{\pm} = \mp \delta(y-\eta) \pi \left(\frac{x-3}{\sqrt{(x-3)^2 + (y-\eta)^2}} + 1 \right)$$

The expression in brackets for $z=0$ and $(y-\eta) = 0$ is proportional to the Heavyside function.

$$\frac{x-3}{|x-3|} + 1 = 2 H(x-3)$$

$$K_1^{\pm}(x-3, y-\eta) = \pm \frac{1}{2} \delta(y-\eta) H(x-3)$$

Evaluation of χ_1

$$\chi_1^{-} = \lim_{z \rightarrow 0^{-}} \left\{ \frac{e^{-ik(x-3)}}{4\pi} \frac{\partial}{\partial z} \int_{-\infty}^{x-3} \frac{e^{ik\lambda}}{\sqrt{\lambda^2 + r^2}} d\lambda \right\}$$

where

$$r = \sqrt{(y-\eta)^2 + z^2}$$

$$K_1 = -\frac{e^{-ik(x-3)}}{4\pi} \lim_{z \rightarrow 0^{-}} \left\{ \frac{\partial}{\partial z} \int_{-\infty}^0 \frac{e^{ik\lambda}}{(\lambda^2 + r^2)^{1/2}} d\lambda + \frac{\partial}{\partial z} \int_0^{x-3} \frac{e^{ik\lambda}}{\sqrt{\lambda^2 + r^2}} d\lambda \right\}$$

We define two functions to be evaluated separately

$$F_1 = \lim_{z \rightarrow 0^-} \left\{ \frac{\partial}{\partial z} \int_{-\infty}^0 \frac{e^{ik\lambda}}{\sqrt{\lambda^2 + r^2}} d\lambda \right\}$$

$$F_2 = \lim_{z \rightarrow 0^-} \left\{ \frac{\partial}{\partial z} \int_0^{x-3} \frac{e^{ik\lambda}}{\sqrt{\lambda^2 + r^2}} d\lambda \right\}$$

Following the method of ref. (6) for a similar kernel function we make the following substitution in F_2 .

$$\lambda = r \sin \theta$$

$$F_2 = \lim_{z \rightarrow 0^-} \left\{ \frac{\partial}{\partial z} \int_0^{\sin^{-1} \frac{x-3}{r}} e^{ikr \sin \theta} d\theta \right\}$$

Performing the indicated differentiation we obtain

$$F_2 = \lim_{z \rightarrow 0^-} \left\{ ik \frac{z}{r^2} \int_0^{\sin^{-1} \frac{x-3}{r}} \frac{\lambda e^{ik\lambda}}{\sqrt{\lambda^2 + r^2}} d\lambda - \frac{z}{r^2} e^{\frac{ik(x-3)}{\sqrt{(x-3)^2 + r^2}}} \right\}$$

But from the evaluation of K_1 we have found that

$$\lim_{z \rightarrow 0^-} \left\{ -\frac{z}{r^2} \right\} = \pi \delta(y-\eta)$$

$$F_2 = -\pi \delta(y-\eta) \left[ik \int_0^{x-3} \frac{\lambda e^{ik\lambda}}{|\lambda|} d\lambda + \frac{(x-3)}{|x-3|} e^{ik(x-3)} \right]$$

The integral in F_2

$$\int_0^{x-3} \frac{\lambda}{|\lambda|} e^{ik\lambda} d\lambda = \int_0^{x-3} \frac{\lambda}{|\lambda|} (\cos k\lambda + i \sin k\lambda) d\lambda$$

$$\int_0^{x-3} \frac{\lambda}{|\lambda|} e^{ik\lambda} d\lambda = \frac{x-3}{|x-3|} \frac{1}{ik} \left(e^{ik(x-3)} - 1 \right)$$

$$F_2 = -\pi \delta(y-4) \left[ik \frac{x-3}{|x-3|} \left(e^{\frac{ik(x-3)}{ik}} - 1 \right) + e^{\frac{ik(x-3)}{ik}} \frac{(x-3)}{|x-3|} \right]$$

$$F_2 = \pi \delta(y-4) \frac{(x-3)}{|x-3|}$$

Evaluation of F_1

$$F_1 = \lim_{z \rightarrow 0^-} \left\{ \frac{d}{dz} \int_{-\infty}^0 \frac{e^{ik\lambda}}{\sqrt{\lambda^2 + r^2}} d\lambda \right\}$$

or

$$F_1 = \lim_{z \rightarrow 0^-} \left\{ -z \int_0^{\infty} \frac{e^{-ik\lambda}}{(\lambda^2 + r^2)^{3/2}} d\lambda \right\}$$

$$F_1 = \lim_{z \rightarrow 0^-} \left\{ -z \int_0^{\infty} \frac{\cos k\lambda d\lambda}{(\lambda^2 + r^2)^{3/2}} + i z \int_0^{\infty} \frac{\sin k\lambda d\lambda}{(\lambda^2 + r^2)^{3/2}} \right\}$$

The evaluation of these integrals may be found in Ref. (13) (Bateman).

$$F_1 = \pi \delta(y - \eta) \lim_{z \rightarrow 0^-} \left\{ k.r K_1(kr) + \frac{i\pi}{2} k.r (J_1(kr) - L_1(kr)) \right\}$$

Since F_1 contains a delta function of $y - \eta$, the Bessel functions must be evaluated at $y - \eta = 0$, $z = 0^-$.

The result for F_1 is

$$F_1 = \pi \delta(y - \eta)$$

The end result for χ_1 is

$$\chi_1 = -\frac{1}{2} \delta(y - \eta) e^{-ik(x-3)} \left(1 + \frac{(x-2)}{|x-3|} \right)$$

which takes a final form similar to K_1

$$\chi_1 = -\frac{e^{-ik(x-3)}}{2} \delta(y - \eta) H(x-3)$$

Evaluation of χ_2 and K_2

$$\chi_2 = -\frac{e^{-ik(x-3)}}{4\pi} \lim_{z \rightarrow 0} \left\{ \frac{\partial^2}{\partial z^2} \int_0^{\infty} \frac{e^{-ik\lambda}}{\sqrt{\lambda^2 + r^2}} d\lambda \right.$$

$$\left. + \frac{\partial}{\partial z} \int_0^{x-3} \frac{e^{ik\lambda}}{\sqrt{\lambda^2 + r^2}} d\lambda \right\}$$

We make the following definitions:

$$H_1 = \frac{\partial^2}{\partial z^2} \int_0^{\infty} \frac{e^{-ik\lambda}}{\sqrt{\lambda^2 + r^2}} d\lambda$$

$$H_2 = \frac{\partial}{\partial z} \int_0^{\infty} \frac{e^{+ik\lambda}}{\sqrt{\lambda^2 + r^2}} d\lambda$$

Evaluation of H_1

$$H_1 = 3z^2 \int_0^{\infty} \frac{e^{-ik\lambda}}{(\lambda^2 + r^2)^{5/2}} d\lambda - \int_0^{\infty} \frac{e^{-ik\lambda}}{(\lambda^2 + r^2)^{3/2}} d\lambda$$

These integrals may be found in Ref(13)

$$H_1 = -\frac{k}{r} \left\{ K_1(kr) + \frac{\pi i}{2} [I_1(kr) - L_1(kr)] - i \right\}$$

$$+ \left(\frac{kr}{r} \right)^2 \left\{ K_2(kr) - \frac{\pi i}{2} [I_2(kr) - L_2(kr)] - \frac{ikr}{3} - \frac{1}{kr} \right\}$$

Evaluation of H_2

By means of the substitution $\lambda = r \sinh \theta$ in the integral

definition for H_2 , we obtain the following result:

$$H_2 = \frac{(y-\eta)^2}{r^3} \left\{ \frac{ik}{r} \int_0^{x-3} \frac{\lambda e^{ik\lambda} d\lambda}{\sqrt{\lambda^2 + r^2}} - \frac{(x-3)c}{r \sqrt{r^2 + (x-3)^2}} e^{ik(x-3)} \right\} \\ + \frac{z^2}{r^2} \left\{ \frac{(2r^2 + (x-3)^2)(x-3)}{(r^2 + (x-3)^2)^{3/2}} e^{i\lambda(x-3)} - \frac{k^2}{r^2} \int_0^{x-3} \frac{\lambda^2 e^{ik\lambda} d\lambda}{\sqrt{\lambda^2 + r^2}} \right.$$

$$\left. - \frac{ik(x-3)^2 e^{ik(x-3)}}{r^2 \sqrt{r^2 + (x-3)^2}} \right\}$$

\bar{K}_2 then becomes

$$\bar{K}_2 = \frac{e^{-ik(x-3)}}{(y-\eta)^2} \frac{1}{4\pi} \left\{ k|y-\eta| K_1(k|y-\eta|) + \frac{i\pi}{2} k|y-\eta| \left[I_1(k|y-\eta|) \right. \right. \\ \left. \left. - L_1(k|y-\eta|) \right] + \frac{x-3}{((x-3)^2 + (y-\eta)^2)^{3/2}} e^{ik(x-3)} + ik|y-\eta| \int_0^{x-3/|y-\eta|} \frac{\tau e^{ik|y-\eta|\tau}}{\sqrt{1+\tau^2}} d\tau \right. \\ \left. - ik|y-\eta| \right\}$$

For steady flow \bar{K}_2 reduces to K_2

$$K_2 = \frac{1}{4\pi(y-\eta)^2} \left(1 + \frac{(x-3)}{\sqrt{(x-3)^2 + (y-\eta)^2}} \right)$$

Evaluation of K_3

$$K_3 = \lim_{z \rightarrow 0^{\pm}} \left\{ \frac{z}{2z} \left(\frac{1}{\sqrt{(x-3)^2 + (y-\eta)^2 + z^2}} \right) \right\} = \lim_{z \rightarrow 0^{\pm}} \left\{ \frac{-z}{((y-\eta)^2 + (x-3)^2 + z^2)^{3/2}} \right\}$$

We recognize K_3 as a generalized function defining the delta function within a constant of proportionality. To solve for this constant, we require that

$$\int_{-\infty}^{\infty} \int_{-\infty}^{\infty} \delta(x, y) dx dy = 1$$

We evaluate the integral

$$-z \int_{-\infty}^{\infty} \int \frac{dx dy}{((x-3)^2 + (y-7)^2 + z^2)^{3/2}} = -2\pi \frac{z}{|z|}$$

Therefore

$$\lim_{z \rightarrow 0^{\pm}} \left\{ \frac{-z}{((x-3)^2 + (y-7)^2 + z^2)^{3/2}} \right\} = \mp 2\pi \delta(x-3, y-7)$$

and

$$K_3 = \mp 2\pi \delta(y-7, x-3)$$

Appendix 11 The Kernel Function for Nonplanar Surfaces

The kernel function for a nonplanar surface in an infinite fluid is

$$K^{\infty} = -\frac{1}{4\pi} \frac{\partial}{\partial n_1} \frac{\partial}{\partial n_2} e^{-ik(x-s)} \int_{-\infty}^{x-s} \frac{e^{ik\lambda}}{\sqrt{\lambda^2 + r_-^2}} d\lambda \quad (11.1)$$

The correction to the kernel function for a nonplanar surface near a free surface at infinite Froude number is

$$K^{F=\infty} = -\frac{1}{4\pi} \frac{\partial}{\partial n_1} \frac{\partial}{\partial n_2'} e^{-ik(x-s)} \int_{-\infty}^{x-s} \frac{e^{ik\lambda}}{\sqrt{\lambda^2 + r_+^2}} d\lambda \quad (11.2)$$

where

$$r_- = \sqrt{(y-\eta)^2 + (z-f)^2} \quad (11.3)$$

$$r_+ = \sqrt{(y-\eta)^2 + (z+f)^2} \quad (11.4)$$

$$\frac{\partial}{\partial n_1} = \cos \psi(\eta) \frac{\partial}{\partial z} - \sin \psi(\eta) \frac{\partial}{\partial y} \quad (11.5)$$

$$\frac{\partial}{\partial n_2} = \cos \psi(\eta) \frac{\partial}{\partial z} - \sin \psi(\eta) \frac{\partial}{\partial y} \quad (11.6)$$

$$\frac{\partial}{\partial n_2'} = \cos \psi(\eta) \frac{\partial}{\partial z} + \sin \psi(\eta) \frac{\partial}{\partial y} \quad (11.7)$$

If we make the following definitions

$$F_1^\pm = \int_0^\infty \frac{e^{-ik\lambda}}{\sqrt{\lambda^2 + r_\pm^2}} d\lambda \quad (11.8)$$

$$F_2^\pm = \int_0^{x-3} \frac{e^{ik\lambda}}{\sqrt{\lambda^2 + r_\pm^2}} d\lambda \quad (11.9)$$

Then the kernel function in equation (11.1) becomes

$$\begin{aligned} \chi^\infty = & -\frac{e^{-ik(x-3)}}{4\pi} \left\{ \cos \psi(y) \cos \psi(\eta) \frac{\partial^2}{\partial z^2} (F_1^- + F_2^-) \right. \\ & \left. + \sin \psi(y) \sin \psi(\eta) \frac{\partial^2}{\partial y^2} (F_1^- + F_2^-) - \sin(\psi(\eta) + \psi(y)) \frac{\partial^2}{\partial y \partial z} (F_1^- + F_2^-) \right\} \quad (11.10) \end{aligned}$$

And the correction term in equation (11.2) becomes

$$\begin{aligned} \chi^{F=\infty} = & -\frac{e^{-ik(x-3)}}{4\pi} \left\{ \cos \psi(y) \cos \psi(\eta) \frac{\partial^2}{\partial z^2} (F_1^+ + F_2^+) - \right. \\ & \left. \sin \psi(y) \sin \psi(\eta) \frac{\partial^2}{\partial y^2} (F_1^+ + F_2^+) + \sin(\psi(\eta) - \psi(y)) \frac{\partial^2}{\partial y \partial z} (F_1^+ + F_2^+) \right\} \quad (11.11) \end{aligned}$$

Since both F_1^\pm and F_2^\pm are functions of y and z only in the combination $r_\pm = \sqrt{(y-\eta)^2 + (z \pm \rho)^2}$

$$\frac{\partial^2 F_{1,2}^\pm}{\partial z^2} = \frac{(y-\eta)^2}{r^3} \frac{\partial F_{1,2}^\pm}{\partial r} + \frac{(z \pm \rho)^2}{r^2} \frac{\partial^2 F_{1,2}^\pm}{\partial r^2} \quad (11.12)$$

$$\frac{\partial^2 F_{1,2}^{\pm}}{\partial y^2} = \frac{(z \pm \rho)^2}{r_{\pm}^3} \frac{\partial F_{1,2}^{\pm}}{\partial r} + \frac{(y-\eta)^2}{r_{\pm}^2} \frac{\partial^2 F_{1,2}^{\pm}}{\partial r^2} \quad (11.13)$$

$$\frac{\partial^2 F_{1,2}^{\pm}}{\partial y \partial z} = \frac{(z \pm \rho)(y-\eta)}{r_{\pm}^2} \frac{\partial^2 F_{1,2}^{\pm}}{\partial r^2} - \frac{(z \pm \rho)(y-\eta)}{r_{\pm}^3} \frac{\partial F_{1,2}^{\pm}}{\partial r} \quad (11.14)$$

The functions in equations (11.12) to (11.14) can be evaluated using ref. (12) and ref. (7). They are:

$$\frac{\partial F_1^{\pm}}{\partial r} = -k \left(K_1(kr_{\pm}) + \frac{\pi i}{2} \left(I_1(kr_{\pm}) - L_1(kr_{\pm}) \right) - i \right) \quad (11.15)$$

$$\begin{aligned} \frac{\partial^2 F_1^{\pm}}{\partial r} = & -\frac{k}{r} \left(K_1(kr_{\pm}) + \frac{\pi i}{2} \left[I_1(kr_{\pm}) - L_1(kr_{\pm}) \right] - i \right) \\ & + k^2 \left(K_2(kr_{\pm}) - \frac{i\pi}{2} \left[I_2(kr_{\pm}) - L_2(kr_{\pm}) \right] + \frac{ikr}{3} - \frac{i}{kr} \right) \end{aligned} \quad (11.16)$$

$$\frac{\partial F_2^{\pm}}{\partial r} = \frac{ikr}{r_{\pm}} \int_0^{x-3} \frac{\lambda e^{ik\lambda}}{\sqrt{\lambda^2 + r_{\pm}^2}} d\lambda - \frac{(x-3) e^{ik(x-3)}}{r_{\pm} \sqrt{r_{\pm}^2 + (x-3)^2}} \quad (11.17)$$

$$\frac{\partial^2 F_2^{\pm}}{\partial r^2} = \frac{2r_{\pm}^2 + (x-3)^2}{(r_{\pm}^2 + (x-3)^2)^{3/2}} \frac{e^{ik(x-3)}}{r_{\pm}^2} - \frac{ck(x-3)^2 e^{ik(x-3)}}{r_{\pm}^2 \sqrt{r_{\pm}^2 + (x-3)^2}} - \frac{k^2}{r_{\pm}^2} \int_0^{x-3} \frac{\lambda^2 e^{ik\lambda}}{\sqrt{\lambda^2 + r_{\pm}^2}} d\lambda \quad (11.18)$$

The combination of these functions as in equation (11.10) — (11.14) will give the very complicated form of the kernel function.

The behavior of the kernel function near the line $y=\eta, z=f$ may be found by expanding the expression

$$\chi \approx -\frac{e}{4\pi} \frac{\partial^2}{\partial n^2} \int_{-\infty}^{x-3} \frac{e^{ik\lambda} d\lambda}{\sqrt{\lambda^2 + n^2 + t^2}} \quad (11.19)$$

for small $r, r = \sqrt{n^2 + t^2}$ n is the normal to the surface, t is the tangent to the surface.

For small r

$$\frac{\partial F_1}{\partial r} \approx -k \left(\frac{1}{kr} + \dots \right) \quad (11.20)$$

$$\frac{\partial^2 F_1}{\partial r^2} = -\frac{k}{r} \left(\frac{1}{kr} + \dots \right) + k^2 \left(\frac{2}{(kr)^2} + \dots \right) \quad (11.21)$$

$$\frac{\partial F_2}{\partial r} \approx -\frac{1}{r} \frac{|x-3|}{(x-3)} + \dots \quad (11.22)$$

$$\frac{\partial^2 F_2}{\partial r^2} = \frac{1}{r^2} \frac{|x-3|}{(x-3)} + \dots \quad (11.23)$$

$$\chi \approx -\frac{e}{4\pi} \frac{e^{-ik(x-3)}}{\left[\frac{t^2}{(n^2+t^2)^{3/2}} \left(\frac{\partial F_1}{\partial r} + \frac{\partial F_2}{\partial r} \right) + \frac{n^2}{r^2} \left(\frac{\partial^2 F_1}{\partial r^2} + \frac{\partial^2 F_2}{\partial r^2} \right) \right]} \quad (11.24)$$

Thus

$$\chi \approx \frac{e}{4\pi} \frac{e^{-ik(x-3)}}{\left\{ \frac{1}{n^2+t^2} - \frac{2n^2}{n^2+t^2} \right\} \left\{ 1 + \frac{(x-3)}{|x-3|} \right\}} + \dots \quad (11.25)$$

APPENDIX 111 Transformation of the Fourier Inversion Integral

We consider the transformation $s = -s$, $\beta = \tau s$ applied to the Fourier inversion integral

$$\phi(x, y) = \frac{1}{2\pi} \iint_{-\infty}^{\infty} \Phi(s, \beta) e^{isx + i\beta y} ds d\beta \quad (111.1)$$

This integral is also written

$$\begin{aligned} \phi(x, y) &= \frac{1}{2\pi} \int_0^{\infty} \int_{-\infty}^{\infty} \bar{\Phi}(s, \beta) e^{isx + i\beta y} d\beta ds \\ &+ \frac{1}{2\pi} \int_0^{\infty} \int_{-\infty}^{\infty} \bar{\Phi}(-s, \beta) e^{-isx + i\beta y} d\beta ds \end{aligned} \quad (111.2)$$

Applying the transformation $s = -s$, $\beta = \tau s$,

$$\begin{aligned} \phi(x, y) &= \frac{1}{2\pi} \int_0^{\infty} \int_{-\infty}^{\infty} \bar{\Phi}(s, \tau s) e^{isx + i\tau s y} s ds d\tau \\ &+ \frac{1}{2\pi} \int_0^{\infty} \int_{-\infty}^{\infty} \bar{\Phi}(-s, \tau s) e^{-isx + i\tau s y} s ds d\tau \end{aligned} \quad (111.3)$$

Let $s = -s$ in the second integral in equation (111.3)

$$\begin{aligned} \phi(x, y) &= \frac{1}{2\pi} \int_0^{\infty} \int_{-\infty}^{\infty} \bar{\Phi}(s, \tau s) e^{isx + i\tau s y} s ds d\tau \\ &- \frac{1}{2\pi} \int_{-\infty}^0 \int_{-\infty}^{\infty} \bar{\Phi}(s, -\tau s) e^{isx - i\tau s y} s ds d\tau \end{aligned} \quad (111.4)$$

We then let $\tau = -\tau$ in the second integral of (111.4)

$$\begin{aligned} \phi(x, y) &= \frac{1}{2\pi} \int_0^{\infty} \int_{-\infty}^{\infty} \Phi(s, \tau s) e^{isx + i\tau y} s ds d\tau \\ &\quad - \frac{1}{2\pi} \int_0^{\infty} \int_{-\infty}^{\infty} \Phi(s, \tau s) e^{isx + i\tau y} s ds d\tau \end{aligned} \quad (111.5)$$

Written in more compact form, this becomes

$$\phi(x, y) = \frac{1}{2\pi} \int_{-\infty}^{\infty} \int_{-\infty}^{\infty} \Phi(s, \tau s) e^{isx + i\tau y} |s| d\tau ds \quad (111.6)$$

Therefore if,

$$\phi(x, y) = \frac{1}{2\pi} \iint_{-\infty}^{\infty} \Phi(s, \beta) e^{isx + i\beta y} ds d\beta \quad (111.7)$$

then

$$\phi(x, y) = \frac{1}{2\pi} \iint_{-\infty}^{\infty} \Phi(s, s\tau) e^{isx + i\tau y} |s| ds d\tau \quad (111.8)$$